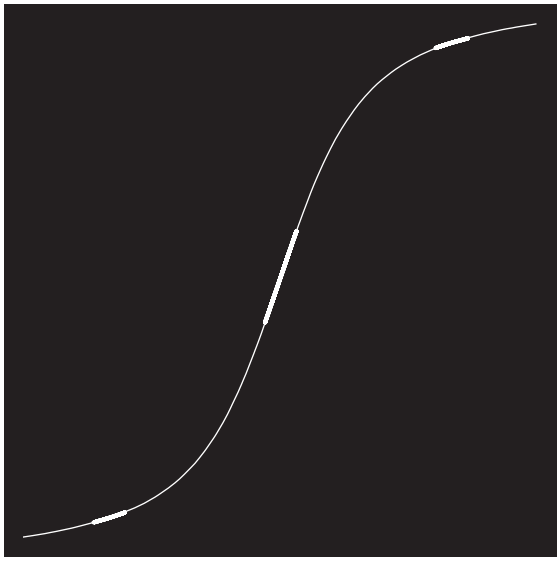

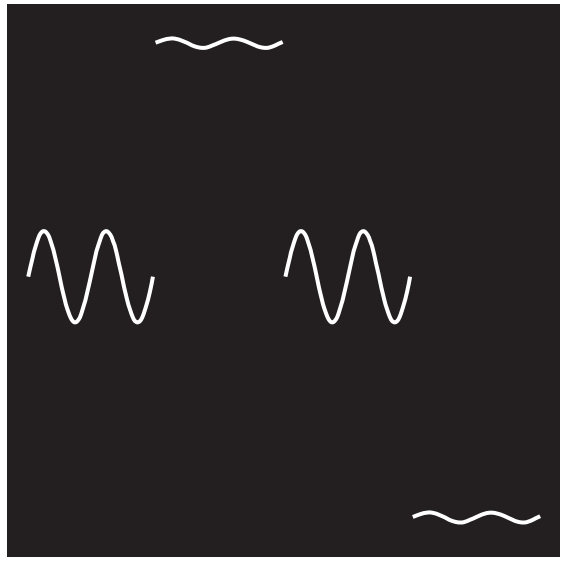

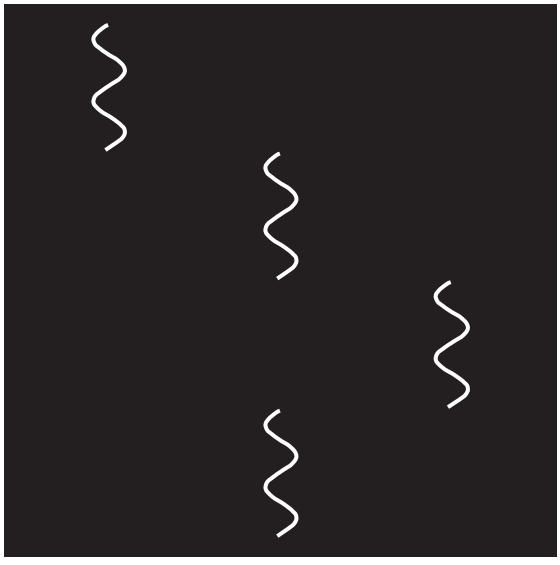

detection of magnetic nanoparticles for clinical interventions

martijn visscher

Detection of magnetic nanoparticles for clinical interventions

Martijn Visscher

Members of the dissertation committee:

Prof. dr. ir. J.W.M. Hilgenkamp (chairman)	University of Twente
Prof. dr. ir. W. Steenbergen (promotor)	University of Twente
Dr. B. ten Haken (assistent promotor)	University of Twente
Prof. dr. Q.A. Pankhurst	University College London
Prof. dr. A. Heerschap	Radboud University Nijmegen
Dr. J.M. Klaase	Medisch Spectrum Twente
Prof. dr. J.F.J. Engbersen	University of Twente
Dr. M.M.J. Dhallé	University of Twente

The work in this thesis was carried out at the Faculty of Science and Technology and the MIRA Institute for Biomedical Engineering and Technical Medicine at the University of Twente.

Nederlandse titel:
Detectie van magnetische nanodeeltjes voor klinische interventies

Publisher:
Martijn Visscher
MIRA Institute for Biomedical Engineering and Technical Medicine
University of Twente
P.O.Box 217, 7500 AE Enschede, The Netherlands
http://www.utwente.nl/MIRA
m.visscher@alumnus.utwente.nl

Cover design: Martijn Duifhuizen, Berkenwoude - atelierduifhuizen.nl
Printed by: Gildeprint Drukkerijen - Enschede

ISBN: 978-90-365-3701-8
DOI: http://dx.doi.org/10.3990/1/9789036537018

DETECTION OF MAGNETIC NANOPARTICLES FOR CLINICAL INTERVENTIONS

PROEFSCHRIFT

ter verkrijging van
de graad van doctor aan de Universiteit Twente,
op gezag van de rector magnificus,
Prof. dr. H. Brinksma,
volgens besluit van het College voor Promoties
in het openbaar te verdedigen
op woensdag 27 augustus 2014 om 14.45 uur

door

Martijn Visscher

geboren op 23 december 1983

te Apeldoorn

Dit proefschrift is goedgekeurd door de promotor:

Prof. dr. ir. W. Steenbergen

en de assistent-promotor:

Dr. ir. B. ten Haken

Contents

1 Introduction

The application of magnetic nanoparticles (MNPs) for biomedical purposes has been developing over the last decades, driven by technological developments [1, 2]. A variety of diagnostic and therapeutic routes has been developed and tested, taking advantage of the specific magnetic characteristics of MNPs. Still, the ongoing development of MNPs and magnetic methods to use them, have a high potential to improve diagnostic and therapeutic methods. The goal of the research presented in this thesis, is to investigate the aspects of MNP detection for surgical interventions. Focusing on magnetic detection of the sentinel lymph node, the feasibility and possibilities of MNP detection for a broader range of clinical interventions is investigated. In the following sections the clinical utility of MNPs and the application in clinical interventions is introduced. In the final section a synopsis of the following chapters is given.

1.1 Clinical utility of magnetic nanoparticles

The development of biomedical use of MNPs is stimulated by the typical magnetic characteristics that make them suitable for clinical application. The high magnetic susceptibility of MNPs provides good contrast with the low susceptibility of the body. Since magnetic detection can be performed in a safe and harmless way, MNPs are concurring with other sources of contrast in medicine, like radio-isotopes. The magnetic properties of MNPs enable distant detection in nontransparent environments, which is advantageous for *in vivo* applications. Under specific conditions, magnetic fields can be used to manipulate MNPs for transportation, localization or activation.

The second point facilitating MNP application in medicine, is the availability of magnetic materials with a safe and biocompatible profile. Particles based on iron oxide have been proven to be safe for clinical application and can be secreted or degraded, followed by uptake in the iron blood pool for hemoglobin [3, 4]. MNPs

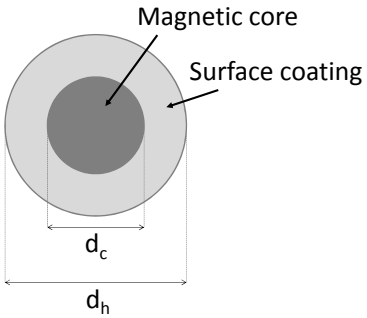

Figure 1.1: *A simple structure of a magnetic nanoparticle with a magnetic core with diameter d_c. The surface coating determines the final hydrodynamic size d_h of the particle.*

with other magnetic materials are in development and can be applied *in vivo* as long as good biocompatibility and low toxicity can be guaranteed by optimal coating and particle engineering [5].

In biomedical context, the hydrodynamic size of MNPs is important for optimal performance (fig. 1.1). Nanometer sized particles are well suited to overcome biological barriers, entering the interstitial space, cells and vesicles [2]. Fortunately, the magnetic moment of nanometer-sized iron oxide particles is still sufficient for contrasting detection in biomedical samples. For most biomedical applications, it is feasible to produce particles with a magnetic moment large enough for good magnetic performance and a hydrodynamic size small enough for adequate physiological distribution. Since particle size and type of coating largely determine the biodistribution and lifetime for *in vivo* applications, the production of magnetic core materials and coatings with different characteristics are still a topic of research [5, 6].

Compared to optical tracers used for biomedical applications, like fluorescent dye or ink, a magnetic tracer can be detected in deeper tissue layers. Where optical methods achieve a maximum of 1-1.5 cm detection depth [7, 8], magnetic systems can detect the MNPs deep in the human body, with magnetic resonance imaging (MRI) suitable for whole body detection [9]. Furthermore, fluorescent detection restricts the use of a standard light source, which makes the performance of a clinical intervention more complicated and time consuming.

In contrast to radio-active medical tracers, with usually a relatively short half-life, the MNPs can be magnetically stable over much longer time. Shelf life of MNP tracers is long and clinical procedures involving MNPs are less time critical, since they are less influenced by a signal decay. In addition, the balance in clinical nuclear procedures between a tracer dose large enough for good detection rates and minimization of radiation exposure of patients and clinical staff [10–13], is eliminated with the use of magnetic tracers. These aspects, combined with the safe character of magnetism, can help to make clinical procedures less expensive and logistically less complex, compared to radionuclide-based procedures [14, 15].

Detection of magnetic nanoparticles in medical interventions

While biomedical research has resulted in a variety of MNPs for different applications, the clinical application of MNPs is still very little. Currently, the main *in vivo* application is the use of MNPs as an MRI contrast agent after intravenous administration [16]. MRI is able to visualize the effect of a concentration of MNPs in a specific area on whole body scale. Another approach, currently in development for whole body detection, is magnetic particle imaging (MPI), which specificly detects the magnetic response of MNPs with increased sensitivity compared to MRI [2, 17]. In general, in clinical context MNPs are used to indicate a typical area of interest. A

Figure 1.2: *Operating room during surgery with the sentinel lymph node procedure using a gamma probe which is placed on the cart. The available space and materials of surgical equipement limit the use of large magnetic detection systems.*

few milligrams of MNPs are injected in the large 80 kg human body and is subsequently sensed by a suitable detection system. The whole body methods can provide important diagnostic preoperative or post-operative information.

During surgical interventions MNP detection can help to localize lesions and other spots of interest labeled with MNPs. However, for surgical use in a complex operating theater (fig. 1.2), high sensitive and MNP-specific magnetic detection systems are not available. The existing detection technology with MRI and MPI, requires large systems with high magnetic fields, which is not compatible with the surgical environment (fig. 1.3). For optimal surgical assistance, a small magnetic (handheld) sensor for local detection is suitable to minimize detection of the operating table and surgical instruments, is minimally interfering with surgical practice and enables the surgeon to control the detection area. For successfull introduction of MNP detection in surgical practice, the greatest challenge one faces is the detection of tiny amounts of MNPs -in the order of micrograms- accumulated in a large tissue mass, since the magnetism of the MNPs should be discriminated from the magnetism of a much larger amount of tissue of several hundred grams. Existing probes based on alternating field magnetometry with a constant, single frequency lack MNP specificity and also detect tissue contributions.

A magnetic detection method that more specificly detects the MNPs and eliminates the contribution from tissue, has a better for clinical *in vivo* applications. For more selective MNP detection, clinically suitable detection technology is presently not available.

Synopsis

In the present thesis, the clinical use of MNP detection is explored with a focus on interventional application using relatively small, uncomplicated and not expensive detection technology. Both, the clinical and technical possibilities and challenges of local interventional MNP detection are topic of the present thesis. Magnetic sentinel lymph node detection was adopted as a leading clinical case. For this type of clinical magnetic detection, a new algorithm for excitation and high sensitive, specific sensing of MNPs has been developed, using standard copper coils, low field amplitudes and small systems. The work is almost entirely based on commercially available and clinically approved tracers. Synthesis and development of better MNP tracers is certainly possible, but beyond the scope of the thesis.

Chapter 2 gives an introduction into MNP detection with a focus on local detection for clinical interventions. The current status of detection clinical detection methods is discussed regarding the suitability for *in vivo* MNP detection during surgery. The chapter concludes with a model-based quantitative evaluation of constant, single frequency alternating field magnetometry, which is frequently applied for MNP detection. The goal is to obtain insight in the limitations for clinical practice and to define the conditions and challenges for improved detection methods with alternating field magnetometry.

Chapter 3 shows the feasibility of vibrating sample magnetometry (VSM) for magnetic sentinel lymph node detection. MNP content is quantified with VSM in lymph nodes obtained from *ex vivo* sentinel lymph node procedures in colorectal cancer. For the soft tissue samples with variable volume, an accurate fixation system was prepared to eliminate parasitic movement. To quantify the amount of MNPs a

(a) **(b)**

Figure 1.3: *(a). Clinical 3T MRI system from Siemens. (b). The preclinical Magnetic Particle Imaging system from Bruker with a selection field gradient of 1.8 T/m. (Reproduced with permission from [18, 19].)*

model is fitted to the measured magnetic moment response of the lymph nodes, using the Langevin model for the superparamagnetic component and a parameter for the linear contribution of varying tissue volume. Using the VSM protocol developed in chapter 3, chapter 4 discusses the magnetic ex vivo sentinel lymph node procedure for colorectal cancer in clinical perspective and makes a comparison with the most standard use of optical tracers and radio-isotopes. The results of this small-scale study indicate a promising method with technical and practical advantages for ex vivo sentinel lymph node mapping in colorectal cancer patients.

In chapter 5 a new, fast concept of magnetic detection, called *DiffMag*, is introduced and tested for several tracers. The DiffMag concept is developed to achieve selective detection of MNPs in tissue, by comparing the MNP response to a continuous alternating field in the presence of an offset field and zero field. The non-modulating linear response of tissue is eliminated by subtraction.

The observed discrepancy between quantification of MNPs in lymph nodes with VSM and DiffMag in Chapter 5 was he motivation to perform the study described in chapter 6. Using the calibration of DiffMag with MNP suspensions the MNP content in SLNs was underestimated. In chapter 6 the suspected effect of a change in Brownian relaxation after MNP accumulation in lymph nodes was investigated using MNP samples with different conditions for Brownian relaxation. The results show a tracer dependent effect of viscosity and particle volume on the reduction of the measured DiffMag response and confirm the hypothesis of a changed DiffMag response after MNP uptake in lymph node tissue. The effect is an important factor to consider in clinical application of (quantitative) magnetic detection systems based on alternating field excitation.

The final chapter closes with a general discussion about detection of MNPs for clinical interventions, based on the results in previous chapters. The developed DiffMag technique, feasible for fast specific MNP detection with small systems in clinical environment, is considered for different possibilities of future clinical application. Recommendations are given to improve the sensor and measurement protocol and to further investigate clinical MNP detection with DiffMag.

References

[1] Q. A. Pankhurst, N. K. T. Thanh, S. K. Jones, and J. Dobson, “Progress in applications of magnetic nanoparticles in biomedicine”, Journal of Physics D: Applied Physics **42** (2009).

[2] K. M. Krishnan, “Biomedical nanomagnetics: A *Spin* through possibilities in imaging, diagnostics, and therapy”, Magnetics, IEEE Transactions on **46**, 2523–2558 (2010).

[3] H. Onishi, T. Murakami, T. Kim, M. Hori, S. Hirohashi, M. Matsuki, Y. Narumi, Y. Imai, K. Sakurai, and H. Nakamura, “Safety of ferucarbotran in mr imaging of the liver: A pre- and postexam-

ination questionnaire-based multicenter investigation", Journal of Magnetic Resonance Imaging **29**, 106–111 (2009).

[4] M. Bañobre-López, A. Teijeiro, and J. Rivas, "Magnetic nanoparticle-based hyperthermia for cancer treatment", Reports of Practical Oncology & Radiotherapy **18**, 397 – 400 (2013), selected Papers Presented at the {XVII} {SEOR} Congress, Vigo, 1821 June 2013.

[5] A. Figuerola, R. Di Corato, L. Manna, and T. Pellegrino, "From iron oxide nanoparticles towards advanced iron-based inorganic materials designed for biomedical applications", Pharmacological Research **62**, 126–143 (2010).

[6] S. Laurent, D. Forge, M. Port, A. Roch, C. Robic, L. Vander Elst, and R. N. Muller, "Magnetic iron oxide nanoparticles: Synthesis, stabilization, vectorization, physicochemical characterizations, and biological applications", Chemical Reviews **108**, 2064–2110 (2008).

[7] J. C. Hebden, S. R. Arridge, and D. T. Delpy, "Optical imaging in medicine: I. experimental techniques", Physics in Medicine and Biology **42**, 825 (1997).

[8] A. P. Gibson, J. C. Hebden, and S. R. Arridge, "Recent advances in diffuse optical imaging", Physics in Medicine and Biology **50**, R1 (2005).

[9] R. Di Corato, F. Gazeau, C. Le Visage, D. Fayol, P. Levitz, F. Lux, D. Letourneur, N. Luciani, O. Tillement, and C. Wilhelm, "High-resolution cellular MRI: Gadolinium and iron oxide nanoparticles for in-depth dual-cell imaging of engineered tissue constructs", ACS Nano **7**, 7500–7512 (2013).

[10] E. C. Glass, R. Essner, and A. E. Giuliano, "Sentinel node localization in breast cancer", Seminars in Nuclear Medicine **29**, 57–68 (1999).

[11] S. Povoski, R. Neff, C. Mojzisik, D. OMalley, G. Hinkle, N. Hall, D. Murrey, M. Knopp, and E. Martin, "A comprehensive overview of radioguided surgery using gamma detection probe technology", World Journal of Surgical Oncology **7**, 11 (2009).

[12] A. H. Strickland, N. Beechey-Newman, C. B. Steer, and P. G. Harper, "Sentinel node biopsy: an in depth appraisal", Critical Reviews in Oncology/Hematology **44**, 45–70 (2002).

[13] R. A. Valdés Olmos, P. J. Tanis, C. A. Hoefnagel, O. E. Nieweg, S. H. Muller, E. J. T. Rutgers, M. L. K. Kooi, and B. B. R. Kroon, "Improved sentinel node visualization in breast cancer by optimizing the colloid particle concentration and tracer dosage", Nuclear Medicine Communications **22**, 579–586 (2001).

[14] S. K. Somasundaram, D. W. Chicken, and M. R. S. Keshtgar, "Detection of the sentinel lymph node in breast cancer", British Medical Bulletin **84**, 117–131 (2007).

[15] M. Douek, J. Klaase, I. Monypenny, A. Kothari, K. Zechmeister, D. Brown, L. Wyld, P. Drew, H. Garmo, O. Agbaje, Q. Pankhurst, B. Anninga, M. Grootendorst, B. Haken, M. Hall-Craggs, A. Purushotham, and S. Pinder, "Sentinel node biopsy using a magnetic tracer versus standard technique: The sentimag multicentre trial", Annals of Surgical Oncology 1–9 (2013).

[16] C. Corot, P. Robert, J. M. Idée, and M. Port, "Recent advances in iron oxide nanocrystal technology for medical imaging", Advanced Drug Delivery Reviews **58**, 1471–1504 (2006).

[17] B. Gleich and J. Weizenecker, "Tomographic imaging using the nonlinear response of magnetic particles", Nature **435**, 1214–1217 (2005).

[18] "Siemens Web Site", `http://www.healthcare.siemens.nl`, (Accessed: 2014-05-27).

[19] "Bruker Corporation Website", `http://www.bruker.com`, (Accessed: 2014-05-27).

2

Detection of magnetic nanoparticles and biomedical applications*

Abstract: The suitability of magnetic nanoparticles (MNPs) for biomedical applications is largely dependent on the physical and chemical properties of magnetic core materials and coating. Various laboratory detection methods are available to characterize MNPs and use them for different applications. The main (pre-)clinical applications of MNPs, are magnetic resonance imaging and magnetic particle imaging. In both techniques the MNPs are used as an *in vivo* tracer, to visualize anatomical structures of interest. The increasing interest for local detection of magnetic nanoparticles (MNPs) during clinical interventions, like sentinel lymph node biopsy, requires the development of suitable probes that unambiguously detect the MNPs at a depth of several centimeters in the body. The final part of this chapter quantitatively evaluates the limitations of a simple magnetometry method using a constant amplitude alternating field with a single frequency. This method is limited by the variability of the magnetic susceptibility of the surrounding diamagnetic tissue. Two different sensors are evaluated in a theoretical model of MNP detection in a tissue volume. For a coil which completely encloses the sample volume, the MNPs can be detected if the total mass contributing to the signal is larger than $4.1{\cdot}10^{-7}$ times the tissue mass. For a handheld surface coil, intended to search for the MNPs in a larger tissue volume, an amount of 1 μg of iron cannot be detected by sensors with a diameter larger than 2 cm. To detect a spot with MNPs at 5 cm depth in tissue, it should contain at least 120 μg iron. Therefore, for high-sensitive clinical MNP detection in surgical interventions, techniques with increased specificity for the nonlinear magnetic properties of MNPs are indispensable.

*Part of this chapter is submitted as: Martijn Visscher, Sebastiaan Waanders, Joost Pouw, Bennie ten Haken, Depth Limitations for *In Vivo* Magnetic Nanoparticle Detection with a Compact Handheld Device. Journal of Magnetism and Magnetic Materials: Conference Proceedings of the 10^{th} International Conference on the Scientific and Clinical Applications of Magnetic Carriers, 2014

The present chapter introduces the different aspects of MNP detection and focuses more specifically on clinical detection of MNPs during (surgical) interventions. Only general MNP characteristics and a short overview of biomedical MNP applications is given. The possibilities and aspects of MNPs regarding biomedical (*in vivo*) performance and detection, is shortly discussed. A short explanation is given on MNP detection with MRI and MPI, which can be valuable in combination with interventional MNP detection. To determine the quantitative limitations of (local)interventional MNP detection using a single alternating field, a theoretical detector model is developed and evaluated in the final part of this chapter.

2.1 Magnetic and chemical properties of MNPs

The magnetic and chemical properties of MNPs are crucial for optimal performance in biomedical applications. Both aspects, shortly discussed in this section, are of great importance in the development of MNP tracers.

Most MNPs used in biomedical applications, are made of magnetic core materials with a nonmagnetic coating for stability and biocompatibility. The core materials determine the magnetic properties of a MNP sample by the bulk saturation magnetization, the size and the shape and structure of the crystal. MNPs with the same core materials, but produced with different chemical production processes, show large differences in magnetic properties, due to differences in crystallographic order, surface structure and impurities [1, 2].

The majority of MNPs for clinical applications have a superparamagnetic characteristic at room or body temperature. This means that the particles are non-interacting single domain particles. In zero field the net magnetization of an ensemble of particles decays to zero by the thermal energy of the system. Such a system can be described by the Langevin equation, introduced by Bean [3]. For increasing particle diameter, the particles become ferromagnetic with a multidomain structure. After first excitation, these particles show remanent magnetization in zero field and particle interactions may cause agglomeration of MNPs. For most medical applications particle agglomeration is undesired, because of risks of blood clots in the cardiovascular system. Therefore, the main focus in medical MNP application is on superparamagnetic nanoparticles [4].

A change in magnetization of MNPs occurs by (re-)orientation of the magnetic moment, called relaxation. The magnetic energy of an MNP system depends on the magnetic field conditions. The relaxation process of MNPs restores the energy balance between thermal and magnetic energy of the particles. Thus, the state of MNP samples depends both on temperature and magnetic field. A magnetic field change or a change in temperature can initiate a relaxation process. Magnetometers based on Faraday induction use this relaxation process to detect the MNPs in a sample.

Since magnetic detection of MNPs is relaxation dependent, factors influencing the particle relaxation can also be used to monitor MNP conditions. This feature is used for smart detection or monitoring of chemical and biological processes involving MNPs [5]. MNPs prepared to take part in a specific molecular or cellular reaction, may show altered relaxation behavior after the reaction took place and can thus be used as an indirect tool for detection of (bio)molecular reactions [2, 6, 7] (see also Chapter 6).

The coating of MNPs prevents the magnetic core from clustering and degradation by oxidation or biological processes [2]. Therefore, the coating in itself should be stable and insensitive for biological degradation. Using a proper coating, the MNPs become water soluble resulting in a stable dispersion, suitable for biomedical environments [4]. Depending on the purpose of the MNPs, the coating can be engineered for optimal performance. For specific targeting, particles can be labeled with an antigen [2, 6]. To increase circulation time for vascular imaging, the particles can be made less recognizable for the immune system [1]. Functional molecules, such as specific dyes, can be attached to the coating for multimodal detection. Finally, association with therapeutic agents can be used for MNP related drug delivery [4].

The thickness of the coating defines final particle size and can be optimized for certain applications. Particles larger than 200 nm are easily caught by the spleen and subsequently removed by the phagocyte system. Particles smaller than 10 nm are rapidly removed by renal clearance and extravasation. Therefore, for long blood circulation times after intravenous injection, the most optimal particle size is in the range of 10-100 nm [2, 6]. Also in this context the type of coating material is essential, since the effective particle size may increase after *in vivo* administration due to adhesion of biomolecules. This can be reduced by choosing a suitable coating material with a lower affinity for biomolecules.

Different laboratory methods can be used for MNP detection and characterization of the physical properties, as is discussed in the next section.

2.2 Laboratory techniques for magnetic nanoparticle detection

Different techniques can be used for the characterization of the physical characteristics of MNPs. In biomedical research, a variety of laboratory systems is used for detection and characterization of MNPs, like vibrating sample magnetometry (VSM), AC-susceptometry (or more appropriate alternating field susceptometry), superconducting quantum interference device (SQUID) and nuclear magnetic resonance (NMR) . In a few biomedical applications Hall-effect sensors are used for MNP detection [8, 9]. Techniques not requiring sample destruction for MNP detection are applicable to analyse samples that have to be subjected to additional clinical

post-processing methods (e.g. histologic analysis by light microscopy).

Closely related to clinical practice, MRI is used to measure the relaxivity of an MNP, so as to determine the suitability as a contrast agent [10]. Since MRI is usually based on proton relaxation, MRI analysis of MNPs is a more indirect method, measuring the effect of the MNPs on proton relaxation. Unless a great sensitivity, the interventional use of MRI detection is limited, since the system requirements are not compatible with a standard surgical environment. The application of MRI for clinical use of MNPs is introduced in section 2.3.1.

VSM measurements are mostly used to determine the magnetic properties of MNPs in a (quasi-)static field up to a few Tesla and can especially provide a good measure of the saturation magnetization. This method is rather time consuming, requires careful sample preparation and a suitable coil design for high field excitation, which makes it a rather expensive technique.

Methods based on alternating field excitation are developed in several variants for MNP characterization or specific applications. Using relatively low field amplitudes and simple systems, high sensitive detection can be achieved. Frequency dependent MNP behavior is investigated by measurements at a range of excitation frequencies [11–14]. Excitation with dual frequencies is exploited to specificly measure the nonlinear response of MNPs [15, 16]. Magnetic particle imaging (MPI) is a method for (clinical) MNP tracer imaging based on (single frequency) alternating field excitation and the nonlinear response of MNPs. For MPI tracer characterization the higher harmonics content or field derivative of the magnetization response is analyzed [17, 18]. Alternating field magnetometry is further discussed later in this chapter and also in the chapters 5 and 6, since it is strongly related to the measurement technique developed in this thesis.

MNP characterization with SQUID systems has been used to determine MNP relaxation properties, mainly for Brownian relaxation. After a period with a relatively weak static excitation field, the demagnetization response is measured over longer time scales ($>$1s). The magnetization decay is used to determine the characteristic relaxation times of the MNP sample [5, 19, 20], while the amplitude can be used to determine the amount of MNPs contributing to the response [21–24]. This technique can only detect MNP processes which are significantly longer than the period of dead time after excitation. The use of the high sensitive but costly SQUIDs for MNP detection normally requires a magnetically shielded room which makes the technique more expensive and less attractive for clinical applications.

Non-magnetic detection methods for MNPs comprise optical methods such as, transmission electron microscopy (TEM), dynamic light scattering (DLS) [14, 25], light microscopy and photoacoustic detection [26–28]. Light microscopic analysis and photoacoustic detection are mostly used for specific MNP applications, especially to investigate MNP distribution in tissue. TEM and DLS are used for MNP

characterization, mainly to determine the particle size distribution. TEM is applied to analyse the core size distribution of an MNP population, which is an expensive and time consuming procedure because of critical sample preparation and laborious image analysis. Hydrodynamic particle size and clustering of MNPs can be investigated by DLS, which uses optical scattering to determine the particle size of MNPs in suspension. DLS cannot be applied for samples with opaque media and, since the technique is not MNP specific, the results can be biased by other structures in the suspension. Therefore, a complementary analysis is often applied with techniques selectively sensitive for MNPs and suitable for non-transparent samples [29, 30].

2.3 Clinical detection of magnetic nanoparticles

Biomedical detection of MNPs has been developing along different routes for *in vivo*, *ex vivo* and *in vitro* samples. Several reviews have described the current applications of MNPs in MRI, magnetic hyperthermia, magnetic labeling of cells and molecules, magnetic particle imaging and drug delivery [2, 31–33]. The main clinical *in vivo* application of MNPs so far is as a T_2 contrast agent in MRI [1]. Emerging applications for clinical detection of MNPs are MPI and sensors for local detection during interventions. These applications and the use of MNPs for MRI are discussed in the following sections.

2.3.1 Magnetic resonance imaging

In addition to the widely applied gadolinium based MRI contrast agent, the use of superparamagnetic iron oxides (SPIOs) as a contrast agent for MRI is one of the most important and well developed applications of MNPs in medicine [1, 34]. The magnetic susceptibility of SPIOs is much higher compared to the susceptibility of bodily tissue. The magnetic field gradient produced by the MNPs, increases the field dependent proton relaxation. Therefore, inhomogeneous distribution of SPIO particles in tissue cause large differences in the MR-signal between voxels. The MNPs cause a disturbed, inhomogeneous field, which highly affects both longitudinal and transverse proton relaxation time (T_1 and T_2). Most applications use the effect of MNPs on transverse proton relaxation time (T_2), where the MNP induced field inhomogeneities cause an increased loss of phase coherence of the spins contributing to the MRI-signal. After contrast agent administration, the areas with MNP uptake are recognized by the increased signal loss. Particle clustering or aggregation can result in a stronger signal decrease, as the local field gradient around a cluster becomes larger.

For MNP-based contrast in MRI, the tracer is usually administered intravenously and accumulates in specific organ systems in the body, depending on the particle

characteristics and the progress of disease. In only a few studies a local, interstitial injection of MNP tracer was used for preoperative staging of sentinel lymph nodes (see also section 2.3.3) [35, 36]. The main applications for SPIO based contrast, is imaging of organs or processes related to macrophage function, like liver and lymph nodes [37, 38]. The response of the reticuloendothelial system (RES) depends on particle size and thus aggregation of particles can be used to investigate RES-function [1, 39]. For healthy regions, SPIO uptake is optimal and a large contrast agent effect is observed. The pathological areas of interest are those, where macrophage uptake of SPIO-MNPs is affected by tumor growth. Diseased areas show therefore signal intensities not affected by MNP presence, while the healthy regions with normal macrophage function show a large signal reduction.

For lymph node imaging, so called ultra-small SPIOs (USPIOs, $<$50 nm) are used, since smaller particles with minor macrophage uptake have a prolonged blood half-life and give better access to the lymphatic system [40–43]. Nodal staging using SPIO tracers has been successful, but still tumors smaller than 5 mm may remain undetected [44].

The USPIO particles may also be beneficial for imaging of increased macrophage content in diseased tissue in inflammatory or degenerative diseases [45]. Finally, for medical indications currently requiring blood vessel imaging based on gadolinium T_1 contrast, MNPs with prolonged blood half-life can be useful as a tool for angiography, tumor permeability, tumor blood volume, cerebral blood volume and vascular size measurements [1].

2.3.2 Magnetic particle imaging

Magnetic particle imaging (MPI) was introduced by Gleich and Weizenecker in a Nature publication in 2005 as a new medical imaging modality [46]. The concept of MPI is based on the nonlinear magnetization response of superparamagnetic nanoparticles in a magnetic field. Using an alternating field with a fixed frequency between 1 and 100 kHz, the higher harmonics generated by the nonlinear MNP response are detected by the receive coil. The higher harmonics content is used as a representation for the MNPs in a sample. Spatial encoding of the signal is achieved by addition of large, opposing, static fields, with a field free line or point in between. The static fields are used to saturate the magnetization of the MNPs outside the field free area, which prohibits the MNPs to respond to the alternating field. The field free area is scanned over the sample space to obtain spatial information of the MNP distribution. The magnetically nonsaturated MNPs in the field free area give the strongest response to the alternating field. An image reconstruction with MNP densities is made, by combining the received MNP response with the known field free area positions.

Since tissue has a linear magnetic response, only the MNP tracer appears in the image, as is shown on the left side in figure 2.1. Anatomic information can therefore

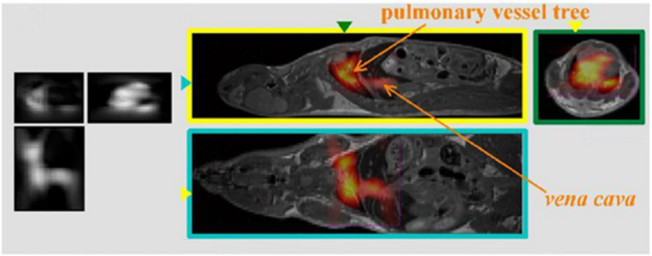

Figure 2.1: *A selected registration out of a series of in vivo dynamic MPI images fused with static MRI images of a mouse. On the left the MPI images before fusion with MRI, showing only the spatial MNP distribution. (Reproduced with permission from [47].)*

only be retrieved from the areas reached by the MNPs. MPI is therefore a tracer imaging technique, since the MNPs are not used as a conventional agent for contrast enhancement. For more detailed anatomical information of MNP distribution, the MPI image has to be merged with anatomical images obtained from other imaging modalities.

The imaging performance of MPI is heavily based on the amplitude and quality of the static magnetic field gradients. For human MPI scanners with a good imaging resolution, the permanent magnets or superconducting magnets to produce the static field gradient should be much heavier compared to the presently developed small prototypes [48]. Therefore, to limit the load on clinical infrastructure and costs, functional applicability with relatively inexpensive magnets outside a magnetically shielded room has still to be shown.

The advantages of MPI are that it is a relatively fast and MNP specific method, suitable for vascular imaging (figure 2.1). Especially for patients with chronic kidney disease, MPI can provide a safe alternative for iodine contrast computed tomography angiography with a similar imaging resolution [33, 48]. Furthermore, the MNP specificity of MPI exceeds that of MRI, where the negative contrast effect is sometimes confused with air filled space and various artifacts [49–51]. Unambiguous MNP specific MRI could be realized by laborious and expensive use of two MRI systems with different field strength (see figure 2.2) [52]. Compared to the speed of MR-angiography which is physically limited, the MPI method can be significantly faster and with the ultimate perspective of real time imaging. If MPI sensitivity can be further improved, a sensitivity similar to positron emission tomography is expected because of the tracer specific detection [33].

2.3.3 Local magnetic nanoparticle detection

One of the developing applications is local MNP detection during clinical interventions. The most prominent case in this category is magnetic sentinel lymph node

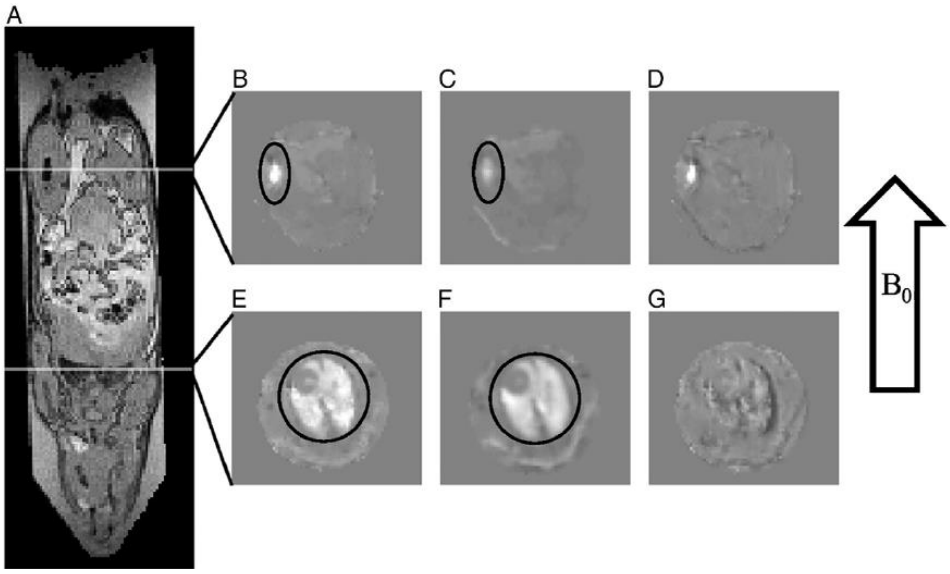

Figure 2.2: *(A) MRI gradient echo image of a mouse at 3 T. Both lung (lower cross-section) and the SPIO injection region appear to be signal void regions. (B and C) susceptibility reconstructions using quantitative susceptibility mapping at the cross section that contains the SPIO injection region from 1.5 and 3 T, respectively. (D) Difference between B and C. (E and F) Susceptibility reconstructions at the cross section that contains lung. (G) Difference between E and F. (Reprinted with Elsevier's permission from [52].)*

detection with surgical probes [53, 54]. Especially in diagnostics and (surgical) interventions, local MNP detection has a great potential as is demonstrated by the first studies on magnetic sentinel lymph node biopsy. However, despite the for magnetic detection very suitable superparamagnetic MNP properties, the development of clinically suitable probes for interventions is still in an early phase.

Magnetic sentinel lymph node detection

Sentinel lymph node biopsy (SLNB) is a standard procedure in the surgical treatment of several types of cancer [55, 56]. The sentinel lymph node is the lymph node that receives first drainage from the tumor area and thus most likely may contain metastatic cells. It is therefore an important site with diagnostic and prognostic value to determine the progress of disease and the best therapeutic strategy. During the

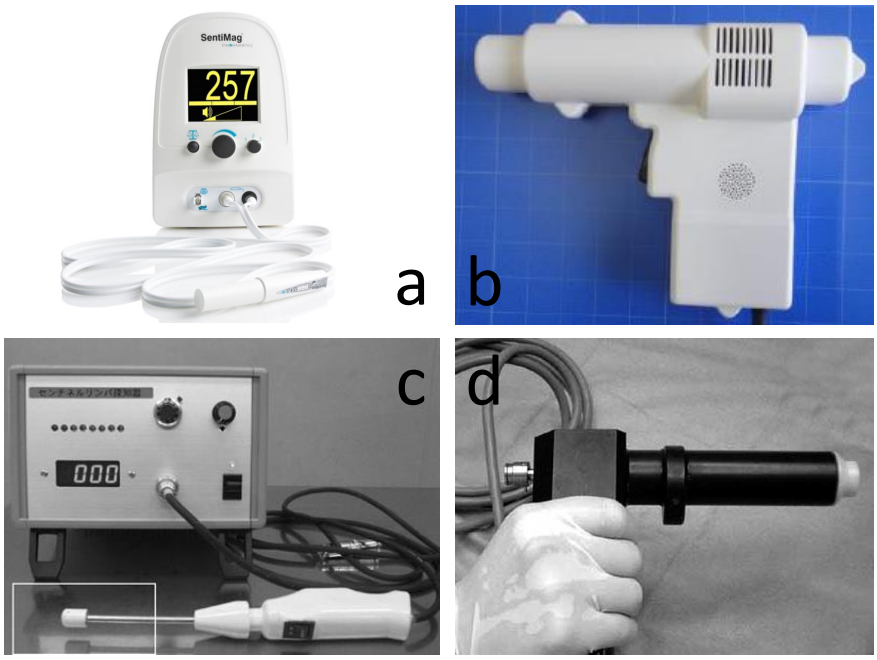

Figure 2.3: *Different magnetic probes developed for intraoperative sentinel lymph node localization. a. The SentiMag developed by Endomagnetics in the UK and used in breast cancer studies [53, 57]. (Reproduced with permission from [58].) b. A Japanese probe based on hall sensors. No clinical studies using this probe are known yet [8, 59] (Reproduced with permission from [8].). c. The probe used in a Japanese breast cancer study [60]. d. The probe used in the lung cancer studies in Japan. (Reprinted with permission from [61].)*

SLNB procedure, a tracer, most often a radioisotope and/or a blue dye, is injected in or near the tumor area. The distribution of tracer through the tissue and lymphatics, mimics the flow of metastatic cells from the tumor area with final accumulation in the sentinel lymph node. The sentinel lymph node is identified by a detector sensitive for the accumulated tracer. After resection of the SLN, the node is histologically analyzed by microscopy to determine the presence of (micro-)metastases.

In the last decade, several studies have been presented about the application of MNPs for sentinel lymph node (SLN) detection. Some examples of different magnetic probes for intraoperative hand held detection are shown in figure 2.3 Especially the disadvantages accompanying the use of radioisotopes in SLNB, concerning radiation exposure, complicated logistics and legislation, have stimulated the search for other tracers and detection methods, leading to the introduction of MNPs in SLNB. In the first studies, magnetic tracer (Endorem or Resovist) was injected around the

tumor for intra-operative sentinel lymph node detection in lung cancer [54, 61–63]. A handheld probe guided the surgeon to localize the lymph node with accumulated MNP tracer. The identification rate of about 80% was similar to other SLNB studies in lung cancer [64]. However, in this context, the limited depth sensitivity of the sensor of 5 mm could be the cause of not identified deeper SLNs.

More recently, several studies have been published about magnetic sentinel lymph node detection in breast cancer. In a study combining CT and MRI with interstitial injection of contrast agent, preoperative detection of macro-metastases was successful, whereas 40% of the micro-metastases were missed as a consequence of a too low MRI resolution [35]. Another Japanese group used MRI and a handheld magnetic probe to localize SLNs filled with MNP tracer (Resovist) [36, 60]. Using the handheld probe, the SLN identification rate was 77% in the first 30 patients. In a larger European multicenter non-inferiority trial, a magnetic handheld probe was used during intra-operative sentinel lymph node biopsy. All 160 patients received the standard SLNB procedure and the magnetic procedure. Both procedures show a similar identification rate, indicating the magnetic SLNB procedure to be feasible and non-inferior to the standard technique [53].

Finally, a single study was published about magnetic SLNB in only 3 tongue cancer patients. In all cases successful SLN localization was performed by MRI after submucosal SPIO (Resovist) injection around the tumor. For further development of the procedure, the intra-operative use of a handheld magnetic probe is proposed [65].

The present practice of SLNB in various cancers is diverse and for different types of cancer the SLNB procedures can be optimized in terms of quality as well as efficiency. Especially for SLN detection in cancers where the use of blue dye alone is insufficient and radioisotopes are undesired, the magnetic tracer can be beneficial. Therefore, the magnetic approach of SLNB can be developed along different routes. In all cases, a simple, unambiguous method of magnetic detection that can assists with real time information during SLN localization and resection, is regarded as essential for clinical users. To realize this, the availability of sensitive handheld probes with high MNP specificity is required.

The probes used in the clinical studies mentioned above, have still some limitations and drawbacks regarding intra-operative use, which concern (thermal) stability, sterilisability and, more importantly, sensitivity and MNP specificity in combination with detection depth. Compared to MRI and MPI, which require high fields and large systems, the principle of alternating field magnetometry is very suitable for clinical interventions, since it can operate at relatively low field amplitudes using simple technology. However, the intrinsic linear magnetic properties of the body have to be taken into account in MNP detection. Methods based on constant alternating field detection with a single frequency (also: conventional alternating field magnetometry), for example as is used in the SentiMag probe [53], also detect the linear magnetic tissue.

For a very low response from deeply located or a small amount of MNPs, the tissue response can predominate the particle response. Simply increasing excitation field strength to increase depth sensitivity will not solve the problem, since the signal-to-noise-ratio will decrease by an increased contribution of a larger tissue area and field limits, heat dissipation and sensor stability may affect the clinical usability of the probe. In the next section the intrinsic limitations of conventional alternating field magnetometry for clinical MNP detection are quantitatively demonstrated.

2.4 Is conventional alternating field magnetometry feasible for local clinical MNP detection?

Alternating field magnetometry has been widely applied for magnetic analysis and measurements of MNPs. A few clinical applications for MNP detection are based on the use of a detection coil and a single frequency excitation field with constant amplitude [53]. Detection of MNPs is successful when its signal provides a good contrast with the surrounding medium, e.g. the tissue. The magnetic susceptibilities of the sample materials are the basis of contrast, where materials with a large susceptibility give a much larger signal compared to the medium or surrounding materials with a low magnetic susceptibility. However, the weight of contributions of materials with different (dimensionless) susceptibilities is based on the volume or mass ratio. In other words, for a certain mass of MNPs, the measured signal equals the signal contribution of the tissue or medium mass. This ratio determines the detectability of MNPs in a typical application.

Especially for applications with a relatively large contribution from tissue volumes and very low amounts of MNPs or MNPs at distant locations, the detection limits for MNPs are crucial. For SLNB in breast cancer, adequate depth sensitivity of an MNP probe is crucial , because axillary sentinel lymph nodes can be found 1.5-8 centimeters deep in the body [66]. In the following sections, alternating field susceptometry of MNPs in an aqueous medium (e.g. tissue) is quantitatively evaluated. To achieve a result that can be compared in fairness with other optimized magnetic detection techniques, the analysis is based on general and the most optimistic assumptions. The evaluation is based on two different sensor types, both consisting of an excitation coil and a single detection coil. In the first approach the MNP detection limit is calculated for a sample enclosing coil. The second model evaluates MNP detection in a large tissue volume with a surface coil.

The evaluation is based on some general assumptions that are applied to both sensor models. The alternating excitation field H is assumed to be homogeneous over the whole sample, with an amplitude of 10 mT μ_0^{-1} and an excitation frequency of $f = 1$ kHz. The geometry of the excitation coil is therefore not included. The amplitude of the excitation field is assumed to be low; for larger amplitudes the nonlinear

magnetic properties of MNPs become of importance and the situation turns to the disadvantage of the detectability of MNPs. In the detected signal, the contribution from the excitation field is assumed to be effectively eliminated, e.g. by electronic compensation.

For tissue the volume susceptibility of water $\chi_{tis} = -9.05 \cdot 10^{-6}$ is assumed, with 20% variation taking into account tissue differences ($-11 \cdot 10^{-6} < \chi_{tis} < -7 \cdot 10^{-6}$) [67]. For iron oxide MNPs the (optimistic) value of $\chi_{MNP} = 50$ is assumed. The respective mass densities are $\rho_{tis} = 1000$ kg m^{-3} and $\rho_{MNP} = 5180$ kg m^{-3}.

The detected voltage U [V] in the coil is the sum of the contributions from tissue and MNPs,

$$U = U_{tis} + U_{MNP}. \tag{2.1}$$

In practice, the tissue component can be eliminated by subtracting the signal U_{tis} of a tissue sample or region not containing MNPs (U_{MNP}=0). After this compensation procedure, the resulting response of tissues with MNPs can be fully attributed to the MNPs. However, because of the susceptibility variations of tissues in the human body, some uncertainty is introduced in the compensation, which affects the detectability of MNPs. This uncertainty can be expressed as a variability in the effective tissue susceptibility in the range of $\chi_{tis,var} = -4.0 \cdot 10^{-6}$. Because adequate reduction of this uncertainty during clinical procedures is difficult to verify, we use this full range of variability for the definition of the detection limit. For both sensor models it is therefore assumed that MNPs can be detected when the amplitude of the MNP contribution exceeds the potential signal variability of tissue: $U_{MNP} > -U_{tis,var}$.

2.4.1 Sample volume enclosing coil: detection limit determined by mass balance

The first sensor model considers a setup typically for magnetic analysis of small (*ex vivo*) samples, with a coil that encloses the entire sample volume, containing the tissue and MNPs (figure 2.4). Assuming a detection coil with a homogeneous sensitivity profile in the coil, the whole sample space is assumed to be detected with a spatially constant coil sensitivity S [TA^{-1}], i.e. every sample volume element is detected with equal sensitivity. The space outside the coil is neglected in the signal contribution.

The signal U received by the detection coil can be written as,

$$U = -2\pi f \cdot m \cdot S, \tag{2.2}$$

with m [Am^2] the magnetic moment of the entire sample. For the magnetic moment we write

$$m = M \cdot V = \chi \cdot H \cdot V, \tag{2.3}$$

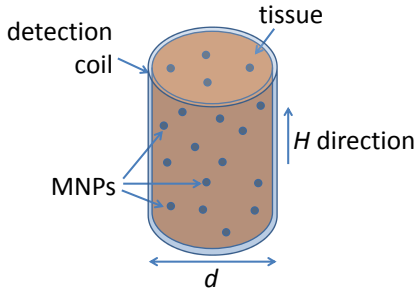

Figure 2.4: *Model of the sample enclosing sensor with diameter d and a tissue volume which contains distributed MNPs. The tissue volume is assumed as an homogeneous medium filling the coil volume. The excitation field is homogeneous and parallel to the axis of the coil.*

with M [Am^{-1}] the magnetization, V [m^3] the volume of sample material and H [Am^{-1}] the applied field. The detected voltage U is proportional to the total magnetic moment m of the sample. The individual susceptibilities of diamagnetic and superparamagnetic materials determine their respective partial contributions to the signal. According to the definition of MNP detectability, the MNPs are defined to be detectable if the magnetic moment of the MNPs m_{MNP} equals the opposite magnetic moment variability of the tissue $m_{tis,var}$,

$$m_{MNP} = -m_{tis,var} \longrightarrow \chi_{MNP} \cdot H \cdot V_{MNP} = -\chi_{tis,var} \cdot H \cdot V_{tis}. \tag{2.4}$$

Since the excitation field is assumed to be homogeneous, both the tissue and the MNPs experience the same field. Thus, the susceptibilities of MNPs and tissue provide us the ratio of MNP and tissue volumes that produce the same magnetic moment:

$$\frac{V_{MNP}}{V_{tis}} = \frac{-\chi_{tis,var}}{\chi_{MNP}} = \frac{4.0 \cdot 10^{-6}}{50} = 8.0 \cdot 10^{-8}. \tag{2.5}$$

Using the mass densities of tissue ρ_{tis} and iron oxide ρ_{MNP}, the mass ratio $\mathfrak{m}_{tis} : \mathfrak{m}_{MNP}$ of equally detected MNPs and tissue variations can be calculated:

$$\frac{\mathfrak{m}_{MNP}}{\mathfrak{m}_{tis}} = \frac{V_{MNP}}{V_{tis}} \frac{\rho_{MNP}}{\rho_{tis}} = 8.0 \cdot 10^{-8} \cdot \frac{5180}{1000} = 4.1 \cdot 10^{-7}. \tag{2.6}$$

To summarize, under the most optimal conditions for alternating field magnetometry using a sample enclosing coil with a spatially homogeneous sensitivity, a homogeneous excitation field and compensated tissue contribution, the MNP mass that can be detected is 2.4 million times smaller than the contributing tissue mass.

For comparison this value can be translated to the clinically realistic case of localization of a MNP containing lymph node in a tissue hemisphere with a radius of 5 cm. The lymph node can be detected if it contains at least 107 μg Fe_3O_4, equivalent to 77 μg iron. However, for clinical *in vivo* detection these calculations provide too optimistic values for the MNP detection limit, since the sample enclosing coil is not a realistic detector in that case. Therefore, in the following section the calculations are continued for a single sided surface coil placed on a tissue volume.

2.4.2 Single sided detection of MNPs in a homogeneous tissue volume

For *in vivo* applications with a clinical handheld MNP sensor, the sample volume is positioned at one side of the detection coil. Such a sensor is typically used in the search for clinically relevant MNP spots in tissue. A relatively large diamagnetic tissue volume is present, which contributes to the signal in the magnetometer. In this context, it is important whether the presence of a small volume of MNPs at a certain location can be determined. To obtain a quantitative indication for MNP detection with a single sided magnetometer, a model is defined with a single detection coil and an infinite, large tissue volume containing a small spot with MNPs (see figure 2.5).

In addition to the general assumptions mentioned above, some additional conditions are formulated. The detection coil has n=100 windings and zero length and is placed at position $x = 0$ on the tissue surface. The spot with MNPs is positioned on the coil axis at different positions x.

According to equation 2.1, the signal U received by the detection coil contains the individual contributions of the different materials in the sample. The signal contribution U_{tis} is calculated using Faraday's law of induction,

$$U_{tis} = -\frac{n}{2}\frac{d\Phi_{tis}}{dt} = -\frac{n}{2}\frac{dB_{tis}}{dt}A, \tag{2.7}$$

with Φ_{tis} the magnetic flux through the coil due to the magnetization of tissue and $A = \pi R^2$ the coil surface. The factor $1/2$ is added to account for the half-sided tissue volume. In this model, the tissue is assumed to be an infinite homogeneous medium at one side of the coil. The magnetization of the tissue M_{tis} produces the magnetic field B_{tis} that is detected by the sensing coil:

$$B_{tis} = \mu_0 M_{tis} = \mu_0 \cdot \chi_{tis} \cdot H. \tag{2.8}$$

The spatially dependent contribution of MNPs containing 1 μg iron is calculated using the equations 2.2 and 2.3, assuming a homogenous sensitivity $S(x)$ over the very small MNP volume at position x on the axis of the detection coil. The coil sensitivity $S(x)$ is calculated using the Biot-Savart law, defined for the magnetic field strength on the axis of a single loop, divided by the applied current and multiplied by

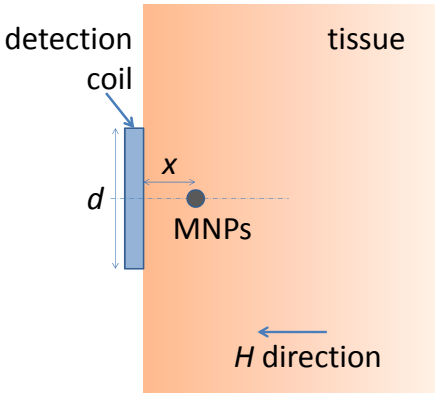

Figure 2.5: *Model of the single sided sensor with diameter d and a tissue volume which contains a spot with MNPs. The tissue volume is assumed as an homogeneous infinite medium at the right side of the probe. The excitation field is homogeneous and parallel to the axis of the coil. The MNP spot is positioned on the axis of the coil at a distance x between 0 and d from the coil.*

the number of turns:

$$S(x) = \frac{B(x)}{I} = \frac{n\mu_0 R^2}{2(R^2+x^2)^{3/2}}, \tag{2.9}$$

with B the magnetic field at position x on the axis of a coil with diameter $d = 2R$ and I [A] the current through the coil. The location dependent coil sensitivity thus represents the field strength produced per unit current through the detection coil.

Assuming a homogeneous excitation field of H=10 mTμ_0^{-1}, the signal U_{MNP} of a small volume of MNPs containing 1 μg iron at positions x between 0 and 25 mm on the coil axis and the uncertainty of the compensation signal for the tissue volume $U_{tis,var}$ are calculated. The results for four different coil diameters are shown in figure 2.6. For a coil with a diameter of 10 mm, 1 μg iron in MNPs can be detected up to a depth of 9 mm in tissue (see figure 2.6).

Similar to the calculations for a sample enclosing coil, the MNP detection limit increases with coil diameter, because the tissue contribution increases and the amplitude of the maximum MNP signal decreases. From figure 2.6 it is clear that the MNP signal of 1 μg iron does not exceed the detection limit for coil diameters larger than approximately 2.0 cm, even if the MNPs are positioned close to the coil.

Using the definition of the detection limit, for a sensor with radius R the de-

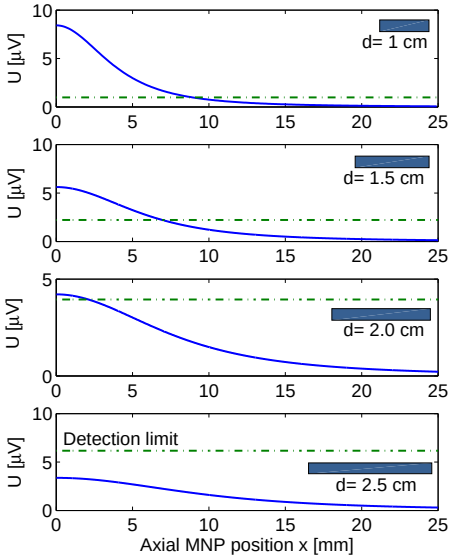

Figure 2.6: *The detected signals for different coil diameters calculated for a 1 µg iron sample. The calculated signals from tissue U_{tis} and MNPs U_{MNP} are detected by a coil with 100 windings and a homogeneous excitation field of 10 mT alternating at f=1 kHz. Larger tissue volumes are detected with larger coil diameters, which reduces distant detection of MNPs.*

tectable iron mass at position x is given by

$$\mathfrak{m}_{MNP} = \pi(R^2 + x^2)^{3/2} \cdot \frac{-\chi_{tis,var}}{\chi_{MNP}} \cdot \rho_{MNP}. \tag{2.10}$$

The detection limits for coil diameters between 0.1 and 5 cm and five different axial MNP positions are shown in figure 2.7. For example, using a large coil with a diameter of 5 cm, a minimum of about 15 µg iron ($72\% \cdot \mathfrak{m}_{MNP}$) can be detected at the coil-tissue interface. At a distance of 5 cm, the MNP spot is only detectable if it contains more than 117 µg iron, even for the smallest coil.

In conclusion, for the single sided detection coil only for small coils (d <2.0 cm) and short MNP distances (x <1.0 cm) the detectable iron mass is below 1 µg. Thus for cases with superficial MNP locations, it is worth to consider small diameter coils. For deeply located MNP spots the variability of tissue dominates the response, while for a larger coil diameter the increased tissue contribution prevails the MNP signal even for close positions.

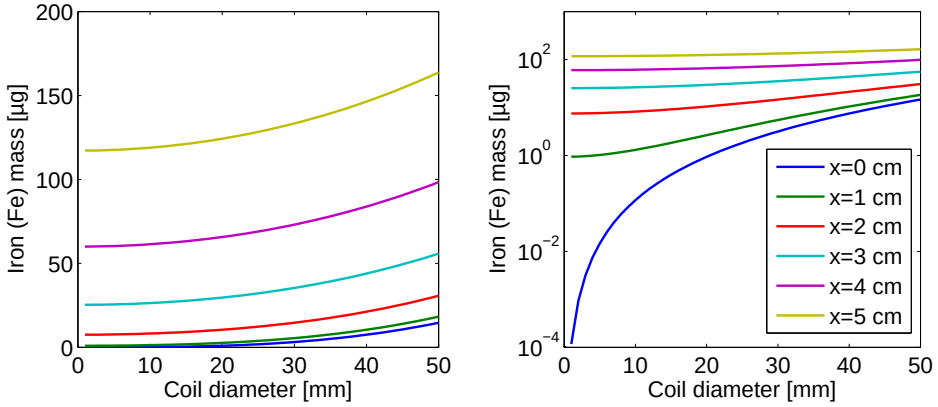

Figure 2.7: *The iron mass detection limit for iron oxide MNPs in tissue vs. detection coil diameter, calculated for five axial distances to the coil. The mass detection limit increases rapidly with MNP distance and with coil diameter. For clarity, the mass values are plotted on linear (a) and logarithmic (b) scale.*

2.4.3 Conventional alternating field magnetometry not suitable for high sensitive *in vivo* MNP detection

The quantitative analysis of MNP detection using conventional alternating field magnetometry in the previous sections has shown the limitations for clinical application. The variability of the diamagnetic susceptibility of tissue prohibits the detection of small MNP amounts deeply located in larger tissue volumes in patients. The analysis was performed with specific assumptions simplifying the calculations, but also providing the most optimal conditions for sensitive MNP detection with a local probe.

The assumption of a homogeneous detection field is to the advantage of the MNP detection limit, since the MNP signal becomes less dependent on location. Especially for the single sided detector, a single sided excitation coil would reduce the detection depth, since the spatial decay of the excitation field results in a reduced MNP magnetization and thus a lower MNP signal contribution.

The results presented above, cannot be improved by choosing another amplitude or frequency of the excitation field. The results may even get worse, since the diamagnetic magnetization is frequency independent and linearly related to the excitation field, whereas the magnetic response of MNPs is strictly nonlinear and depends on the excitation frequency [11, 68]. The assumption of a frequency independent linear MNP susceptibility in the present model is therefore the most optimistic case for MNP detection with conventional alternating fields.

Neither signal phase nor higher harmonics were included in the present evalua-

tion. These signal features may be used to discriminate nonlinear materials from the linear magnetic tissue. The signal phase is not suitable to improve MNP detection, because all electrically conducting materials, including biological tissue and surgical instruments, will contribute to the out-of-phase component via eddy currents. For higher harmonic detection, the filter requirements will significantly affect the final sensitivity of the sensor, which makes it therefore unattractive for more specific MNP detection. In addition, the alternating field amplitude should be considerably large to produce the higher harmonic response, which is undesirable in specific clinical applications.

The geometric simplification of the single sided detection coil with zero length is the most sensitive design for a surface coil. For realistic, longer detection coils the sensitivity will only decrease. A detection coil with gradiometer configuration can achieve limited improvement for only nearby positions of the MNPs. At larger distances from the probe, the MNP contribution in the pick-up coil is increasingly cancelled by the compensation part of the gradiometer which limits detection depth, while the contribution from tissue remains [69].

The MNP detection limit derived from the tissue susceptibility variation is homogeneously applied to the modeled tissue volume. The detection limit may only decrease if the compensation measurement can be performed with increased accuracy. Then the tissue susceptibility of the reference spot is similar to the tissue susceptibility around the MNP spot. For cases with a larger variability in tissue susceptibility, the detection limit of MNPs increases, while the depth detection limit of the single sided probe reduces.

The MNP susceptibility used for the calculations is based on what is found for a typical MRI contrast agent (Resovist). Although this value is optimistic, there are of course MNP formulations possible with a larger susceptibility. However, for biomedical applications it is unlikely to find materials for MNPs with a significantly larger susceptibility that would eliminate the limitations of conventional alternating field magnetometry.

2.5 Conclusion

Magnetic nanoparticles have shown good applicability in biomedical applications because of the distinct magnetic properties and the availability of biocompatible materials. MRI and future MPI applications of MNP detection are valuable for (preoperative and postoperative) diagnostics. However, the technical requirements of MRI and MPI are not compatible with the upcoming MNP detection during clinical interventions. For those cases, handheld magnetic sensors that can operate during surgery are preferred, since they are minimally interfering with the procedure and can provide location specific real-time information.

The present quantitative analysis clearly shows that conventional alternating field magnetometry for local MNP detection is limited by the significant contribution from tissue susceptibility variations. In clinical applications, both sensor diameter and detection depth are essential for optimal implementation of magnetic detection. For example, in surgical interventions small sensors are preferred for optimal accessibility and operator view. Although a small sensor detects only small tissue contributions, it has a limited detection depth and requires a more careful search by the operator over large volumes. Detection depth can be increased by increasing sensor diameter, but the larger contribution from tissue and accompanying susceptibility variations will increase the minimum amount of MNPs that can be detected. For a wide clinical acceptance of MNP detection in (surgical) interventions a clinical probe is required which has a selective sensitivity for nonlinear MNPs. The probe should be able to detect micrograms iron oxide at a depth of several centimeters, by eliminating the linear magnetic contribution of tissue and exploiting the nonlinear properties of MNPs.

References

[1] C. Corot, P. Robert, J. M. Idée, and M. Port, "Recent advances in iron oxide nanocrystal technology for medical imaging", Advanced Drug Delivery Reviews **58**, 1471–1504 (2006).

[2] S. Laurent, D. Forge, M. Port, A. Roch, C. Robic, L. Vander Elst, and R. N. Muller, "Magnetic iron oxide nanoparticles: Synthesis, stabilization, vectorization, physicochemical characterizations, and biological applications", Chemical Reviews **108**, 2064–2110 (2008).

[3] C. P. Bean and I. S. Jacobs, "Magnetic granulometry and super-paramagnetism", Journal of Applied Physics **27**, 1448–1452 (1956).

[4] A. Figuerola, R. Di Corato, L. Manna, and T. Pellegrino, "From iron oxide nanoparticles towards advanced iron-based inorganic materials designed for biomedical applications", Pharmacological Research **62**, 126–143 (2010).

[5] D. Eberbeck, F. Wiekhorst, U. Steinhoff, and L. Trahms, "Aggregation behaviour of magnetic nanoparticle suspensions investigated by magnetorelaxometry", Journal of Physics Condensed Matter **18** (2006).

[6] A. K. Gupta and M. Gupta, "Synthesis and surface engineering of iron oxide nanoparticles for biomedical applications", Biomaterials **26**, 3995–4021 (2005).

[7] J. W. M. Bulte and D. L. Kraitchman, "Iron oxide MR contrast agents for molecular and cellular imaging", NMR in Biomedicine **17**, 484–499 (2004).

[8] M. Abe, T. Ueda, T. Masaki, Y. Kitamoto, N. Matsushita, and H. Handa, "Detecting ferrite nanobeads for sentinel lymph node mapping with a highly sensitive hall differential magnetic field sensor", Journal of Physics: Conference Series **352**, 012015 (2012).

[9] G. Mihajlovic, P. Xiong, S. von Molnar, M. Field, G. Sullivan, K. Ohtani, and H. Ohno, "Submicrometer hall sensors for superparamagnetic nanoparticle detection", Magnetics, IEEE Transactions on **43**, 2400–2402 (2007).

[10] J. Bulte, R. Brooks, B. Moskowitz, L. Bryant, and J. Frank, "Relaxometry and magnetometry of the MR contrast agent MION-46L", Magnetic Resonance in Medicine **42**, 379–384 (1999).

[11] B. H. Erné, K. Butter, B. W. M. Kuipers, and G. J. Vroege, "Rotational diffusion in iron ferrofluids", Langmuir **19**, 8218–8225 (2003).

[12] B. W. M. Kuipers, I. A. Bakelaar, M. Klokkenburg, and B. H. Erné, "Complex magnetic susceptibility setup for spectroscopy in the extremely low-frequency range", Review of Scientific Instruments **79**, – (2008).

[13] K. Enpuku, H. Watanabe, Y. Higuchi, T. Yoshida, H. Kuma, N. Hamasaki, M. Mitsunaga, H. Kanzaki, and A. Kandori, "Characterization of magnetic markers for liquid-phase immunoassays using brownian relaxation", Japanese Journal of Applied Physics **51** (2012).

[14] F. Ludwig, E. Heim, and M. Schilling, "Characterization of magnetic core-shell nanoparticles by fluxgate magnetorelaxometry, ac susceptibility, transmission electron microscopy and photon correlation spectroscopy - A comparative study", Journal of Magnetism and Magnetic Materials **321**, 1644–1647 (2009).

[15] H. J. Krause, N. Wolters, Y. Zhang, A. Offenhusser, P. Miethe, M. H. F. Meyer, M. Hartmann, and M. Keusgen, "Magnetic particle detection by frequency mixing for immunoassay applications", Journal of Magnetism and Magnetic Materials **311**, 436–444 (2007).

[16] L. Tu, T. Klein, W. Wang, Y. Feng, Y. Wang, and J.-P. Wang, "Measurement of Brownian and Néel relaxation of magnetic nanoparticles by a mixing-frequency method", Magnetics, IEEE Transactions on **49**, 227–230 (2013).

[17] H. Arami, R. M. Ferguson, A. P. Khandhar, and K. M. Krishnan, "Size-dependent ferrohydrodynamic relaxometry of magnetic particle imaging tracers in different environments", Medical Physics **40**, 071904–14 (2013).

[18] S. Biederer, T. Knopp, T. F. Sattel, K. Ldtke-Buzug, B. Gleich, J. Weizenecker, J. Borgert, and T. M. Buzug, "Magnetization response spectroscopy of superparamagnetic nanoparticles for magnetic particle imaging", Journal of Physics D: Applied Physics **42** (2009).

[19] D. Eberbeck, M. Kettering, C. Bergemann, P. Zirpel, I. Hilger, and L. Trahms, "Quantification of the aggregation of magnetic nanoparticles with different polymeric coatings in cell culture medium", Journal of Physics D: Applied Physics **43**, 405002 (2010).

[20] N. L. Adolphi, D. L. Huber, H. C. Bryant, T. C. Monson, D. L. Fegan, J. Lim, J. E. Trujillo, T. E. Tessier, D. M. Lovato, K. S. Butler, P. P. Provencio, H. J. Hathaway, S. A. Majetich, R. S. Larson, and E. R. Flynn, "Characterization of single-core magnetite nanoparticles for magnetic imaging by SQUID relaxometry", Physics in Medicine and Biology **55**, 5985 (2010).

[21] F. Wiekhorst, C. Seliger, R. Jurgons, U. Steinhoff, D. Eberbeck, L. Trahms, and C. Alexiou, "Quantification of magnetic nanoparticles by magnetorelaxometry and comparison to histology after magnetic drug targeting", Journal of Nanoscience and Nanotechnology **6**, 3222–3225 (2006).

[22] H. Hathaway, K. Butler, N. Adolphi, D. Lovato, R. Belfon, D. Fegan, T. Monson, J. Trujillo, T. Tessier, H. Bryant, D. Huber, R. Larson, and E. Flynn, "Detection of breast cancer cells using targeted magnetic nanoparticles and ultra-sensitive magnetic field sensors", Breast Cancer Research **13**, R108 (2011).

[23] H. Richter, F. Wiekhorst, K. Schwarz, S. Lyer, R. Tietze, A. Ch, and L. Trahms, "Magnetorelaxometric quantification of magnetic nanoparticles in an artery model after ex vivo magnetic drug targeting", Physics in Medicine and Biology **54**, N417 (2009).

[24] C. Knopke, F. Wiekhorst, D. Eberbeck, I. Gemeinhardt, M. Ebert, J. Schnorr, S. Wagner, M. Taupitz, and L. Trahms, "Quantification of magnetic nanoparticle uptake in cells by temperature dependent magnetorelaxometry", IEEE Transactions on Magnetics **49**, 421–424 (2013).

[25] D. X. Chen, A. Sanchez, E. Taboada, A. Roig, N. Sun, and H. C. Gu, "Size determination of superparamagnetic nanoparticles from magnetization curve", Journal of Applied Physics **105** (2009).

[26] D. J. Grootendorst, R. M. Fratila, M. Visscher, B. T. Haken, R. J. A. van Wezel, S. Rottenberg, W. Steenbergen, S. Manohar, and T. J. M. Ruers, "Intra-operative ex vivo photoacoustic nodal staging in a rat model using a clinical superparamagnetic iron oxide nanoparticle dispersion", Journal of Biophotonics **6**, 493–504 (2013).

[27] D. J. Grootendorst, J. Jose, R. M. Fratila, M. Visscher, A. H. Velders, B. Ten Haken, T. G. Van Leeuwen, W. Steenbergen, S. Manohar, and T. J. M. Ruers, "Evaluation of superparamagnetic iron oxide nanoparticles (Endorem) as a photoacoustic contrast agent for intra-operative nodal staging", Contrast Media & Molecular Imaging **8**, 83–91 (2013).

[28] E. I. Galanzha, M. S. Kokoska, E. V. Shashkov, J.-W. Kim, V. V. Tuchin, and V. P. Zharov, "In vivo fiber-based multicolor photoacoustic detection and photothermal purging of metastasis in sentinel lymph nodes targeted by nanoparticles", Journal of Biophotonics **2**, 528–539 (2009).

[29] D. Eberbeck, F. Wiekhorst, S. Wagner, and L. Trahms, "How the size distribution of magnetic nanoparticles determines their magnetic particle imaging performance", Applied Physics Letters **98**, 182502–3 (2011).

[30] D. X. Chen, N. Sun, and H. C. Gu, "Size analysis of carboxydextran coated superparamagnetic iron oxide particles used as contrast agents of magnetic resonance imaging", Journal of Applied Physics **106**, 063906–9 (2009).

[31] Q. A. Pankhurst, J. Connolly, S. K. Jones, and J. Dobson, "Applications of magnetic nanoparticles in biomedicine", Journal of Physics D: Applied Physics **36** (2003).

[32] Q. A. Pankhurst, N. K. T. Thanh, S. K. Jones, and J. Dobson, "Progress in applications of magnetic nanoparticles in biomedicine", Journal of Physics D: Applied Physics **42** (2009).

[33] K. M. Krishnan, "Biomedical nanomagnetics: A *Spin* through possibilities in imaging, diagnostics, and therapy", IEEE Transactions on Magnetics **46**, 2523–2558 (2010).

[34] R. Weissleder and P. Reimer, "Superparamegnetic iron oxides for MRI", European Radiology **3**, 198–212 (1993).

[35] K. Motomura, M. Ishitobi, Y. Komoike, H. Koyama, A. Noguchi, H. Sumino, Y. Kumatani, H. Inaji, T. Horinouchi, and K. Nakanishi, "SPIO-enhanced magnetic resonance imaging for the detection of metastases in sentinel nodes localized by computed tomography lymphography in patients with breast cancer", Annals of Surgical Oncology **18**, 3422–3429 (2011).

[36] M. Shiozawa, S. Kobayashi, Y. Sato, H. Maeshima, Y. Hozumi, A. T. Lefor, K. Kurihara, N. Sata, and Y. Yasuda, "Magnetic resonance lymphography of sentinel lymph nodes in patients with breast cancer using superparamagnetic iron oxide: a feasibility study", Breast Cancer 1–8 (2012).

[37] D. D. Stark, R. Weissleder, G. Elizondo, P. F. Hahn, S. Saini, L. E. Todd, J. Wittenberg, and J. T. Ferrucci, "Superparamagnetic iron oxide: clinical application as a contrast agent for MR imaging of the liver.", Radiology **168**, 297–301 (1988), pMID: 3393649.

[38] R. Weissleder, G. Elizondo, L. Josephson, C. C. Compton, C. J. Fretz, D. D. Stark, and J. T. Ferrucci, "Experimental lymph node metastases: enhanced detection with MR lymphography", Radiology **171**, 835–839 (1989), pMID: 2717761.

[39] P. Reimer and T. Balzer, "Ferucarbotran (Resovist): A new clinically approved RES-specific contrast agent for contrast-enhanced MRI of the liver: Properties, clinical development, and applications", European Radiology **13**, 1266–1276 (2003).

[40] J. O. Barentsz, J. J. Fütterer, and S. Takahashi, "Use of ultrasmall superparamagnetic iron oxide in lymph node MR imaging in prostate cancer patients", European Journal of Radiology **63**, 369–372 (2007).

[41] M. A. Saksena, A. Saokar, and M. G. Harisinghani, "Lymphotropic nanoparticle enhanced MR imaging (LNMRI) technique for lymph node imaging", European Journal of Radiology **58**, 367–374 (2006).

[42] M. G. Harisinghani, M. A. Saksena, P. F. Hahn, B. King, J. Kim, and R. Torabi, Maha T. Weissleder, "Ferumoxtran-10-enhanced MR lymphangiography: Does contrast-enhanced imaging alone suffice for accurate lymph node characterization?", American Journal of Roentgenology **186**, 144–148 (2006).

[43] I. Raynal, P. Prigent, S. Peyramaure, A. Najid, C. Rebuzzi, and C. Corot, "Macrophage endocytosis of superparamagnetic iron oxide nanoparticles: Mechanisms and comparison of ferumoxides and ferumoxtran-10", Investigative Radiology **39**, 56–63 (2004).

[44] F. D. Birkhuser, U. E. Studer, J. M. Froehlich, M. Triantafyllou, L. J. Bains, G. Petralia, P. Vermathen, A. Fleischmann, and H. C. Thoeny, "Combined ultrasmall superparamagnetic particles of iron oxideenhanced and diffusion-weighted magnetic resonance imaging facilitates detection of metastases in normal-sized pelvic lymph nodes of patients with bladder and prostate cancer", European Urology **64**, 953 – 960 (2013).

[45] J. S. Weinstein, C. G. Varallyay, E. Dosa, S. Gahramanov, B. Hamilton, W. D. Rooney, L. L. Muldoon, and E. A. Neuwelt, "Superparamagnetic iron oxide nanoparticles: Diagnostic magnetic resonance imaging and potential therapeutic applications in neurooncology and central nervous system inflammatory pathologies, a review", Journal of Cerebral Blood Flow and Metabolism **30**, 15–35 (2010).

[46] B. Gleich and J. Weizenecker, "Tomographic imaging using the nonlinear response of magnetic particles", Nature **435**, 1214–1217 (2005).

[47] J. Weizenecker, B. Gleich, J. Rahmer, H. Dahnke, and J. Borgert, "Three-dimensional real-time in vivo magnetic particle imaging", Physics in Medicine and Biology **54**, L1 (2009).

[48] P. W. Goodwill, E. U. Saritas, L. R. Croft, T. N. Kim, K. M. Krishnan, D. V. Schaffer, and S. M. Conolly, "X-Space MPI: Magnetic nanoparticles for safe medical imaging", Advanced Materials **24**, 3870–3877 (2012).

[49] J. Langley, W. Liu, E. K. Jordan, J. A. Frank, and Q. Zhao, "Quantification of SPIO nanoparticles in vivo using the finite perturber method", Magnetic Resonance in Medicine **65**, 1461–1469 (2011).

[50] W. Liu and J. A. Frank, "Detection and quantification of magnetically labeled cells by cellular MRI", European Journal of Radiology **70**, 258–264 (2009).

[51] Q. Zhao, J. Langley, S. Lee, and W. Liu, "Positive contrast technique for the detection and quantification of superparamagnetic iron oxide nanoparticles in MRI", NMR in Biomedicine **24**, 464–472 (2011).

[52] T. Liu, P. Spincemaille, L. de Rochefort, R. Wong, M. Prince, and Y. Wang, "Unambiguous identification of superparamagnetic iron oxide particles through quantitative susceptibility mapping of the nonlinear response to magnetic fields", Magnetic Resonance Imaging **28**, 1383 – 1389 (2010).

[53] M. Douek, J. Klaase, I. Monypenny, A. Kothari, K. Zechmeister, D. Brown, L. Wyld, P. Drew, H. Garmo, O. Agbaje, Q. Pankhurst, B. Anninga, M. Grootendorst, B. Haken, M. Hall-Craggs, A. Purushotham, and S. Pinder, "Sentinel node biopsy using a magnetic tracer versus standard technique: The SentiMAG Multicentre Trial", Annals of Surgical Oncology 1–9 (2013).

[54] T. Nakagawa, Y. Minamiya, Y. Katayose, H. Saito, K. Taguchi, H. Imano, H. Watanabe, K. Enomoto, M. Sageshima, T. Ueda, and J. I. Ogawa, "A novel method for sentinel lymph node mapping using magnetite in patients with non-small cell lung cancer", Journal of Thoracic and Cardiovascular Surgery **126**, 563–567 (2003).

[55] H. Schraffordt Koops, M. H. E. Doting, J. d. Vries, A. T. M. G. Tiebosch, J. T. Plukker, H. J. Hoekstra, and D. A. Piers, "Sentinel node biopsy as a surgical staging method for solid cancers", Radiotherapy and Oncology **51**, 1–7 (1999).

[56] M. R. S. Keshtgar and P. J. Ell, "Sentinel lymph node detection and imaging", European Journal of Nuclear Medicine **26**, 57–67 (1999).

[57] M. Thill, A. Kurylcio, R. Welter, V. van Haasteren, B. Grosse, G. Berclaz, W. Polkowski, and N. Hauser, "The Central-European SentiMag study: Sentinel lymph node biopsy with superparamagnetic iron oxide (SPIO) vs. radioisotope", The Breast **23**, 175 – 179 (2014).

[58] "Endomagnetics Ltd., Web Site ©", `http://www.endomagnetics.com/?page_id=1534`, Accessed: 2014-06-14.

[59] Y. Kitamoto, T. Masaki, S. Trisnanto, T. Ueda, and M. Abe, "Magnetic sensor for sentinel lymph node biopsy using superparamagnetic beads", in *2012 IEEE Sensors*, 1–4 (2012).

[60] M. Shiozawa, A. T. Lefor, Y. Hozumi, K. Kurihara, N. Sata, Y. Yasuda, and M. Kusakabe, "Sentinel lymph node biopsy in patients with breast cancer using superparamagnetic iron oxide and a magnetometer", Breast Cancer **20**, 223–229 (2013).

[61] Y. Minamiya, M. Ito, Y. Katayose, H. Saito, K. Imai, Y. Sato, and J. I. Ogawa, "Intraoperative sentinel lymph node mapping using a new sterilizable magnetometer in patients with nonsmall cell lung cancer", Annals of Thoracic Surgery **81**, 327–330 (2006).

[62] Y. Minamiya, M. Ito, Y. Hosono, H. Kawai, H. Saito, Y. Katayose, S. Motoyama, and J.-i. Ogawa, "Subpleural injection of tracer improves detection of mediastinal sentinel lymph nodes in non-small cell lung cancer", European Journal of Cardio-Thoracic Surgery **32**, 770–775 (2007).

[63] T. Ono, Y. Minamiya, M. Ito, H. Saito, S. Motoyama, H. Nanjo, and J. Ogawa, "Sentinel node mapping and micrometastasis in patients with clinical stage IA non-small cell lung cancer", Interactive CardioVascular and Thoracic Surgery **9**, 659–661 (2009).

[64] A. T. Kermani, R. Bagheri, S. Tehranian, P. Shojaee, R. Sadeghi, and D. N. Krag, "Accuracy of sentinel node biopsy in the staging of non-small cell lung carcinomas: Systematic review and meta-analysis of the literature", Lung Cancer **80**, 5 – 14 (2013).

[65] D. Mizokami, S. Kosuda, M. Tomifuji, K. Araki, T. Yamashita, H. Shinmoto, and A. Shiotani, "Superparamagnetic iron oxide-enhanced interstitial magnetic resonance lymphography to detect a sentinel lymph node in tongue cancer patients", Acta Oto-Laryngologica **133**, 418–423 (2013).

[66] C. Mathelin, S. Salvador, D. Huss, and J.-L. Guyonnet, "Precise localization of sentinel lymph nodes and estimation of their depth using a prototype intraoperative mini γ-camera in patients with breast cancer", Journal of Nuclear Medicine **48**, 623–629 (2007).

[67] J. F. Schenck, "The role of magnetic susceptibility in magnetic resonance imaging: Mri magnetic compatibility of the first and second kinds", Medical Physics **23**, 815–850 (1996).

[68] T. Yoshida, K. Ogawa, K. Enpuku, N. Usuki, and H. Kanzaki, "AC susceptibility of magnetic fluid in nonlinear brownian relaxation region: Experiment and comparison with numerical simulation", Japanese Journal of Applied Physics **49**, 053001 (2010).

[69] S. Uzunbajakau, "Development of a highly balanced gradiometer for fetal magnetocardiography", Ph.D. thesis, University of Twente, Enschede, The Netherlands (2008).

3

Quantitative analysis of superparamagnetic contrast agent in sentinel lymph nodes using ex vivo vibrating sample magnetometry*

Abstract: As the first step in developing a new clinical technique for the magnetic detection of colorectal sentinel lymph nodes (SLNs), a method is developed to measure the magnetic content in intact, formalin fixated lymph nodes using a Vibrating Sample Magnetometer (VSM). A suspension of superparamagnetic nanoparticles is injected ex vivo around the tumor in the resected colon segments. A selection of 3 lymph nodes is excised from the region around the tumor and is separately measured in the VSM. The iron content in lymph nodes is quantified from the magnetic moment curve using the Langevin model for superparamagnetism and a bimodal particle size distribution. Adverse, parasitic movements of the sample were successfully reduced by tight fixation of the soft tissue and using a small vibration amplitude. Iron content in the lymph nodes is detected with 0.5 μg accuracy and ranged from 1-51 μg. Histological staining confirmed iron presence. The current method of measuring intact biological tissue in a VSM, is suitable to show the feasibility and merit of magnetic detection of SLNs in colorectal cancer. For clinical validation of magnetic SLN selection in colorectal cancer, a new magnetometer with high specificity for superparamagnetic nanoparticles is required.

*This chapter is published as: M. Visscher , J.J. Pouw , J. van Baarlen , J.M. Klaase , B. Ten Haken, Quantitative analysis of superparamagnetic contrast agent in sentinel lymph nodes using *ex vivo* vibrating sample magnetometry, IEEE Transactions on Biomedical Engineering. 2013 vol.60(9): p2594-602.

3.1 Introduction

Magnetic nanoparticles have become increasingly important in both non-invasive and minimally invasive medical applications [1, 2]. Superparamagnetic nanoparticles have already been used as contrast agents in magnetic resonance imaging (MRI) for a long time [3, 4]. Furthermore, the use of magnetic nanoparticles for drug delivery [5–8] and hyperthermia treatment [9] remains under development. One of the new developments is the use of magnetic nanoparticles for sentinel lymph node (SLN) detection. In Japan and The United Kingdom, magnetic detection of sentinel lymph nodes using a handheld probe was developed for lung [10, 11] and breast cancer [12–14]. Similar experiments using a high-T_C SQUID gradiometer were demonstrated in a rat model [15]. A recent study shows the applicability of magnetic nanoparticles as contrast agent for photoacoustic imaging which can provide intra-operative lymph node staging [16]. The present clinical procedure of SLN detection includes selection of the lymph nodes that drain the tumor area by a technetium marker and blue dye to apply advanced microscopic analysis (ultrastaging) to detect metastasis [17, 18]. The presence of metastasis is important for disease staging and subsequent clinical decisions. SLN biopsy helps the pathologist to select nodes with the highest chance for (micro)metastasis. When no metastasis is found with normal hematoxylin and eosin (H&E) staining, ultrastaging - which is time consuming - can be exclusively restricted to the sentinel lymph nodes.

The introduction of magnetic nanoparticles in sentinel lymph node procedures can improve diagnosis and therapy for various tumors. In case of colorectal cancer, diagnosis can be improved by more specific selection of the SLNs, leading to increased staging accuracy and a more adequate therapeutic path [19]. In breast cancer and melanoma magnetic SLN detection has to compete with the well performing, but logistically more complex, combined method using radioactive tracer and blue dye. Magnetic detection largely simplifies logistics and safety protocols and makes potentially as accurate SLN detection accessible for hospitals that do not have a department for nuclear medicine. In those hospitals significant therapeutic improvements can be achieved by introduction of a reliable SLN procedure.

In surgical procedures of colorectal cancer, a complete colon segment is resected including all lymph nodes surrounding the tumor. Sentinel lymph node mapping (SLNM) for this type of cancer is still in development and is potentially highly beneficial [20–25]. The procedure is introduced to obtain a more precise diagnosis and is technically still developing regarding tracers and surgical approach. The majority of studies use only a blue dye as contrast agent and are performed either *in vivo* or *ex vivo* [19]. A suspension of superparamagnetic iron oxide (SPIO) nanoparticles is an attractive alternative for both blue dye and technetium in colorectal cancer.

The added value of magnetic nanoparticles compared to the generally used technetium and blue dye tracers, is that they are stable and therefore detectable and quan-

tifiable over time. The restricted lifetime of technetium-99m and the fluidity of blue dye limit the time frame of reliable detection of the SLN after surgery. The use of a physically more stable tracer allows *ex vivo* detection several hours after surgery. In such an *ex vivo* procedure, the SLN detection aims to make an accurate selection out of all harvested lymph nodes, rather than a search in a tissue mass for one specific tracer containing lymph node. All lymph nodes are individually selected as SLN based on the presence of magnetic tracer. This post-operative procedure reduces the burden on costly operating time.

Another advantage of a tracer with particles is to reduce the chance to select higher echelon nodes. The particles in a magnetic tracer are more easily trapped in the sentinel lymph node compared to the fluidic blue dye that may spread further to higher echelon nodes [26]. At present, it is still unkown whether these nanoparticles will end up in the SLNs (first echelon) after *ex vivo* injection. Physiological processes in the lymphatic system, like macrophage activity, are expected to stop soon after resection. Moreover, detection of *ex vivo* particle uptake can be limited because the lymph nodes in the mesenterium are rather small in size and *ex vivo* infiltration of particles might be low. The experiments in this first study have to show whether the nanoparticles can still accumulate in the SLNs in *ex vivo* circumstances.

The stability of a magnetic tracer provides the opportunity for a feasibility study to *ex vivo* magnetic sentinel lymph node detection in colorectal cancer in an extramural laboratory. Therefore, a clinically suitable instrument is not needed *a priori*. Detection of SPIO in a SLNM procedure serves to decide whether a particular lymph node is a candicate for additional microscopic analysis. The detection system has to give a decisive answer about the presence of tracer. Therefore a highly sensitive and specific detection system is required. Spatial imaging of tracer is inferior to a more reliable indicator of tracer presence. Therefore, magnetometry methods selectively sensitive for nonlinear magnetic properties of SPIO are prefered over less specific laborious quantitative MRI techniques that are susceptible to assumptions about background signals from tissue, (geometry of) SPIO distribution and detection thresholds [27]. Different spectroscopic methods that have been developed to quantify SPIO content in cell samples, require sample digestion and are therefore not compatible with histopathologic analysis in a SLNM procedure [28]. In the present study, the SLNs were quantitatively analyzed using a standard vibrating sample magnetometer (VSM). Quantification of particle uptake serves to determine technical requirements for development of a clinically suitable magnetometer.

The magnetic analysis of fresh or formalin-fixated biological tissue using a VSM, is a challenging procedure. In several studies, magnetometry of biological tissue was achieved at rather low temperatures ($T < 273$ K) or after freeze-drying the sample to enable a firm fixation [29–34]. Such a procedure is problematic if the sample has to remain intact for clinical histological analysis. Therefore, in the present study a reli-

able, non-destructive VSM-method was developed to measure the magnetic content of SPIO particles in intact diamagnetic biological samples at room temperature. Despite the time-consuming and clinically impractical technique of VSM, the measurements provide important information for the development of a clinical magnetometer to replace the VSM in the methodology presented here.

The objective of this chapter is first to show, with a limited number of experiments, the feasibility of magnetic nanoparticles as tracer for *ex vivo* SLNM in colorectal cancer. The second objective is to determine the quantitative requirements for a clinically suitable magnetometer, that can perform fast *ex vivo* analysis of colorectal lymph nodes. Since the focus in this chapter is on the technical feasibility of magnetic nanoparticles in *ex vivo* colorectal tissue, the patient-specific clinical results and their consequences are topic of the next chapter.

3.2 Experiments

3.2.1 Superparamagnetic particles and clinical application

The Endorem MRI contrast agent (Guerbet Nederland B.V., Gorinchem, The Netherlands) is chosen as superparamagnetic tracer for identification of the SLNs. This tracer is a suspension of superparamagnetic iron oxide nanoparticles coated with dextran in a concentration of 11.2 mg iron per mL. The hydrodynamic particle size is reported in a range of 58-186 nm [35, 36]. Lymph nodes are harvested from resected tissue of patients with colorectal cancer who underwent a standard surgical procedure. Immediately after resection, the colon part containing the tumor is brought to a separate field and is injected submucosally around the tumor with 1.5-2.0 mL of Endorem and massaged for about 5 minutes to induce particle flow into the lymphatic system. Macrophage activity responsible for *in vivo* lymphatic processing of magnetic nanoparticles [37], is expected to stop immediately after resection. Therefore mechanical transport of particles through the interstitial space and the lymphatics should be maintained *ex vivo* to get the SLNs filled with tracer. Since VSM analysis of all lymph nodes in each specimen would be very time consuming and magnetic detection of lymph nodes *in situ* was not possible, a parallel SLN selection procedure with blue dye is used. Patent Blue V (Guerbet Nederland B.V., Gorinchem, The Netherlands) is injected additionally after Endorem, to enable the visual selection of SLNs by the pathologist. For each patient the blue lymph nodes nearest to the tumor, with a maximum of three, are considered as SLNs and are resected for analysis of iron content and placed in formalin for 24-72 hours. The local ethics committee of the hospital Medisch Spectrum Twente in Enschede was informed and agreed with the experimental procedure.

(a)

(b)

Figure 3.1: *(a) Lymph node sample fixated with plastic system in glass tube. (b) VSM detection coil set with bore diameter 10.6 mm.*

3.2.2 Sample placement

All samples are placed in a NMR glass tube (Wilmad-LabGlass, Vineland, New Jersey, USA) with an inner diameter of 8.16 mm and an outer diameter of 10 mm. To prevent uncontrolled movement during VSM-measurements, the samples are fixated between two plastic parts inside the tube (fig. 3.1a). The upper part is adjustable in length to allow for different sample sizes; typically for lymph nodes between 2 and 10 mm. In addition, the soft lymphatic tissue with some surrounding fat can be compactly fixated. To reduce noise from liquid movement, the level of remnant formalin in the tube is as low as possible. Automatic offset detection by the VSM-system itself is often not accurate because of low or absent magnetization in biological tissue. Therefore the axial distance from the bottom of the tube to the center of the sample is measured manually, to determine the optimal VSM-offset position in the detection coil set.

3.2.3 VSM procedure

Measurements are performed using the VSM of a physical property measurement system (PPMS, Quantum Design Inc., San Diego, California, USA) with a maximum magnetic field capacity of $\mu_0 H$ = 9T. The applied field range is lower ($\mu_0 H$ = 4T), to prevent samples from large forces while approaching magnetic saturation for Endorem particles. The vibration frequency was 40 Hz, whereas the vibration amplitude was 0.5 mm. This low amplitude reduces the forces acting on the sample by a factor of 4, compared to the default amplitude of 2 mm. Consequently, noise caused by interfering, parasitic movements due to soft tissue is reduced. The lymph nodes are relatively large compared to most samples normally measured in a VSM. To fit the NMR tube containing the lymph node, a custom-made VSM detection coil was

used with an inner diameter of 10.6 mm (see fig. 3.1b).

To investigate sensitivity of magnetic detection and to calibrate the VSM for Endorem containing lymph nodes, a series of calibration samples was prepared. Small glass containers were filled with 15 μL diluted Endorem ranging from 1:1 to 1:150, which corresponds with 168 to 1.12 μg iron in a sample. In addition, some larger samples containing 500 and 1568 μg iron were used to increase accuracy of the calibration factor. Furthermore, a known Endorem sample is measured while immersed in formalin to investigate the noise contributions from free liquid formalin. Samples with Patent Blue V and formalin are measured to exclude the effect of superparamagnetic or ferromagnetic contributions when present in lymph node samples. To determine the correction for the demagnetization of the superconducting magnet [38], a paramagnetic palladium sample is measured in the same field range as applied to the lymph nodes.

3.2.4 Data analysis

VSM measurements of lymph nodes placed in the NMR tube with plastic fixation parts, are assumed to exhibit a superparamagnetic component originating from the nanoparticles, a diamagnetic component originating from the tissue and a paramagnetic component originating from the sample holder. Magnetic moment versus field curves of the sample were analyzed in MATLAB (The Mathworks Inc., Natick, Massachusetts, USA) by a parameter optimization of a model that includes the three different magnetic components. Before the optimization, some preprocessing of the data was necessary to remove some additional effects from the data, which is explained hereafter.

In the first step, a correction is made to the measured field to compensate for demagnetization of the superconducting magnet in the PPMS [38]. The palladium measurement should theoretically show a strictly anhysteretic linear curve. Any hysteresis observed in this measurement can be attributed to the demagnetization of the magnet during the measurement. This causes an inaccurate field measurement that should be corrected to obtain coinciding ascending and descending branches in measurements of anhysteretic materials. To compensate for demagnetization of the superconducting magnet, a field correction of 1750 Am^{-1} is applied to each dataset. Then the assumption is made that no hysteresis is present in the Endorem sample at ambient temperatures [39] and the Langevin model for superparamagnetism can be applied.

The strength of the linear components in the measurements vary over different samples and are eliminated from the optimization by subtracting the linear approximation of the magnetic moment in the high field region. In most studies this component is determined by a 'background' measurement. There are three reasons why this cannot be done in this experiment: (i) the magnetic contribution from tissue cannot

be determined in a separate measurement before tracer administration and, moreover, it depends on the size of a lymph node and the amount of surrounding fat and thus differs for each lymph node, (ii) the amount of formalin surrounding the sample varies, (iii) the variable size of the calibration samples and lymph nodes needs fine-tuning of the fixation system, as a result of which the paramagnetic contribution of the sample holder in the detection coil differs from sample to sample. Therefore the sample dependent linear component is approximated by a linear fit of the data measured from 90% of the field maxima ($|H|_{max}$). The superparamagnetic component of the magnetic moment of the sample is assumed to be saturated in this region. Although this is not true for contributions of very small superparamagnetic particles, this approach can be used when the model describing the superparamagnetic component is subjected to the same procedure. Therefore, also the model is subjected to a linear subtraction, which is based on the slope of the modeled superparamagnetic component in the same high field range as the measured data. So, to obtain the most likely parameters describing the curvature of the magnetic moment curve, the model and the data are matched in the high field region by linear approximation, while the particle size distribution parameters in the fitting algorithm that describe the unsaturated nonlinear superparamagnetic part, are optimized by minimization of the error between data and fit.

Asymmetry in the positive and negative branches of the measured curve were treated by an offset correction. Finally the magnetic moment curve is normalized in order to exclude the saturation value from the parameters to be optimized. Then a normalized model for the superparamagnetic component can be compared with the normalized data.

The optimization procedure is now only dependent on the *shape* of the superparamagnetic components, which is determined by the particle characteristics in the sample. The superparamagnetic component is modeled by the Langevin model for superparamagnetism [40], described by

$$L(x_k H) = \coth(x_k H) - \frac{1}{x_k H}, \tag{3.1}$$

with

$$x_k H = \frac{m_k \mu_0 H}{k_B T}. \tag{3.2}$$

The constants μ_0, k_B and parameter T represent vacuum permeability, the Boltzmann constant and absolute temperature (always 300 K in our case) respectively. The Langevin function is specific for a particle size with magnetic moment m_k [Am^2] and depends on the applied magnetic field strength H [Am^{-1}]. Since the size of a magnetic nanoparticle determines its magnetic moment, a sample with a certain particle size distribution has also a certain magnetic moment distribution. Therefore the

model describing the experimental data has to take into account a distribution of magnetic moments [41]. The magnetic moment of a superparamagnetic particle is related to its diameter D_k [m] by the bulk saturation magnetization M_s [Am^{-1}] of iron oxide Fe_3O_4 ($\mu_0 M_s$= 0.60 T, [41]) via

$$m_k = \frac{\pi D_k^3 M_s}{6}. \tag{3.3}$$

For magnetic nanoparticles an unimodal lognormal particle size distribution is generally accepted [42], because it is physically very likely and can be explained by physical phenomena during the production process [43]. Furthermore, transmission electron microscopy results of Endorem indicated a lognormal core size distribution [39]. The numerical approach of the lognormal particle size distribution is defined as

$$f(D_k|D_1,\sigma_1) = \frac{1}{D_k\sigma_1\sqrt{2\pi}} e^{\frac{-ln(D_k-D_1)}{2\sigma_1^2}},\ k = (1,\ldots,K), \tag{3.4}$$

where D_1 and σ_1 are the mean diameter and standard deviation of the associated normal distribution, respectively. The distribution is calculated for a broad range of K different particle diameters with diameter step size D_{step}. By substituting equation 3.3 for each D_k in equation 3.1 and 3.2 and multiplying each resulting Langevin function by its weight from the distribution $f(D_k|D_1,\sigma_1)\cdot D_{step}$, the contribution from each particle size is computed.

However, the model of the magnetic moment curve using a unimodal lognormal distribution for Endorem did not result in a suitable approach of the data. Especially in the region of the strongest curvature the model can not match the data. Therefore the unimodal lognormal distribution cannot represent the core size distribution of Endorem and a core size distribution with other shape parameters has to be used. Since particle production processes often result in lognormal distributed populations, it is reasonable to add a second lognormal distribution in the fit, which gives more degrees of freedom to the modeling curve. The bimodality of the particle size distributions may originate from the production process of the nanoparticles. A chemical growth processes, such as precipitation used for Endorem production [39, 44], comprises initial nucleation and growth, after which some original (smaller) seeds may remain in the colloid, which gives rise to two lognormal distributed particle size populations [45]. In present analysis, the bimodal distribution is only a way to model the most probable experimental magnetic moment curve using the most relevant parameters of the size distribution. Implementation of a bimodal lognormal distribution requires three additional parameters to be optimized: a second mean and standard deviation for the distribution and the relative weight factors p and $(1-p)$ for each distribution.

Finally, the sum of all modeled Langevin functions for the bimodal lognormal

distribution describes the model to be optimized

$$m(H) = \sum_{k=1}^{K} n\frac{\pi D_k^3 M_s}{6} \cdot L(x_k H) \cdot f(D_k|D_1, D_2, \sigma_1, \sigma_2, p) \cdot D_{step}, \quad (k = 1, \ldots, K), \quad (3.5)$$

where m represents the total field dependent magnetic moment of the sample and n the number of particles. This model, as well as the data, is normalized and the best parameters are determined by minimization of the root of the sum of squares of the logarithmic differences between the model $m(H)$ and measurement data $m_{sample}(H)$ [46]:

$$Error = \sqrt{\sum_{H=H_{min}}^{H_{max}} \left(log\,|m(H)| - log\,|m_{sample}(H)|\right)^2}. \quad (3.6)$$

This minimization for five parameters is performed using the Nelder-Mead simplex algorithm, which is an unconstrained nonlinear optimization algorithm, implemented in the MATLAB software package [47].

The original superparamagnetic component, which is lost in the normalization, is reconstructed adding again the linear component which was subtracted from the model. This component is added to both the normalized model and the normalized measured data. The total magnetic moment responsible for superparamagnetism in a sample, is determined by the sum of magnetic moments of the individual particles. This can be derived from the factor that was used for normalization of the data. To finish the quantitative reconstruction of the superparamagnetic component, both model and data were multiplied by this factor, which is basically the saturated magnetic moment.

For relatively large linear contributions in lymph node measurements, the quantification of the superparamagnetic component is very sensitive for noise, since after linear correction the relatively small errors made at high fields have a large effect on the small amplitude of the superparamagnetic component. Therefore, reduction of movement noise is particularly important for the quantification of samples with low amounts of iron. Determination of all parameters of the bimodal particle size distribution is therefore not suitable for each individual lymph node measurement. For that reason, the parameters of the particle size distributions found for the individual calibration samples are averaged and used in the model to quantify the iron content in lymph nodes. This average bimodal distribution is based on all measurements of calibrationn samples with an fit error lower than 0.5 (see eq. 3.6). Thereby it is assumed that the particle size distribution of the superparamagnetic cores in the lymph nodes is the same as in the original tracer. The hydrodynamic size distribution of the

particles that enter the lymph nodes might be different from the distribution in the original tracer, because the tissue and lymphatic system can be considered as a filter that may trap the larger particles. In the lymph node analysis presented here, the core size distribution in lymph nodes is assumed to be the same as in the original tracer, which supposes that hydrodynamic size is not directly related to magnetic core size. Finally, there remain three parameters to be estimated for the lymph node measurement. The first parameter is the saturated magnetic moment m_s, which corresponds to the amount of iron. The second parameter is the linear component χH, added to estimate the volumetric susceptibility χ of paramagnetic or diamagnetic material. The last estimate is an offset correction that is applied to correct for asymmetry.

3.2.5 Light microscopic analysis of lymph nodes

Following VSM-measurements, the lymph nodes are sliced (2-4 μm) for histological analysis by a pathologist. The presence of metastases is revealed by H&E and Cam 5.2 histological staining. Pearls Prussian Blue staining is used to indicate iron content in the lymph nodes.

3.3 Results and discussion

3.3.1 Calibration and parameter modeling

Different samples with a known quantity of Endorem were used as reference measurement to calibrate the system, as well as to develop the parameter modeling of the total magnetic moment of a sample. The model achieved for the measured data and the accompanying bimodal particle size distribution is shown in figure 3.2. For the average particle size distribution, further used for lymph node quantification, the following parameters were found: D_1= 4.5 nm, σ_1= 0.47, D_2= 8.3 nm, σ_1= 0.29, p= 0.52. These values are in the same range as was found using a unimodal lognormal distribution for TEM analysis of Endorem nanoparticles [39, 48, 49]. The bimodal core size distribution has a more broadened peak compared to a unimodal lognormal distribution, but does not show two clear separate maximums. The use of the bimodal lognormal distribution does give more freedom to the shape of the distribution and does not implicate that there are two clearly distinguishable populations of particle sizes.

The deviation of the model from the measured data, revealed a systematic measurement error (fig. 3.2). The ascending and descending branches of the loop do not coincide, which causes dissimilar differences between the measurement data and the model. This may indicate hysteresis in the sample, but the asymmetric and inconsistent pattern of deviation argues for measurement errors.

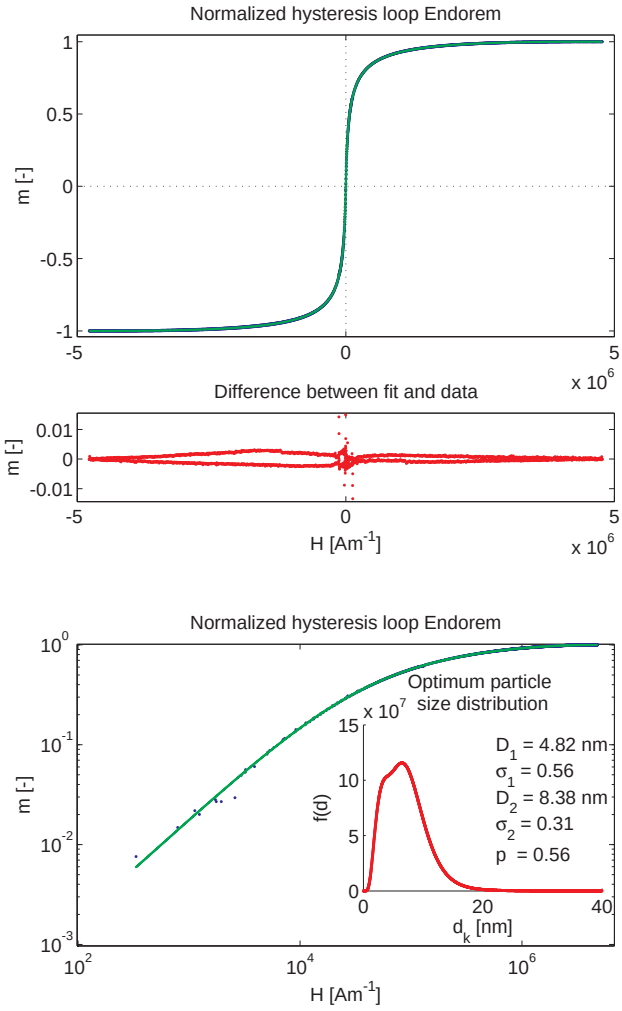

Figure 3.2: *The normalized magnetic moment versus field curve. The* upper panel *shows the normalized measurement and the curve of the optimized model on linear scale. The* mid panel *shows the difference between the model and the measured data. The negative and positive differences indicate that the model is well positioned in between the descending and ascending branch of the loop, showing some unphysical hysteresis due to measurement error. The* lower panel *on bilogarithmic scale gives more insight in the quality of measured data and the model in the low field region. Superparamagnetism is confirmed by the absence of significant hysteresis in the low field region. The bimodal lognormal particle size distribution that resulted in the best modeling curve is shown in the* inset.

Since the saturated magnetization at a high field strength is used as calibration to estimate iron content in other samples, the model should be as precise as possible in

this region. The calibration with the lowest amount of 1 μg iron could not accurately be quantified, but still shows a minor superparamagnetic component, indicating the detection limit. The lowest amount of Endorem that could be quantified corresponds to 1.5 μg Fe with an error of ± 0.5 μg. This detection limit depends strongly on the quality of the measurement and the contribution of linear magnetic materials. The calibration constant used to quantify lymph node samples with a saturation field of $3.18 \cdot 10^6$ Am^{-1} was $7.76 \cdot 10^{-8}$ Am$^2\mu$g^{-1} iron.

Measurements of samples with Patent Blue V and formalin did not show any nonlinear magnetic contribution that may interfere with the superparamagnetic contribution from particles accumulated in the tissue (results not shown). Therefore, the presence of Patent Blue V and formalin in or around lymph node samples will not affect an accurate estimation of the superparamagnetic component from the tracer.

3.3.2 Lymph node analysis

The magnetic content in lymph nodes is determined based on the average particle size distribution found in the calibration samples. The Endorem mass in the lymph nodes is determined using the Langevin model with the bimodal distribution described in section 3.2.4. Although in most cases a significant linear contribution was present, a superparamagnetic nonlinear component could be well estimated by the algorithm and therefore a background measurement became unnecessary. This is important, because a background measurement for the lymph nodes would even be impossible for this clinical application.

The magnetic moment curve of two lymph nodes is shown in figure 3.3. There is an obvious difference with the curve in figure 3.2 because of the linear contribution from sample holder and tissue. Both the superparamagnetic and the linear component are estimated by fitting the parameters m_s and χ, respectively. The calibration constant derived from a series of known Endorem samples (see sec. 3.3.1) is used to determine the iron mass in the lymph node. Over all, from 13 patients and 33 lymph nodes included in the study, Endorem content was detected in 24 lymph nodes and was found in the range of 1.1 to 51.4 μg iron. The mean quantity of iron found in lymph nodes was 17.1 μg. Light microscopic analysis of the lymph nodes with Pearls Prussian Blue staining confirmed iron presence in each lymph node that was detected by magnetometry (fig. 3.3). The iron presence was observed in the interstitial space in all but one lymph node. In that particular lymph node, macrophages stained positive for iron.

Some measurements suffered from significant noise and possibly sample displacement. Lymph node samples with a substantial proportion of fat tissue are more susceptible to abusive, parasitic, lateral movements. This is overcome by a stronger fixation of the sample, resulting in lower noise and subsequent accurate quantification of the amount of iron. The remaining effect of motion-generated errors is rep-

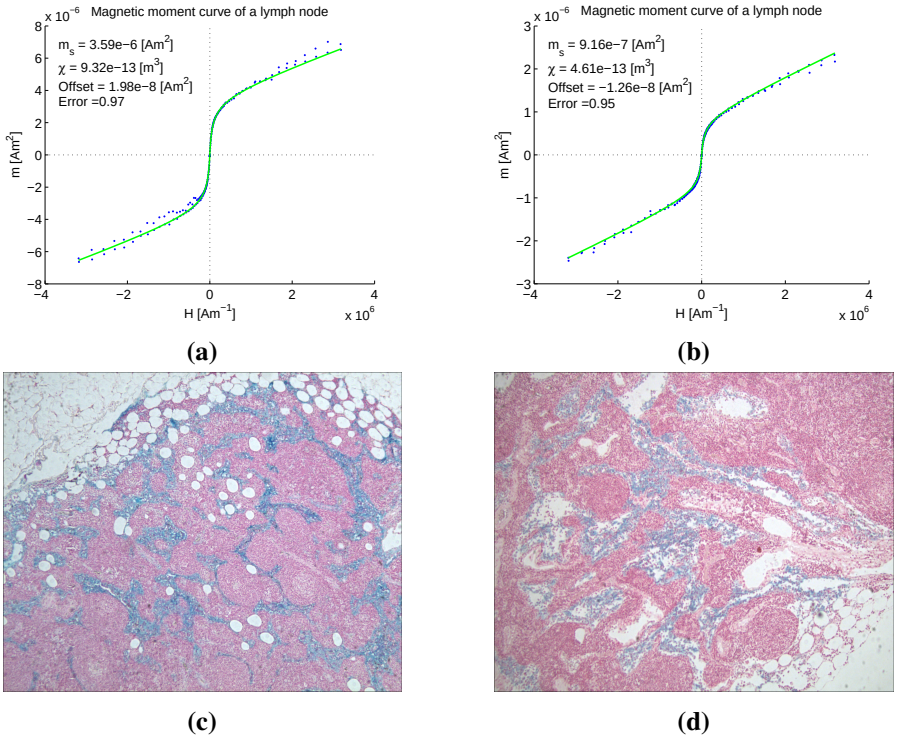

Figure 3.3: *Two examples of a VSM measurement of a lymph node containing Endorem and the corresponding microscopy images with Pearls Prussian Blue staining. Endorem content corresponds with* ***(a)*** *46.7 µg and* ***(b)*** *11.9 µg iron. The green line indicates the model applied to the data points measured, including a linear (χ) and nonlinear component with amplitude m_s. The corresponding histology images (**c** and **d**) with Pearls Prussian Blue confirm the presence of SPIO and indicate interstitial spread of the particles throughout the sinuses of the lymph nodes.*

resented in the error of the fit procedure (see eq. 3.6), which is on average 1.61 for lymph nodes compared to 0.24 for the calibration samples. However, for the present study this error is small enough to obtain a quantitative indication of Endorem filling of colorectal lymph nodes in an *ex vivo* sentinel node procedure. Future systems for magnetic lymph node analysis need to be designed such that this kind of errors do not occur.

There are two possible reasons that some blue nodes that were selected as SLNs by definition, did not contain iron. First, the definition of the SLN may have failed by selecting lymph nodes that are not true SLNs. The probably more selective magnetic tracer has only reached the true SLNs in that case. This cannot be verified, since lymph node mapping is unable to reveal whether a lymph node is a first or higher echelon node. The second reason could be that the *ex vivo* circumstances reduced

magnetic tracer migration towards lymph nodes. Therefore, some of the SLNs may be missed by the magnetic tracer. These aspects of the procedure should be investigated in a more elaborate clinical study that allows magnetic measurements on all the lymph nodes in a specimen.

Interestingly, the results show that *ex vivo* SLN mapping with magnetic nanoparticles is feasible. Lymphatic drainage of Endorem particles from the tumor in *ex vivo* colorectal tissue is possible by mechanical actuation, such as massage. Other physiological mechanisms of lymphatic transport, including macrophage uptake which is normally present in living tissue [37], are therefore not necessary for the selection of SLNs in colorectal cancer. After *ex vivo* injection, the particles flow via the interstitial space through the lymphatics to the SLNs, driven by mechanical pressure induced by massage. In *in vivo* cases, SPIO accumulates normally in macrophages, but this activity is believed to cease soon after resection of the specimen. Other studies have shown the utility of *ex vivo* SLNM in colorectal cancer using a non-colloidal blue dye [20–25]. The present study has shown that, despite the use of particles in *ex vivo* SLNM, the tracer ends up in lymph nodes. The use of particles might even be contributing to accurate sentinel node selection, since the chance of selection of second echelon nodes might be reduced. The specific clinical value of the use of magnetic nanoparticles in colorectal SLN mapping should be investigated in a more elaborate patient study.

The accumulated particles in SLNs are detectable by highly sensitive laboratory equipment. Although Endorem was a pragmatic choice for reasons of availability, it performed well as tracer for SLNs. However, further development of magnetic SLNM in colorectal cancer should consider the optimal magnetic and hydrodynamic particle size and composition. The success of radioisotope based SLN procedures has shown to be dependent on the particle size of the applied colloid [50, 51]. The development of magnetic nanoparticles with a higher (magnetic) yield, will lower the requirements for new clinical instruments to be developed, or may increase the sensitivity of the procedure.

For several reasons, an experimental laboratory VSM system is not suitable for clinical applications. The large magnetic fields and helium cooling, as well as sample mounting and long measuring time are significant drawbacks for clinical use of a VSM. Therefore further development of fast, high-sensitive magnetic detectors is desirable. Exploiting the nonlinear behavior of the SPIO particles in AC-susceptometry or a frequency mixing technique [52], the detection can be very specific, which is mandatory for samples with unknown diamagnetic content. In colorectal cancer, the SLNs have to be selected out of a series of about 10-25 resected lymph nodes per patient. Therefore, a clinical magnetic detection instrument with high sensitivity and short processing time would enable pathologists to use their specific microscopy techniques for ultrastaging on magnetically selected SLNs, so as to find high-risk patients

who may benefit from adjuvant therapy.

3.3.3 Other techniques of SPIO quantification

In literature, several other techniques to quantify SPIO in biological samples are described. Besides magnetometry, optical and mass spectroscopy are used to analyse SPIO content in cell samples. Inductively coupled plasma spectroscopy is a highly sensitive but expensive method that is not suitable for routine sample analysis. These techniques are very sensitive for SPIO, but require sample digestion, which is not compatible with histopathologic analysis in SLNM [28, 53, 54].

Since Endorem is developed as MRI contrast agent, the uptake of particles can be revealed by MRI. MRI techniques to quantify SPIO concentrations in samples are based on the field inhomogeneities produced by the particles. These field inhomogeneities can be quantified by measuring a reduction in relaxation time [53] or by model-based reconstruction using a measured phase map [55, 56]. Boutry and colleagues could quantify magnetic nanoparticle content in cell samples by relaxometry [53], however their procedure is not applicable in SLNM because it requires sample digestion and thus impedes histopathologic analysis of intact samples. Problematic in SPIO quantification with MRI are other sources of field inhomogeneities in a sample, like gradient instabilities and tissue-tissue or air-tissue interfaces, that all may cause the contribution from SPIO nanoparticles to be indistinguishable [27, 56]. Therefore (background) measurements that allow identification of these other components are often required to determine the exact contribution from SPIO [55, 57, 58]. This makes MRI procedures much more complex and time consuming, since, in case of SLNM, the SLNs also have to be measured before tracer administration. For *ex vivo* procedures, this would postpone the time-critical tracer injection and therefore the identification rate of the procedure may become affected. Finally, MRI is an expensive technique which is less specific for nonlinear magnetic properties and therefore less suitable for *ex vivo* SLNM with SPIO. Therefore, magnetometry methods that are more selective for the specific nonlinear characteristics of SPIO, can be much more accurate, less expensive and easier to implement in clinical practice.

3.4 Conclusion

Sentinel lymph node mapping using superparamagnetic nanoparticles is successfully applied in colorectal cancer patients. Although a dispersion of nanoparticles is used in the *ex vivo* tissue, the tracer ends up in lymph nodes. This chapter shows that non-destructive VSM measurements on fresh or formalin-fixated lymph nodes, can reveal the magnetic properties inside, provided that the lymph nodes are firmly fastened. The nonlinear superparamagnetic contribution, arising from the magnetic nanoparti-

cles in the tracer, is distinguishable and quantifiable by modeling the magnetic moment curve with the Langevin model and a bimodal lognormal core size distribution. Furthermore, detection and selection of Endorem-filled SLNs in *ex vivo* colorectal tissue was proven to be possible by a detection limit of 1 μg iron. Selection of the SLN in colorectal cancer using a selective colloidal magnetic tracer can help to accurately intensify standard histopathological analysis, by additional staining of those nodes that most probably contain metastases. To facilitate the clinical application of magnetic SLN detection in colorectal cancer, a clinical magnetometer has to be developed that allows quick and specific detection of the nonlinear properties of superparamagnetic tracer in lymph nodes.

References

[1] Q. A. Pankhurst, N. T. K. Thanh, S. K. Jones, and J. Dobson, "Progress in applications of magnetic nanoparticles in biomedicine", Journal of Physics D: Applied Physics **42**, 224001 (2009).

[2] S. Laurent, D. Forge, M. Port, A. Roch, C. Robic, L. Vander Elst, and R. N. Muller, "Magnetic iron oxide nanoparticles: Synthesis, stabilization, vectorization, physicochemical characterizations, and biological applications", Chemical Reviews **108**, 2064–2110 (2008).

[3] C. Corot, P. Robert, J.-M. Idée, and M. Port, "Recent advances in iron oxide nanocrystal technology for medical imaging", Advanced Drug Delivery Reviews **58**, 1471 – 1504 (2006).

[4] J. W. M. Bulte and D. L. Kraitchman, "Iron oxide MR contrast agents for molecular and cellular imaging", NMR in Biomedicine **17**, 484–499 (2004).

[5] A. Ito, M. Shinkai, H. Honda, and T. Kobayashi, "Medical application of functionalized magnetic nanoparticles", Journal of Bioscience and Bioengineering **100**, 1 – 11 (2005).

[6] T. Islam and L. Josephson, "Current state and future applications of active targeting in malignancies using superparamagnetic iron oxide nanoparticles", Cancer Biomarkers **5**, 99–107 (2009).

[7] R. Ivkov, S. DeNardo, W. Daum, A. Foreman, R. Goldstein, V. Nemkov, and G. DeNardo, "Application of high amplitude alternating magnetic fields for heat induction of nanoparticles localized in cancer", Clinical Cancer Research **11**, 7093s–7103s (2005).

[8] T. Jain, J. Richey, M. Strand, D. Leslie-Pelecky, C. Flask, and V. Labhasetwar, "Magnetic nanoparticles with dual functional properties: Drug delivery and magnetic resonance imaging", Biomaterials **29**, 4012–4021 (2008).

[9] R. Hergt and S. Dutz, "Magnetic particle hyperthermia-biophysical limitations of a visionary tumour therapy", Journal of Magnetism and Magnetic Materials **311**, 187–192 (2007), cited By (since 1996) 90.

[10] T. Nakagawa, Y. Minamiya, Y. Katayose, H. Saito, K. Taguchi, H. Imano, H. Watanabe, K. Enomoto, M. Sageshima, T. Ueda, and J. I. Ogawa, "A novel method for sentinel lymph node mapping using magnetite in patients with non-small cell lung cancer", Journal of Thoracic and Cardiovascular Surgery **126**, 563–567 (2003).

[11] Y. Minamiya, M. Ito, Y. Katayose, H. Saito, K. Imai, Y. Sato, and J. I. Ogawa, "Intraoperative sentinel lymph node mapping using a new sterilizable magnetometer in patients with nonsmall cell lung cancer", Annals of Thoracic Surgery **81**, 327–330 (2006).

[12] T. Joshi, Q. A. Pankhurst, S. Hattersley, A. Brazdeikis, M. Hall-Craggs, E. De Vita, A. Bainbridge, R. Sainsbury, A. Sharma, and M. Douek, "Magnetic nanoparticles for detecting cancer spread", 30th Annual San Antonio Breast Cancer Symposium - December 13-16, 2007 - Breast Cancer Research and Treatment **106**, S129 (2007).

[13] L. Johnson, Q. A. Pankhurst, A. Purushotham, A. Brazdeikis, and M. Douek, "Magnetic sentinel lymph node detection for breast cancer", Cancer Research **70**, P1–01–23 (2010).

[14] M. Shiozawa, A. Lefor, Y. Hozumi, K. Kurihara, N. Sata, Y. Yasuda, and M. Kusakabe, "Sentinel lymph node biopsy in patients with breast cancer using superparamagnetic iron oxide and a magnetometer", Breast Cancer 1–7 (2012).

[15] S. Tanaka, H. Ota, Y. Kondo, Y. Tamaki, S. Kobayashi, and S. Noguchi, "Detection of magnetic nanoparticles in lymph nodes of rat by high T_c-SQUID", IEEE Transactions on Applied Superconductivity **13**, 377–380 (2003), http://dx.doi.org/10.1109/TASC.2003.813857.

[16] D. J. Grootendorst, J. Jose, R. M. Fratila, M. Visscher, A. H. Velders, B. Ten Haken, T. G. Van Leeuwen, W. Steenbergen, S. Manohar, and T. J. M. Ruers, "Evaluation of superparamagnetic iron oxide nanoparticles (Endorem) as a photoacoustic contrast agent for intra-operative nodal staging", Contrast Media & Molecular Imaging **8**, 83–91 (2013).

[17] A. H. Strickland, N. Beechey-Newman, C. B. Steer, and P. G. Harper, "Sentinel node biopsy: an in depth appraisal", Critical Reviews in Oncology/Hematology **44**, 45–70 (2002).

[18] P. J. Tanis, O. E. Nieweg, R. A. Valdés Olmos, and B. B. Kroon, "Anatomy and physiology of lymphatic drainage of the breast from the perspective of sentinel node biopsy", Journal of the American College of Surgeons **192**, 399 – 409 (2001).

[19] E. S. van der Zaag, W. H. Bouma, P. J. Tanis, D. T. Ubbink, W. A. Bemelman, and C. J. Buskens, "Systematic review of sentinel lymph node mapping procedure in colorectal cancer", Annals of Surgical Oncology **19**, 3449–3459 (2012).

[20] A. Stojadinovic, P. J. Allen, M. Protic, J. F. Potter, C. D. Shriver, J. M. Nelson, and G. E. Peoples, "Colon sentinel lymph node mapping: Practical surgical applications", Journal of the American College of Surgeons **201**, 297 – 313 (2005).

[21] J. Tuech, P. Pessaux, F. D. Fiore, V. Nitu, B. Lefebure, A. Colson, and F. Michot, "Sentinel node mapping in colon carcinoma: In-vivo versus ex-vivo approach", European Journal of Surgical Oncology (EJSO) **32**, 158 – 161 (2006).

[22] E. S. van der Zaag, C. J. Buskens, N. Kooij, H. Akol, H. M. Peters, W. H. Bouma, and W. A. Bemelman, "Improving staging accuracy in colon and rectal cancer by sentinel lymph node mapping: A comparative study", European Journal of Surgical Oncology (EJSO) **35**, 1065 – 1070 (2009).

[23] P. M. van Schaik, J. C. van der Linden, M. F. Ernst, W. A. H. Gelderman, and K. Bosscha, "Ex vivo sentinel lymph node "mapping" in colorectal cancer", European Journal of Surgical Oncology **33**, 1177–1182 (2007).

[24] C. T. Viehl, C. T. Hamel, W. R. Marti, U. Guller, L. Eisner, U. Stammberger, L. Terracciano, H. P. Spichtin, F. Harder, and M. Zuber, "Identification of sentinel lymph nodes in colon cancer depends on the amount of dye injected relative to tumor size", World Journal of Surgery **27**, 1285–1290 (2003).

[25] J. H. Wong, S. Steineman, C. Calderia, J. Bowles, and T. Namiki, "Ex vivo sentinel node mapping in carcinoma of the colon and rectum", Annals of Surgery **233**, 515–521 (2001).

[26] V. Galimberti, S. Zurrida, M. Intra, S. Monti, P. Arnone, G. Pruneri, and C. De Cicco, "Sentinel node biopsy interpretation: The Milan experience", Breast Journal **6**, 306–309 (2000).

[27] W. Liu and J. A. Frank, "Detection and quantification of magnetically labeled cells by cellular MRI", European Journal of Radiology **70**, 258–264 (2009).

[28] E. R. Dadashzadeh, M. Hobson, L. Henry Bryant, D. D. Dean, and J. A. Frank, "Rapid spectrophotometric technique for quantifying iron in cells labeled with superparamagnetic iron oxide nanoparticles: potential translation to the clinic", Contrast Media & Molecular Imaging **8**, 50–56 (2013).

[29] W. Beyhum, D. Hautot, J. Dobson, and Q. A. Pankhurst, "Magnetic biomineralisation in huntington's disease transgenic mice", Journal of Physics: Conference Series **17**, 50 (2005).

[30] J. Dobson and P. Grassi, "Magnetic properties of human hippocampal tissue - evaluation of artefact and contamination sources", Brain Research Bulletin **39**, 255–259 (1996).

[31] D. Hautot, Q. A. Pankhurst, and J. Dobson, "Superconducting quantum interference device measurements of dilute magnetic materials in biological samples", Review of Scientific Instruments **76** (2005).

[32] D. Hautot, Q. A. Pankhurst, C. M. Morris, A. Curtis, J. Burn, and J. Dobson, "Preliminary observation of elevated levels of nanocrystalline iron oxide in the basal ganglia of neuroferritinopathy patients", Biochimica et Biophysica Acta - Molecular Basis of Disease **1772**, 21–25 (2007).

[33] J. L. Kirschvink, A. Kobayashi-Kirschvink, and B. J. Woodford, "Magnetite biomineralization in the human brain", Proceedings of the National Academy of Sciences of the United States of America **89**, 7683–7687 (1992).

[34] Q. A. Pankhurst, D. Hautot, N. Khan, and J. Dobson, "Increased levels of magnetic iron compounds in alzheimer's disease", Journal of Alzheimer's Disease **13**, 49–52 (2008).

[35] I. Raynal, P. Prigent, S. Peyramaure, A. Najid, C. Rebuzzi, and C. Corot, "Macrophage endocytosis of superparamagnetic iron oxide nanoparticles: Mechanisms and comparison of ferumoxides and ferumoxtran-10", Investigative Radiology **39**, 56–63 (2004).

[36] H. Y. Lee, S. H. Lee, C. Xu, J. Xie, J. H. Lee, B. Wu, A. Leen Koh, X. Wang, R. Sinclair, S. X. Wang, D. G. Nishimura, S. Biswal, S. Sun, S. H. Cho, and X. Chen, "Synthesis and characterization of PVP-coated large core iron oxide nanoparticles as an MRI contrast agent", Nanotechnology **19** (2008).

[37] M. A. Saksena, A. Saokar, and M. G. Harisinghani, "Lymphotropic nanoparticle enhanced MR imaging (LNMRI) technique for lymph node imaging", European Journal of Radiology **58**, 367–374 (2006).

[38] D. X. Chen, O. Pascu, A. Roig, and A. Sanchez, "Size analysis and magnetic structure of nickel nanoparticles", Journal of Magnetism and Magnetic Materials **322**, 3834–3840 (2010).

[39] C. W. Jung and P. Jacobs, "Physical and chemical properties of superparamagnetic iron oxide MR contrast agents: Ferumoxides, ferumoxtran, ferumoxsil", Magnetic Resonance Imaging **13**, 661 – 674 (1995).

[40] C. P. Bean and I. S. Jacobs, "Magnetic granulometry and super-paramagnetism", Journal of Applied Physics **27**, 1448–1452 (1956).

[41] D. X. Chen, A. Sanchez, E. Taboada, A. Roig, N. Sun, and H. C. Gu, "Size determination of superparamagnetic nanoparticles from magnetization curve", Journal of Applied Physics **105** (2009).

[42] C. G. Granqvist and R. A. Buhrman, "Ultrafine metal particles", Journal of Applied Physics **47**, 2200–2219 (1976).

[43] L. B. Kiss, J. Söderlund, G. A. Niklasson, and C. G. Granqvist, "New approach to the origin of lognormal size distributions of nanoparticles", Nanotechnology **10**, 25 (1999).

[44] E. V. Groman, L. Josephson, and J. M. Lewis, "Biologically degradable superparamagnetic materials for use in clinical applications", U.S. patent 4827945 (1989).

[45] M. Blanco-Mantecón and K. O'Grady, "Grain size and blocking distributions in fine particle iron oxide nanoparticles", Journal of Magnetism and Magnetic Materials **203**, 50–53 (1999).

[46] S. Biederer, T. Knopp, T. F. Sattel, K. Lüdtke-Buzug, B. Gleich, J. Weizenecker, J. Borgert, and T. M. Buzug, "Magnetization response spectroscopy of superparamagnetic nanoparticles for magnetic particle imaging", Journal of Physics D: Applied Physics **42**, 205007 (2009).

[47] J. C. Lagarias, J. A. Reeds, M. H. Wright, and P. E. Wright, "Convergence properties of the Nelder–Mead simplex method in low dimensions", SIAM J. on Optimization **9**, 112–147 (1998).

[48] J. E. Lima, A. L. Brandl, A. D. Arelaro, and G. F. Goya, "Spin disorder and magnetic anisotropy in Fe_3O_4 nanoparticles", Journal of Applied Physics **99**, 083908 (2006).

[49] L. F. Gamarra, G. E. S. Brito, W. M. Pontuschka, J. B. Mamani, C. A. Moreira-Filho, and E. Amaro Jr., "Study of the ferrofluid drying process for morphological and nanostructutal characterization", Brazilian Journal of Physics **37**, 1288 – 1291 (2007).

[50] M. R. S. Keshtgar and P. J. Ell, "Sentinel lymph node detection and imaging", European Journal of Nuclear Medicine **26**, 57–67 (1999).

[51] M. H. Leidenius, E. A. Leppänen, L. A. Krogerus, and K. A. V. Smitten, "The impact of radiopharmaceutical particle size on the visualization and identification of sentinel nodes in breast cancer", Nuclear Medicine Communications **25**, 233–238 (2004).

[52] H. J. Krause, N. Wolters, Y. Zhang, A. Offenhäusser, P. Miethe, M. H. F. Meyer, M. Hartmann, and M. Keusgen, "Magnetic particle detection by frequency mixing for immunoassay applications", Journal of Magnetism and Magnetic Materials **311**, 436–444 (2007).

[53] S. Boutry, D. Forge, C. Burtea, I. Mahieu, O. Murariu, S. Laurent, L. Vander Elst, and R. N. Muller, "How to quantify iron in an aqueous or biological matrix: a technical note", Contrast Media & Molecular Imaging **4**, 299–304 (2009).

[54] P. Danhier, G. De Preter, S. Boutry, I. Mahieu, P. Leveque, J. Magat, V. Haufroid, P. Sonveaux, C. Bouzin, O. Feron, R. N. Muller, B. F. Jordan, and B. Gallez, "Electron paramagnetic resonance as a sensitive tool to assess the iron oxide content in cells for MRI cell labeling studies", Contrast Media & Molecular Imaging **7**, 302–307 (2012).

[55] P. Cantillon-Murphy, L. L. Wald, M. Zahn, and E. Adalsteinsson, "Measuring SPIO and Gd contrast agent magnetization using 3T MRI", NMR in Biomedicine **22**, 891–897 (2009).

[56] J. Langley, W. Liu, E. K. Jordan, J. A. Frank, and Q. Zhao, "Quantification of SPIO nanoparticles in vivo using the finite perturber method", Magnetic Resonance in Medicine **65**, 1461–1469 (2011).

[57] R. M. Weisskoff and S. Kiihne, "MRI susceptometry: Image-based measurement of absolute susceptibility of MR contrast agents and human blood", Magnetic Resonance in Medicine **24**, 375–383 (1992).

[58] P. H. Mills, T. K. Hitchens, L. M. Foley, T. Link, Q. Ye, C. R. Weiss, J. D. Thompson, W. D. Gilson, A. Arepally, J. A. Melick, P. M. Kochanek, C. Ho, J. W. M. Bulte, and E. T. Ahrens, "Automated detection and characterization of SPIO-labeled cells and capsules using magnetic field perturbations", Magnetic Resonance in Medicine **67**, 278–289 (2012).

4

Ex vivo magnetic metection of sentinel lymph nodes in colorectal cancer: first results of a new approach*

Abstract: *Background:* In this chapter the use of superparamagnetic ironoxide (SPIO) nanoparticles is investigated as a possibly more specific tracer in *ex vivo* sentinel lymph node mapping (SLNM) in colorectal cancer (CRC) to improve diagnosis of stage I and II patients. *Materials and Methods:* After standard resection of the tumor in 10 patients, the colonic or rectal segment was opened and Endorem and Patent Blue V was injected submucosally around the tumor. At histopathologic dissection, the three blue nodes closest to the tumor were selected as the sentinel nodes (SN). The SNs were subjected to vibrating sample magnetometry (VSM) and histologic staining to determine Endorem content. To determine nodal status, multi-level sectioning and immunohistochemistry was applied. *Results:* VSM detected nonlinear magnetism from Endorem in 9 patients in the range of 1.1-51.4 μg iron, which was confirmed by histology. The Endorem containing nodes accurately predicted status of the nodal basin in all patients. *Conclusions:* The *ex vivo* circumstances of the procedure did not hamper the distribution of nanoparticles through the lymphatic system. Development of a clinical magnetometer that exploits the nonlinear properties of SPIO will facilitate the introduction of magnetic ex vivo SLNM in CRC as a fast and cost-effective method to improve staging.

*This chapter is to be submitted with contributing authors: M. Visscher, J.J. Pouw, J. van Baarlen, J.M. Klaase, B. ten Haken

4.1 Introduction

Colorectal cancer (CRC) is the fourth most cause of cancer deaths worldwide [1] and reduction of mortality may be achieved by early diagnosis via screening programs, improved diagnostic methods and increased treatment effectiveness. The latter two may be realized by the introduction of sentinel lymph node mapping (SLNM), providing a more precise diagnosis and possibly a more accurate subsequent (adjuvant) treatment. In the search for an accurate and cost-effective procedure, *ex vivo* SLNM using a superparamagnetic tracer is proposed as a suitable alternative for existing approaches.

The idea of lymphatic mapping has been developing since the first half of the last century for various types of cancers. The first application in penile cancer has led to the broader application of the procedure in melanoma, breast cancer and head and neck cancer [2, 3]. The sentinel lymph node (SLN) is the node that receives lymphatic drainage directly from the tumor area. SLNM is a procedure that is used to select the lymph nodes with the highest chance of harboring metastases. A (not tumor targeted) tracer applied by peritumoral injection in SLNM is expected to follow the same pathway to the SLN as a metastatic cell. Therefore, detected accumulation of the tracer in a lymph node is used as identification of a SLN [4]. The laborious and expensive immunohistochemistry or reverse transcription polymerase chain reaction (RT-PCR) techniques can then be focused on selected SLNs. The results of this intensified analysis are regarded as representative for the total nodal basin. For various cancers most often a blue dye is used as a visual tracer, which can be applied in combination with a radioactive tracer, like technetium colloid [5–7]. A handheld gamma probe, gamma camera or SPECT/CT-system can be used to localize non-superficial accumulation of radioactive tracer in tissue [8].

Colorectal cancer is normally treated by segmental resection of the primary tumor and *en-bloc* resection of the lymph nodes in the mesentery. Regional lymphadenectomy provides local-regional control of the disease, the possibility of cancer staging and plays a role in treatment planning. However, still up to 30% of the patients diagnosed with metastatis free lymph nodes, will develop distant metastases and die from colorectal cancer [9–11]. It is supposed that these patients may benefit from more accurate staging of the disease, by intensifying the search for metastases, micro-metastases (MM) and isolated tumor cells (ITC) in lymph nodes, using multi-sectioning and immunohistochemistry or the RT-PCR technique [12–14]. However these procedures are expensive and very time consuming [2, 4, 9, 15–18], since a series of at least 12 harvested nodes is required for accurate nodal staging, according to the guidelines of the American Joint Committee on Cancer [19]. To reduce the time investment and the costs needed for improvement of staging in CRC, sentinel lymph node mapping is expected to be a very acceptable compromise [12, 20–27].

Since the concept of SLNM in CRC is systematically different from SLNM in

other cancers, the detection technique and the procedure to perform SLNM can be reconsidered from this renewed perspective. Especially the *en-bloc* resection of the lymph nodes opens new possibilities that cannot be exploited by procedures that are developed to minimize lymph node resection. The development of SLNM in CRC led to about 100 experimental clinical studies in the past 15 years with a focus on procedural and technical aspects of traditional SLNM techniques. In their extensive reviews Van der Pas and Van der Zaag summarized the main conclusions that can be drawn from the results till now [9, 10]. In contrast to breast cancer and melanoma, the regional lymphadenectomy is standard in primary resection of CRC. Therefore the SLNM approach in CRC is used only in an attempt to improve clinical staging [27, 28]. While there are strong indications about the prognostic impact and implications for clinical decisions, the expectations still have to be confirmed by prospective studies. SLNM can be beneficial for patients with negative nodes (N0) normally not receiving adjuvant chemotherapy [13, 16, 29]. The main question for the coming years is whether patients may benefit from this refined diagnostic tool and subsequent altered clinical decisions. To answer this question, a large phase III multicenter, randomized-control study is performed in The Netherlands [30].

The SLNM procedure for CRC has not been standardized yet, since there remains debate about the optimal procedure in terms of accuracy, costs and technical possibilities [15, 25, 31]. In the context of the different perspective of SLNM in CRC compared to other cancers, it is worth to consider other techniques to identify the SLN. The standard methods using blue dye and radioisotopes have significant drawbacks that complicate the implementation of a reliable and efficient procedure for CRC. Blue dye is used by visual assessment of the lymphatic drainage pattern in the peritumoral region. Radioisotopes are used with systems that allow in-depth detection. Alternative SLNM techniques using fluorescent dye are also developing [32, 33], but require expensive systems, whereas mapping is a time critical procedure that has to be performed directly after injection. Using a magnetic tracer and related detection technology, improvement can be achieved on various aspects of SLNM in colorectal cancer. Magnetic SLNM has already been applied in lung cancer and breast cancer [34–38]. To demonstrate feasibility, this chapter discusses the first results of the use of magnetic tracer in *ex vivo* SLNM in CRC.

The magnetic approach of SLNM in CRC has to be evaluated against the critical aspects of current techniques. For several reasons, *ex vivo* SLNM can be the preferred method of SLNM in CRC. However, the use of these traditional tracers in *ex vivo* SLNM is complicated because of decaying activity of radionuclides or elution of blue dye caused by formalin fixation. This can result in sampling error or a reduced identification rate at post-operative detection, especially when SLN identification is performed at histopathologic dissection [3, 9]. Therefore, radionuclides have never been used for entirely *ex vivo* procedures in CRC. *ex vivo* SLNM using

a superparamagnetic tracer has the capability to improve nodal staging with limited additional costs, whereas the issues accompanying the use of blue dye or radioactive technetium may be solved. The use of physically stable superparamagnetic tracers enables post-operative *ex vivo* SLN detection in CRC with the same quality as during surgery. Compared to traditional tracers, the magnetic tracer can decrease sampling error and improve identification rate, since the characteristic magnetic properties do not decay and elution of tracer is prevented by its colloidal property. Therefore, the *ex vivo* identification of the SLN will be a less time critical procedure that can be performed post-operatively, which reduces the burden on costly operation time. Thus, magnetic tracer eliminates the complexity of the use of radioactive tracers, whereas the advantageous specificity for first echelon nodes of a colloidal tracer [6, 23, 39, 40] can be retained.

To implement magnetic SLNM for CRC, a clinically suitable system is required that can detect magnetic nanoparticles in lymph nodes. A device that can specifically search for magnetic nanoparticle (MNP) containing SLNs or a device that can select MNP containing SLNs out of all harvested LNs can be placed either at the surgery department or at the pathology lab. The most critical parameters for such a device are the sensitivity and specificity for MNP detection. The superparamagnetic tracer can be unambiguously detected because of its nonlinear magnetic properties that are in contrast to the linear magnetic properties of tissue. To obtain a first qualitative and quantitative indication of the feasibility of MNP detection for SLNM in colorectal cancer, we performed an *ex vivo* SLNM procedure on ten patients using the commercially available and clinically approved MRI contrast agent Endorem as superparamagnetic tracer and a standard vibrating sample magnetometer (VSM) for magnetic detection of selected nodes. The results of magnetic measurements reveal both the suitability of MNPs for (*ex vivo*) SLNM and the physical and technical requirements of clinical equipment for routinely use of magnetic SLNM in colorectal cancer.

4.2 Materials and Methods

4.2.1 Patients

Ten patients with clinical stage I-II colorectal carcinoma who were operated on with curative intent in the MST Enschede hospital, were subject of an *ex vivo* SLNM procedure. The number of ten patients was chosen because it allows both demonstration of the applicability of the method and definition of the next step in development, but it is too low to draw statistical conclusions. Exclusion criteria for the SLNM procedure were the presence of distant metastasis (M1) and inter-operative gross nodal involvement. All patients underwent a standard surgical resection and lymphadenectomy dictated by the location of the tumor. Four procedures were performed laparoscopic,

the remaining six were open procedures. The study was done in accordance with the guidelines of the local ethics committee of the MST Enschede.

4.2.2 Sentinel lymph node mapping

The specimen was taken to a separate field in the operating room, immediately after resection. It was inspected and palpated to determine the exact tumor location. The specimen was opened on the antimesentric border, or in the rectal case on the anterior border opposite to the mesorectum, leaving the mesorectum intact. When the tumor involved the complete circumference or the antimesentric border of the wall, the incision was stopped adjacent to the tumor. This was done to not hamper the pathological assessment of the tumor invasion of this border.

First, a total of approximately 1.5-2 ml of Endorem (16.8 - 22.4 mg Fe), (Guerbet Nederland B.V., Gorinchem, The Netherlands) was injected with a 25G-needle submucosally in four sites circumferentially around the tumor. The hydrodynamic size of Endorem nanoparticles is reported in the range of 58-186 nm [41, 42], whereas the mean size of the magnetic cores is reported in the range of 4.8-10 nm [43–45]. After injection of Endorem, a gentle massage of the injection sites was performed for 3 minutes. Subsequently, 1-1.5 ml of Patent Blue V (Guerbet Nederland B.V., Gorinchem, The Netherlands) was injected in the same four sites as the Endorem. We have chosen to first inject the colloidal Endorem and then the Patent Blue, because we suspect the first to be transported more difficult. The second injection was followed by a massage of the injection sites of 5 minutes. After injection and massage the mesocolon or mesorectum was inspected for visible blue nodes.

The specimen was formalin fixated directly after the mapping procedure, and sent to the pathology department. It was then processed according to the regular procedure with some minor modifications, as explained in the next section.

4.2.3 Sentinel lymph node selection

After 24-72h of formalin fixation, the tumor area and adjacent tissue was laminated by a pathologist to assess tumor invasion. Then a search for lymph nodes was performed in the mesocolic or mesorectal tissue. The three blue nodes closest to the tumor were designated as the SLNs and kept aside for measurements, to determine the amount of iron in the nodes. In case the laminating of the tumor area bivalved a SLN, the two halves were kept aside for measurements. All non-sentinel nodes were dissected from the specimen and assessed microscopically for metastasis by regular hematoxylin and eosin (H&E) coloring.

Figure 4.1: *The sample holder used for VSM measurements of lymph nodes. The lymph node is placed in a glass tube between two Delrin parts. The length of the upper part is adjustable to allow for firm fixation of lymph nodes with different size.*

4.2.4 Magnetometry of selected blue nodes

To be able to assess whether and how much of the SPIO contrast material was transported to the blue sentinel nodes, a vibrating sample magnetometer (VSM) was used.

Samples were placed in a 8 inch glass tube with 8.2 mm inner diameter and wall thickness of 0.9 mm (Wilmad Labglass, Vineland, New Jersey, USA). A firm fixation of the sentinel nodes, needed to reduce parasitic movements due to soft tissue, was obtained by a Delrin (DuPont, Dordrecht, The Netherlands) fixation system (see figure 4.1). The sample tube was placed in the VSM detection coil of a physical property measurement system (PPMS, Quantum Design Inc.,San Diego, California, USA) and the magnetic moment of the sample was measured using a magnetic field of $\pm$4.0 T, which is suitable to bring the magnetic nanoparticles into saturation. The amount of iron present in the SLNs is determined by the saturated magnetic moment of the superparamagnetic contribution in the sample. A detailed description of the analysis of magnetic content in lymph nodes can be found in chapter 3.

4.2.5 Microscopic analysis

Succeeding the VSM measurements, microscopic analysis is performed by multi-sectioning the SLNs into 3-5 sections, depending on lymph node size. From each level three 2-4 μm-slices were used for histological analysis using different kinds of staining. First, standard H&E-staining was performed. Additional staining with Cam 5.2, an anti-body against keratin, was used to reveal micrometastases (MM, 0.2-2 mm) and isolated tumor cells (ITC, $<$0.2 mm) that could be missed by analysis of

Characteristics	Value
Average age (yrs ± sd)	69±5
Gender	
Male	6
Female	4
Type of resection	
Open	6
Laparoscopic	4
Tumor location	
Cecum	3
Ascending colon	1
Descending colon	2
Sigmoid colon	1
Rectosigmoid colon	2
Rectum	1
Depth of tumor invasion	
T1	1
T2	0
T3	6
T4	3
Nodal status	
N0	9
N1	0
N2	1

Table 4.1: *Patient and tumor characteristics*

the H&E slices. Finally, Perl's Prussian Blue staining is used as a control, to indicate the presence of iron in the SLNs and to reveal the mechanism of nodal uptake.

4.3 Results

A total of 10 patients was included for this feasibility study, with colon tumors in seven patients, rectosigmoid tumors in two patients and a rectum tumor in one patient. One patient suffered from a T1 tumor in both the proximal and distal end of the rectosigmoid. Both tumors were regarded as separate cases for SLNM. Patient and tumor characteristics, according to the 7th edition of the TNM classification, are shown in table 4.1, which does not include the ultrastaging results from SLNM.

Three blue lymph nodes closest to the tumor, defined as the SLNs, are successfully identified in all included patients. In nine patients at least one blue node also

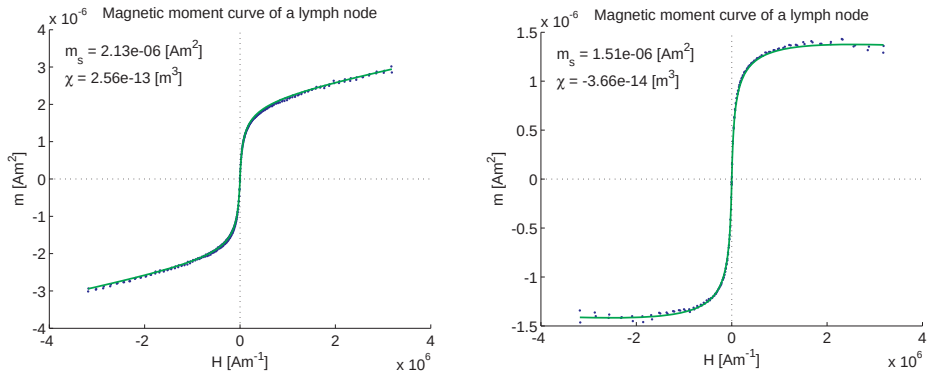

Figure 4.2: *Two representative examples of a VSM measurement of a lymph node. Endorem content corresponds with (a) 27.7 μg and (b) 19.6 μg iron. The green line indicates the model applied to the data points measured, including a nonlinear component with magnetic moment saturation m_s and a linear component (χ). The value of m_s is used to quantify the iron content in the sample. Both samples show a different linear component caused by different contributions of tissue due to lymph node size and sample holder tuning.*

contained Endorem as could be measured by VSM. In total 19 of the selected 33 SLNs (57.6%) contained Endorem particles. The quantified Endorem content in those nodes ranged between 1.1 and 51.4 μg iron (figure 4.2). The presence of iron was confirmed by microscopic analysis with Perl's Prussian Blue. In eight patients, the particles were located in the deeper and/or subcapsular sinuses of the SLNs (see figure 4.3). In one patient some groups of macrophages stained positive for iron, while the sinuses did not show positivity. In only one patient neither VSM nor microscopy revealed Endorem particles in one of the SLNs.

In one patient regular microscopic analysis of all lymph nodes by H&E staining indicated metastases in four non-SLNs, whereas two of the SLNs where involved. The other patients had no tumor involvement of both non-SLNs and SLNs on conventional histopathological analysis (N0).

Using additional microscopy techniques, MM (0.2-2 mm) were detected in two patients and ITC were detected in two patients (see figure 4.4). These findings of occult tumor cells in 44% of conventionally node negative patients can be solely ascribed to the focused staging procedure using SLNM and immunohistochemistry. Since the SLNs are only selected using blue dye, the main question in this study is whether the Endorem containing SLNs have the same predictive value. In the present study, the four patients having occult metastases would also have been upstaged if Endorem was used to select SLNs. Occult metastases were detected in SLNs over the full range of iron content (1.1-51.4 μg). In two patients, occult metastases were

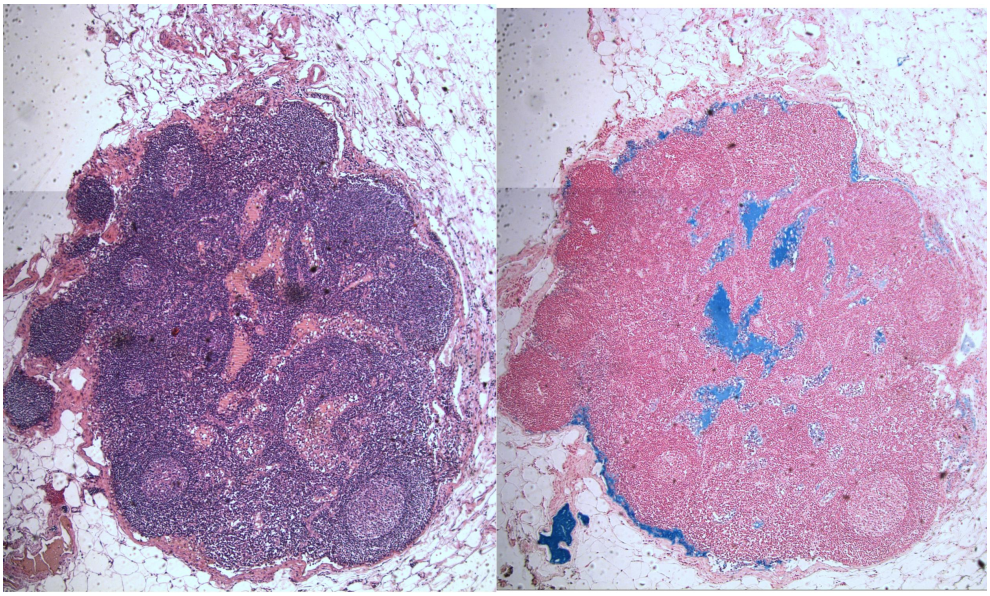

Figure 4.3: *Left: Microscopic H&E slice of an iron containing SLN (7 µg Fe). Right: Perl's Prussian Blue stained slice at approximately the same level as the H&E slice. Blue coloration indicates the presence of iron in the sinuses. (Magnification 40x)*

found in an SLN not containing Endorem. However, at least one of the other Endorem containing nodes from those patients, did also present the same level of occult metastases (MM or ITC) and therefore accurately predicted nodal status.

4.4 Discussion

Since single-level sectioning and H&E-staining of lymph nodes as current standard underestimates the true incidence of tumor cell metastases [12], the implementation of an additional optimal and effective SLNM procedure has to be considered in its various approaches. In this chapter, it is shown that Endorem is a potential tracer that can be used in *ex vivo* SLNM in colorectal cancer. VSM was able to discriminate the nonlinear magnetic component of the tracer from the diamagnetic component from tissue. In only one patient Endorem was not detected in the three blue SLNs. An identification rate of 91% for Endorem in eleven cases is rather good considering the fact that there is a learning-curve effect [9, 10, 21, 25]. The Endorem containing nodes accurately predicted the nodal status of the nodal basin in all patients. The same patients were upstaged by the presence of iron as by Patent Blue. The iron quantity in the lymph nodes was not predictive for the presence of metastases.

The *ex vivo* performance of the procedure did not hamper the distribution of

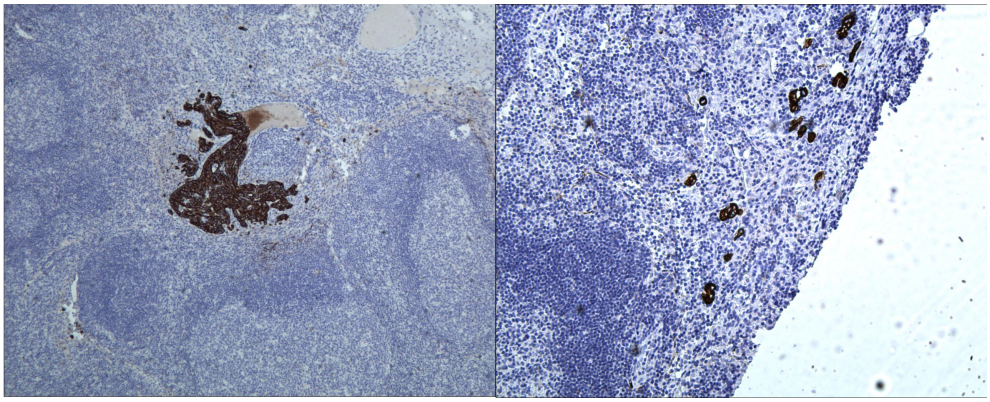

Figure 4.4: *Left: Cam5.2 stained slice showing a micrometastasis of 1.5 mm. (Magnification 40x) Right: Cam5.2 stained slice displaying clusters of isolated tumor cells. (Magnification 100x)*

magnetic nanoparticles through the lymphatic system. *Ex vivo* blue dye migration through the lymphatic system was also observed in other studies [4, 24, 46, 47]. To our knowledge, a complete *ex vivo* SLNM in CRC procedure using a suspension of nanoparticles has not been shown before. Studies with technetium nanocolloid exclusively perform *in vivo* injection [12, 22, 23, 25, 27, 39, 40, 48–53]. The *ex vivo* use of magnetic nanoparticles has many advantages over both technetium and blue dye. The fluidic and magnetic stability of the tracer is shown by limited uptake in only a few nodes, most likely the true SLNs, and by lasting magnetic detectability after surgery and fixation. The safe character and long shelf life of iron oxide does not require complex logistics and safety procedures. Both magnetic detection as well as histologic staining can reveal the presence of superparamagnetic tracer in an SLN. The *ex vivo* application and short time of tracer processing of about 10-15 minutes, explains the interstitial distribution through the sinuses with macrophage uptake in only one patient.

There are many studies about SLNM in CRC using different definitions and methods to select the SLNs. In our study, we chose for practical reasons the three blue nodes closest to the tumor, a variant of definitions used in other studies as well [18, 20, 22, 28, 39, 47, 54] and close to the mean number of SLNs found in most studies [9, 10]. Ideally the magnetic and blue tracer would have been found in the same lymph nodes, i.e. the SLNs. The reason that not all blue SLNs contained iron can be twofold: 1. some of the blue SLNs are not true SLNs (i.e. higher echelon nodes) and are therefore not reached by a more selective tracer [3, 15, 22, 23, 49, 55] with magnetic nanoparticles; 2. the *ex vivo* circumstances reduce the number of true SLNs to be reached by Endorem compared to blue dye, and thus the SLNM with SPIO has failed. Furthermore, some nodes may have been reached by Endorem, but were not

identified as SLNs by blue dye, because they were not blue or exceeded the maximum number of three blue SLNs nearest to the tumor. Since not all harvested LNs were investigated for iron presence, these nodes remain magnetically undetected, although they can be true SLNs. Ideally, all lymph nodes would have been subjected to magnetometry for SLN selection. However, during this study a magnetometer that could quickly measure all LNs, preferably in clinical setting, was not available. Therefore, only the three blue LNs defined as the SLNs, also most probably containing iron, were selected for magnetic assessment by VSM.

Other studies using combined tracers found differences in performance as well. Merrie *et al.*, even using a mixed radiocolloid and blue dye tracer, reported disagreement of hot and blue nodes with only 51% of the blue nodes being radioactive and 19% of the radioactive nodes not being blue [40]. Saha *et al.* found 56% of 156 SLNs detected by only blue dye and 2.6% by only radiocolloid. In addition, they concluded that the radioactive nodes are more likely the true SLNs, since these nodes were histologically positive with higher likelihood compared to the SLNs detected by blue dye only [55]. Patten *et al.* found 54% of 193 blue SLNs to be radioactive and 10 additional SLNs detected by gamma-probe only [51]. Another study found 16.5% and 5.8% of all SLNs detected by only blue dye or radionuclides, respectively [25]. The use of a combined or more selective tracer could reduce the false negative rates and improve accuracy of SLNM. The advantage of a dual tracer with different detection principles is shown by Sandrucci et al. They also found differences in tracer distribution of blue dye and technetium labeled albumin colloid, but even blue and hot SLNs were not always detected by both methods. Blue dye allowed selection of one more SLN, whereas radionuclides localized 14 more SLNs in 31 patients. The detection of these blue and hot nodes can be attributed to the higher penetration depth of radioactive detection, where visual assessment fails [39].

The use of a superparamagnetic tracer is technically a good alternative for the less popular technetium colloid and the fluidic blue dye. Unlike technetium, the SPIO tracer can be safely applied by the surgeon, without the need of qualified personnel, complex safety regulations and logistics [23, 31, 39, 55, 56]. Using dedicated detection technology, SPIO tracer can be detected with comparable penetration depth. The formalin fixation of the specimen was not destructive to the magnetic nanoparticles, which might therefore compensate for errors caused by blue dye elution [21]. The search for blue nodes in SLNM procedures can be hampered in a thick mesentery by the limited penetration depth of visual inspection [2, 23, 25, 29, 31, 50], requiring SLN identification in the formalin-fixated specimen at dissection [18, 49]. Tracers that are detectable with more penetration depth are beneficial in these cases [31]. The physical stability of magnetic nanoparticles in SLNM can resolve this issue, since it enables lasting post-operative quantitative detection with relatively large penetration depth. In addition, the mesenteric lymph nodes are often found to be non-palpable

and smaller than 5 mm and are therefore easily overlooked [12, 18, 21, 51, 56, 57]. A magnetometer, analog to the handheld gamma-probe [29, 39, 50], that can quantitatively detect tiny amounts of magnetic tracer in these lymph nodes *in situ*, can contribute to increased SLN identification and decreased false negative rates.

In this study the SLNM procedure was performed entirely *ex vivo*. The reduced complexity, especially in laparoscopic interventions, as well as the eliminated risk of adverse reactions or harming the patient, argues for the use of an *ex vivo* approach for SLNM in CRC [9, 31, 56]. Furthermore, in studies using blue dye, the *ex vivo* mapping method was found to be as good as the *in vivo* method [24, 46, 54]. *ex vivo* injection of colloidal radionuclides is not reported, but may result in a lower identification rate or accuracy. However, the present study shows that a colloidal tracer can point out the SLN after *ex vivo* injection. In most studies, *in vivo* SLNM is preferred, since it might reveal the presence of aberrant lymphatic drainage which gives the possibility to adjust the planned resection area [20]. Aberrant lymphatic drainage can be observed preoperatively by lymphoscintigraphy after endoscopic *in vivo* injection of radionuclides [15, 58]. Using various SLNM methods, aberrant drainage is reported in 8 studies in a rather broad range of 1.6-22% of all patients, with a mean rate of about 5% [10, 59]. In the study with the highest rate of 22%, 10% of the SLNs identified outside the planned resection area were metastatic [59]. After local *in vivo* injection of SPIO tracer, a preoperative MRI can be used to localize sentinel nodes [60, 61]. After endoscopic administration of SPIO tracer in CRC, preoperative MRI might provide information about aberrant lymphatic drainage and possibly also about lymph node status.

Ex vivo procedures can also be in favor of *in vivo* procedures, because the tumor containing specimen can be brought to a separate (non-sterile) field for injection [4, 16, 17, 26, 54] and inspection [24, 47]. This facilitates the SLNM procedure, because the sample is easily accessible, the subserosal or submucosal injection sites can be easily chosen, risks of tumor cell shedding are eliminated [3, 17] and the surgical procedure is not necessarily delayed by tracer flow and SLN identification [18, 54, 56]. The use of a fully intra-operative *in vivo* procedure most often requires 10-15 min costly operating time [3, 20] inducing potential morbidity [47]. Therefore the development of a clinical magnetic SLNM method in CRC that minimizes intra-operative procedures, while conserving accuracy, can significantly contribute to a cost-effective additional tool in routine CRC treatment [18, 24, 47].

Several aspects regarding the SPIO tracer can potentially be improved. The injection volume of magnetic tracer was in the range of what is mostly used with the regular tracers, but may influence the identification rate [62]. Furthermore, Endorem was chosen because of commercial availability and approval for clinical use. The particle size of this tracer is not optimized for (*ex vivo*) SLNM in CRC. Regarding the use of radionuclides in SLNM, Wilhelm and colleagues concluded that the distribution

of administered particles heavily depends on the particle size. Particles larger than 100 nm usually become trapped in the interstitial space and will not enter the lymphatic system and an optimal particle size between 10 and 50 nm was suggested [63]. Another study investigated SLNM in gastric cancer after pre-operative submucosal technetium injection, using colloid sizes of 500, 100 and 50 nm respectively. They found identification rate, number of SLNs and radioisotope uptake to be significantly lower for 500 nm colloid and recommended the 100 nm colloid for SLNM in gastric cancer [64]. In a study of SLNM in breast cancer by Sato et al., transmission electron microscopy revealed optimal uptake of radiocolloid in the range of 100-150 nm [65]. Although the hydrodynamic size of Endorem nanoparticles [41, 42] is roughly within the range investigated in these studies, optimizing the particle size of the magnetic tracer might result in a higher magnetic yield in the SLNs and more specificity for the first echelon node.

The magnetic nanoparticles in the tracer can be very well detected by the nonlinear magnetic response in contrast to the linear response of tissue. The nonlinear response of superparamagnetic iron oxide nanoparticles depends on the diameter of the cores. The magnetization of particles with a large diameter saturates at lower fields compared to smaller core sizes. A clinical magnetometer that has to be developed for magnetic SLNM in CRC, should exploit this characteristic to achieve maximum sensitivity and specificity. The magnetic excitation fields needed for optimal detection of the nonlinear response, depend on the tracer that is used for SLNM. Therefore, both tracer and magnetic detection system have to be optimized for the procedure to achieve sensitive and specific detection. Techniques like AC-susceptometry using frequency mixing or magnetic particle imaging, are specifically designed to detect the nonlinear magnetic properties of superparamagnetic tracer [66, 67]. A clinical magnetometer for SLNM in CRC requires at least a detection limit of 1 μg iron, according to what is found in the this study. An handheld probe can be used to search for magnetic lymph nodes in the specimen, which facilitates the surgeon or pathologist to find at least the most important lymph nodes. In addition, a clinical magnetometer that is simpler in use and faster to accurately detect superparamagnetic tracer compared to the VSM, will provide quick selection of a few magnetic SLNs out of a large number of harvested LNs in regional lymphadenectomy. Since magnetometers, comparable to the commercially available Sentimag demonstrated in [68], can be developed for relatively low costs, the clinical practice of magnetic SLNM in colorectal cancer can be initiated soon.

4.5 Conclusion

In *ex vivo* SLNM in colorectal cancer, the superparamagnetic tracer Endorem has shown to be a feasible tracer. Using blue dye to select the SLNs, magnetic tracer

was detected in 91% of the procedures and in 57.6% of the selected blue SLNs. This probably indicates more selectivity of magnetic tracer for sentinel nodes. At least one of the Endorem containing nodes accurately predicted nodal status of the patients by ultrastaging. The iron presence varied in the range of 1.1-51.4 μg, which gives a first indication for the required sensitivity of a clinical magnetometer for routine application. The physical stability, the mild safety aspects and simple logistics of superparamagnetic iron oxide tracer, indicate this to be a promising alternative colloidal tracer in SLNM in colorectal cancer.

References

[1] W. H. O. World Health Organization, "Global Health Observatory (GHO) - The data repository", (2008).

[2] S. Saha, A. G. Dan, A. J. Bilchik, Y. Kitagawa, E. Schochet, S. Choudhri, L. T. Saha, D. Wiese, D. Morton, and M. Kitajima, "Historical review of lymphatic mapping in gastrointestinal malignancies", Annals of Surgical Oncology **11**, 245S–249S (2004).

[3] J. Mulsow, D. C. Winter, J. C. O'Keane, and P. R. O'Connell, "Sentinel lymph node mapping in colorectal cancer", British Journal of Surgery **90**, 659–667 (2003).

[4] J. Wong, D. S. Johnson, T. Namiki, and P. Tauchi-Nishi, "Validation of ex vivo lymphatic mapping in hematoxylin-eosin node-negative carcinoma of the colon and rectum", Annals of Surgical Oncology **11**, 772–777 (2004).

[5] P. J. Tanis, O. E. Nieweg, R. A. Valds Olmos, and B. B. R. Kroon, "Anatomy and physiology of lymphatic drainage of the breast from the perspective of sentinel node biopsy", Journal of the American College of Surgeons **192**, 399–409 (2001).

[6] M. R. S. Keshtgar and P. J. Ell, "Sentinel lymph node detection and imaging", European Journal of Nuclear Medicine **26**, 57–67 (1999).

[7] H. Schraffordt Koops, M. H. E. Doting, J. de Vries, A. T. M. G. Tiebosch, J. T. Plukker, H. J. Hoekstra, and D. A. Piers, "Sentinel node biopsy as a surgical staging method for solid cancers", Radiotherapy and Oncology **51**, 1–7 (1999).

[8] I. M. C. Van der Ploeg, O. E. Nieweg, B. B. R. Kroon, E. J. T. Rutgers, M.-J. T. F. D. Baas-Vrancken Peeters, W. V. Vogel, C. A. Hoefnagel, and R. A. Valds Olmos, "The yield of SPECT/CT for anatomical lymphatic mapping in patients with breast cancer", European Journal of Nuclear Medicine and Molecular Imaging **36**, 903–909 (2009).

[9] M. H. G. M. Van der Pas, S. Meijer, O. S. Hoekstra, I. I. Riphagen, H. C. W. de Vet, D. L. Knol, N. C. T. van Grieken, and W. J. H. J. Meijerink, "Sentinel-lymph-node procedure in colon and rectal cancer: a systematic review and meta-analysis", The Lancet Oncology **12**, 540–550 (2011).

[10] E. S. Van der Zaag, W. H. Bouma, P. J. Tanis, D. T. Ubbink, W. A. Bemelman, and C. J. Buskens, "Systematic review of sentinel lymph node mapping procedure in colorectal cancer", Annals of Surgical Oncology **19**, 3449–3459 (2012).

[11] A. Figueredo, M. E. Coombes, and S. Mukherjee, "Adjuvant therapy for completely resected stage II colon cancer", Cochrane Database of Systematic Reviews **3**, The Cochrane Library, Issue 4 (2008).

[12] A. J. Bilchik, D. T. Nora, L. H. Sobin, R. R. Turner, S. Trocha, D. Krasne, and D. L. Morton, "Effect of lymphatic mapping on the new Tumor-Node-Metastasis classification for colorectal cancer", Journal of Clinical Oncology **21**, 668–672 (2003).

[13] E. S. Van der Zaag, W. H. Bouma, H. M. Peters, W. A. Bemelman, and C. J. Buskens, "Implications of sentinel lymph node mapping on nodal staging and prognosis in colorectal cancer", Colorectal Disease **14**, 684–690 (2012).

[14] D. Iddings, A. Ahmad, D. Elashoff, and A. Bilchik, "The prognostic effect of micrometastases in previously staged lymph node negative N0 colorectal carcinoma: A meta-analysis", Annals of Surgical Oncology **13**, 1386–1392 (2006).

[15] R. J. De Haas, D. A. Wicherts, M. G. Hobbelink, I. H. Borel Rinkes, M. E. Schipper, J. A. van der Zee, and R. van Hillegersberg, "Sentinel lymph node mapping in colon cancer: current status", Annals of Surgical Oncology **14**, 1070–1080 (2007).

[16] A. J. Bilchik, D. S. B. Hoon, S. Saha, R. R. Turner, D. Wiese, M. DiNome, K. Koyanagi, M. McCarter, P. Shen, D. Iddings, S. L. Chen, M. Gonzalez, D. Elashoff, and D. L. Morton, "Prognostic impact of micrometastases in colon cancer: Interim results of a prospective multicenter trial", Annals of Surgery **246**, 568–577 (2007).

[17] J. H. Wong, S. Steineman, C. Calderia, J. Bowles, and T. Namiki, "Ex vivo sentinel node mapping in carcinoma of the colon and rectum", Annals of Surgery **233**, 515–521 (2001).

[18] A. E. Faerden, O. Sjo, S. N. Andersen, B. Hauglann, N. Nazir, B. Gravedaug, I. Moberg, A. Svinland, A. Nesbakken, and A. Bakka, "Sentinel node mapping does not improve staging of lymph node metastasis in colonic cancer", Diseases of the Colon and Rectum **51**, 891–896 (2008).

[19] A. J. C. C. American Joint Committee on Cancer, "AJCC cancer staging manual, 7th edition", (2009).

[20] S. Saha, D. Wiese, J. Badin, T. Beutler, D. Nora, B. K. Ganatra, D. Desai, S. Kaushal, M. Nagaraju, M. Arora, and T. Singh, "Technical details of sentinel lymph node mapping in colorectal cancer and its impact on staging", Annals of Surgical Oncology **7**, 120–124 (2000).

[21] J. Paramo, J. Summerall, R. Poppiti, and T. Mesko, "Validation of sentinel node mapping in patients with colon cancer", Annals of Surgical Oncology **9**, 550–554 (2002).

[22] C. A. Quadros, A. Lopes, I. Araujo, J. H. Fregnani, and F. Fahel, "Upstaging benefits and accuracy of sentinel lymph node mapping in colorectal adenocarcinoma nodal staging", Journal of Surgical Oncology **98**, 324–330 (2008).

[23] S. Trocha, D. Nora, S. Saha, D. Morton, D. Wiese, and A. Bilchik, "Combination probe and dye-directed lymphatic mapping detects micrometastases in early colorectal cancer", Journal of Gastrointestinal Surgery **7**, 340–346 (2003).

[24] S. W. Bell, N. Mourra, J. F. Fljou, R. Parc, and E. Tiret, "Ex vivo sentinel lymph node mapping in colorectal cancer", Diseases of the Colon and Rectum **48**, 74–79 (2005).

[25] S. E. Terwisscha van Scheltinga, F. C. Den Boer, R. Pijpers, G. A. Meyer, A. F. Engel, R. Silvis, S. Meijer, and J. R. van der Sijp, "Sentinel node staging in colon carcinoma: value of sentinel lymph node biopsy with radiocolloid and blue staining", Scandinavian Journal of Gastroenterology. Supplement **41**, 153–157 (2006).

[26] T. F. Wood, D. T. Nora, D. L. Morton, R. R. Turner, D. Rangel, W. Hutchinson, and A. J. Bilchik, "One hundred consecutive cases of sentinel lymph node mapping in early colorectal carcinoma: Detection of missed micrometastases", Journal of Gastrointestinal Surgery **6**, 322–330 (2002).

[27] P. Covarelli, R. Cristofani, C. Boselli, A. Servoli, M. F. Burattini, M. Badolato, C. Cini, L. Finocchi, and G. Noya, "Preliminary study on radioguided sentinel node identification in colon cancer", The American Surgeon **73**, 222–226 (2007).

[28] E. S. Van der Zaag, N. Kooij, M. J. van de Vijver, W. A. Bemelman, H. M. Peters, and C. J. Buskens, "Diagnosing occult tumour cells and their predictive value in sentinel nodes of histologically negative patients with colorectal cancer", European Journal of Surgical Oncology (EJSO) **36**, 350–357 (2010).

[29] Y. Kitagawa and M. Kitajima, "Gastrointestinal cancer and sentinel node navigation surgery", Journal of Surgical Oncology **79**, 188–193 (2002).

[30] D. Lips, B. Koebrugge, G. Jan Liefers, J. van de Linden, V. Smit, H. Pruijt, H. Putter, C. van de Velde, and K. Bosscha, "The influence of micrometastases on prognosis and survival in stage I-II colon cancer patients: The Enroute+ Study", BMC Surgery **11**, 11 (2011).

[31] A. Bembenek, A. String, S. Gretschel, and P. M. Schlag, "Technique and clinical consequences of sentinel lymph node biopsy in colorectal cancer", Surgical Oncology **17**, 183–193 (2008).

[32] R. A. Cahill, M. Anderson, L. Wang, I. Lindsey, C. Cunningham, and N. J. Mortensen, "Near-infrared (NIR) laparoscopy for intraoperative lymphatic road-mapping and sentinel node identification during definitive surgical resection of early-stage colorectal neoplasia", Surgical Endoscopy **26**, 197–204 (2012).

[33] M. Hutteman, H. Choi, J. S. Mieog, J. Vorst, Y. Ashitate, P. K. Kuppen, M. Groningen, C. G. M. Löwik, V. H. B. M. Smit, C. H. Velde, J. Frangioni, and A. Vahrmeijer, "Clinical translation of ex vivo sentinel lymph node mapping for colorectal cancer using invisible near-infrared fluorescence light", Annals of Surgical Oncology **18**, 1006–1014 (2011).

[34] L. Johnson, Q. Pankhurst, A. Purushotham, A. Brazdeikis, and M. Douek, "Magnetic sentinel lymph node detection for breast cancer", Cancer Research **70**, P1–01–23 (2011).

[35] T. Joshi, Q. Pankhurst, S. Hattersley, A. Brazdeikis, M. Hall-Craggs, E. De Vita, A. Bainbridge, R. Sainsbury, A. Sharma, and M. Douek, "Magnetic nanoparticles for detecting cancer spread", 30th Annual San Antonio Breast Cancer Symposium December 1316, 2007 - Breast Cancer Research and Treatment **106**, S129 (2007).

[36] Y. Minamiya, M. Ito, Y. Katayose, H. Saito, K. Imai, Y. Sato, and J. I. Ogawa, "Intraoperative sentinel lymph node mapping using a new sterilizable magnetometer in patients with nonsmall cell lung cancer", Annals of Thoracic Surgery **81**, 327–330 (2006).

[37] T. Nakagawa, Y. Minamiya, Y. Katayose, H. Saito, K. Taguchi, H. Imano, H. Watanabe, K. Enomoto, M. Sageshima, T. Ueda, and J. I. Ogawa, "A novel method for sentinel lymph node mapping using magnetite in patients with non-small cell lung cancer", Journal of Thoracic and Cardiovascular Surgery **126**, 563–567 (2003).

[38] M. Shiozawa, A. T. Lefor, Y. Hozumi, K. Kurihara, N. Sata, Y. Yasuda, and M. Kusakabe, "Sentinel lymph node biopsy in patients with breast cancer using superparamagnetic iron oxide and a magnetometer", Breast Cancer 1–7 (2012).

[39] S. Sandrucci, B. Mussa, M. Goss, M. Mistrangelo, M. A. Satolli, A. Sapino, M. Bell, G. Bisi, and A. Mussa, "Lymphoscintigraphic localization of sentinel node in early colorectal cancer: Results of a monocentric study", Journal of Surgical Oncology **96**, 464–469 (2007).

[40] A. E. H. Merrie, A. M. Rij, L. V. Phillips, J. I. Rossaak, K. Yun, and J. L. McCall, "Diagnostic use of the sentinel node in colon cancer", Diseases of the Colon and Rectum **44**, 410–417 (2001).

[41] H. Y. Lee, S. H. Lee, C. Xu, J. Xie, J. H. Lee, B. Wu, A. Leen Koh, X. Wang, R. Sinclair, S. X. Wang, D. G. Nishimura, S. Biswal, S. Sun, S. H. Cho, and X. Chen, "Synthesis and characterization of PVP-coated large core iron oxide nanoparticles as an MRI contrast agent", Nanotechnology **19** (2008).

[42] I. Raynal, P. Prigent, S. Peyramaure, A. Najid, C. Rebuzzi, and C. Corot, "Macrophage endocytosis of superparamagnetic iron oxide nanoparticles: Mechanisms and comparison of ferumoxides and ferumoxtran-10", Investigative Radiology **39**, 56–63 (2004).

[43] L. F. Gamarra, G. E. S. Brito, W. M. Pontuschka, J. B. Mamani, C. A. Moreira-Filho, and E. Amaro Jr, "Study of the ferrofluid drying process for morphological and nanostructural characterization", Brazilian Journal of Physics **37**, 1288–1291 (2007).

[44] C. W. Jung and P. Jacobs, "Physical and chemical properties of superparamagnetic iron oxide MR contrast agents: Ferumoxides, ferumoxtran, ferumoxsil", Magnetic Resonance Imaging **13**, 661–674 (1995).

[45] J. E. Lima, A. L. Brandl, A. D. Arelaro, and G. F. Goya, "Spin disorder and magnetic anisotropy in Fe_3O_4 nanoparticles", Journal of Applied Physics **99**, 083908–10 (2006).

[46] T. F. Wood, S. Saha, D. L. Morton, G. J. Tsioulias, D. Rangel, J. Hutchinson W, L. J. Foshag, and A. J. Bilchik, "Validation of lymphatic mapping in colorectal cancer: In vivo, ex vivo, and laparoscopic techniques", Annals of Surgical Oncology **8**, 150–157 (2001).

[47] P. M. Van Schaik, J. C. van der Linden, M. F. Ernst, W. A. H. Gelderman, and K. Bosscha, "Ex vivo sentinel lymph node "mapping" in colorectal cancer", European Journal of Surgical Oncology **33**, 1177–1182 (2007).

[48] A. Bembenek, B. Rau, T. Moesta, J. Markwardt, C. Ulmer, S. Gretschel, U. Schneider, W. Slisow, and P. M. Schlag, "Sentinel lymph node biopsy in rectal cancer - not yet ready for routine clinical use", Surgery **135**, 498–505 (2004).

[49] K. Dahl, J. Westlin, W. Kraaz, O. Winqvist, L. Bergkvist, and M. Thörn, "Identification of sentinel nodes in patients with colon cancer", European Journal of Surgical Oncology (EJSO) **31**, 381–385 (2005).

[50] Y. Kitagawa, M. Watanabe, H. Hasegawa, S. Yamamoto, H. Fujii, K. Yamamoto, J.-i. Matsuda, M. Mukai, A. Kubo, and M. Kitajima, "Sentinel node mapping for colorectal cancer with radioactive tracer", Diseases of the Colon and Rectum **45**, 1476–1480 (2002).

[51] L. C. Patten, D. H. Berger, M. Rodriguez-Bigas, P. Mansfield, E. Delpassand, K. R. Cleary, S. P. Fagan, S. A. Curley, K. K. Hunt, and B. W. Feig, "A prospective evaluation of radiocolloid and immunohistochemical staining in colon carcinoma lymphatic mapping", Cancer **100**, 2104–2109 (2004).

[52] O. Tiffet, D. Kaczmarek, M. L. Chambonnière, T. Guillan, S. Baccot, N. Prévot, S. Bageacu, E. Bourgeois, E. Cassagnau, P. A. Lehur, and F. Dubois, "Combining radioisotopic and blue-dye technique does not improve the false-negative rate in sentinel lymph node mapping for colorectal cancer", Diseases of the Colon and Rectum **50**, 962–970 (2007).

[53] S. J. Lim, B. W. Feig, H. Wang, K. K. Hunt, M. A. Rodriguez-Bigas, J. M. Skibber, V. Ellis, K. Cleary, and G. J. Chang, "Sentinel lymph node evaluation does not improve staging accuracy in colon cancer", Annals of Surgical Oncology **15**, 46–51 (2008).

[54] J. J. Tuech, P. Pessaux, F. Di Fiore, V. Nitu, B. Lefebure, A. Colson, and F. Michot, "Sentinel node mapping in colon carcinoma: In-vivo versus ex-vivo approach", European Journal of Surgical Oncology **32**, 158–161 (2006).

[55] S. Saha, A. Dan, B. Berman, D. Wiese, E. Schochet, K. Barber, S. Choudhri, S. Kaushal, B. Ganatra, D. Desai, M. Nagaraju, and S. Mannam, "Lymphazurin 1% versus 99mTc sulfur colloid for lymphatic mapping in colorectal tumors: A comparative analysis", Annals of Surgical Oncology **11**, 21–26 (2004).

[56] A. Stojadinovic, P. J. Allen, M. Protic, J. F. Potter, C. D. Shriver, J. M. Nelson, and G. E. Peoples, "Colon sentinel lymph node mapping: Practical surgical applications", Journal of the American College of Surgeons **201**, 297–313 (2005).

[57] J. P. Tiernan, I. Ansari, N. A. Hirst, P. A. Millner, T. A. Hughes, and D. G. Jayne, "Intra-operative tumour detection and staging in colorectal cancer surgery", Colorectal Disease **14**, e510–e520 (2012).

[58] R. J. De Haas, D. A. Wicherts, M. G. Hobbelink, P. J. van Diest, F. P. Vleggaar, I. H. Borel Rinkes, and R. van Hillegersberg, "Sentinel lymph node mapping in colon cancer using radiocolloid as a single tracer: a feasibility study", Nuclear Medicine Communications **33**, 832–837 (2012).

[59] S. Saha, G. Johnston, A. Korant, M. Shaik, M. Kanaan, R. Johnston, B. Ganatra, S. Kaushal, D. Desai, and S. Mannam, "Aberrant drainage of sentinel lymph nodes in colon cancer and its impact on staging and extent of operation", The American Journal of Surgery **205**, 302–306 (2013).

[60] M. Shiozawa, S. Kobayashi, Y. Sato, H. Maeshima, Y. Hozumi, A. T. Lefor, K. Kurihara, N. Sata, and Y. Yasuda, "Magnetic resonance lymphography of sentinel lymph nodes in patients with breast cancer using superparamagnetic iron oxide: a feasibility study", Breast Cancer 1–8 (2012).

[61] D. Mizokami, S. Kosuda, M. Tomifuji, K. Araki, T. Yamashita, H. Shinmoto, and A. Shiotani, "Superparamagnetic iron oxide-enhanced interstitial magnetic resonance lymphography to detect a sentinel lymph node in tongue cancer patients", Acta Oto-Laryngologica **133**, 418–423 (2012).

[62] C. T. Viehl, C. T. Hamel, W. R. Marti, U. Guller, L. Eisner, U. Stammberger, L. Terracciano, H. P. Spichtin, F. Harder, and M. Zuber, "Identification of sentinel lymph nodes in colon cancer depends on the amount of dye injected relative to tumor size", World Journal of Surgery **27**, 1285–1290 (2003).

[63] A. J. Wilhelm, G. S. Mijnhout, and E. J. F. Franssen, "Radiopharmaceuticals in sentinel lymph-node detection - an overview", European Journal of Nuclear Medicine **26** (1999).

[64] Y. Uenosono, S. Natsugoe, H. Higashi, K. Ehi, F. Miyazono, S. Ishigami, S. Hokita, and T. Aikou, "Evaluation of colloid size for sentinel nodes detection using radioisotope in early gastric cancer", Cancer Letters **200**, 19–24 (2003).

[65] K. Sato, D. Krag, K. Tamaki, M. Anzai, H. Tsuda, S. Kosuda, S. Kusano, H. Hiraide, and H. Mochizuki, "Optimal particle size of radiocolloid for sentinel node identification in breast cancer electron microscopic study and clinical comparison", Breast Cancer **11**, 256–263 (2004).

[66] B. Gleich and J. Weizenecker, "Tomographic imaging using the nonlinear response of magnetic particles", Nature **435**, 1214–1217 (2005).

[67] H. J. Krause, N. Wolters, Y. Zhang, A. Offenhusser, P. Miethe, M. H. F. Meyer, M. Hartmann, and M. Keusgen, "Magnetic particle detection by frequency mixing for immunoassay applications", Journal of Magnetism and Magnetic Materials **311**, 436–444 (2007).

[68] B. Anninga, M. Ahmed, M. Hemelrijck, J. Pouw, D. Westbroek, S. Pinder, B. Haken, Q. Pankhurst, and M. Douek, "Magnetic sentinel lymph node biopsy and localization properties of a magnetic tracer in an in vivo porcine model", Breast Cancer Research and Treatment 1–10 (2013).

5

Selective detection of magnetic nanoparticles in biomedical applications using differential magnetometry*

Abstract: This chapter describes a new concept of magnetic detection that can be used for fast, selective measurements on magnetic nanoparticles and which is not influenced by the presence of materials with a linear magnetic susceptibility, like tissue. Using an alternating excitation field ($f \sim 5$kHz) with a sequence of static offset fields, the magnetometer is selectively sensitive for the nonlinear properties of magnetic nanoparticles in samples. The offset field sequence modulates the measured inductive response of nonlinear magnetic materials, in contrast to linear magnetic materials. We demonstrate a detection limit for superparamagnetic iron oxide nanoparticles in the sub-microgram (iron) range. The mass sensitivity of the procedure increases with offset field amplitude and particle size. Compared to the sensitivity for particles in suspension, the sensitivity reduces for particles accumulated in lymph node tissue or immobilized by drying, which is attributed to a change in Brownian relaxation. The differential magnetometry concept is used as a tool to perform non-destructive analysis of magnetic nanoparticles in clinically relevant tissue samples at room temperature. In addition, the differential magnetometer can be used for fundamental quantitative research of the performance of magnetic nanoparticles in alternating fields. The method is a promising approach for in vivo measurements during clinical interventions, since it suppresses the linear contribution of the surrounding body volume and effectively picks out the nonlinear contribution of magnetic tracer.

*This chapter is published as: M. Visscher, S. Waanders, H.J.G. Krooshoop, B. ten Haken, Selective detection of magnetic nanoparticles in biomedical applications using differential magnetometry, 2014, Journal of Magnetism and Magnetic Materials, Vol.365, p31-39, ISSN 0304-8853

5.1 Introduction

The development of applications with magnetic nanoparticles in biology and medicine arises from their typical magnetic properties that can be used for detection or manipulation [1, 2]. In applications like magnetic particle imaging (MPI) and magnetic resonance imaging (MRI), suspensions of superparamagnetic iron oxide (SPIO) nanoparticles are used as a tracer or contrast agent for imaging. The clinical usefulness of a tracer depends on the safety and bio-compatible properties, as well as the possibility to provide unique detection in contrast to the environment. The nonlinear magnetization of magnetic nanoparticles differs from the linear diamagnetism of tissue, which makes it suitable for accurate and sensitive detection. MRI contrast agents based on SPIO nanoparticles use the high magnetic susceptibility of the particles to increase proton relaxation [3]. Relaxometry on magnetic nanoparticles with SQUID based systems is used to investigate particle dynamics and interactions with bio-molecules, magnetic drug targeting and quantification of particles [4–9]. Since 2005, MPI has been developed as a new imaging modality that uses the typical nonlinear magnetic behavior of superparamagnetic nanoparticles in an alternating excitation field [10]. Furthermore, several studies have been published on intra-operative sentinel lymph node mapping using a magnetic tracer and a hand held probe [11, 12]. A handheld magnetic sensor is used to localize sentinel nodes containing magnetic nanoparticles, after a local injection of tracer. The mild safety aspects and physical characteristics of magnetic nanoparticles are an important driving factor behind the development of this new application. Only with excellent performance, the magnetic method may replace the existing and complicated use of radioactive tracers and blue dye that already offer high accuracy in lymph node mapping.

Although magnetic nanoparticles can be very helpful in interventions to determine optimal treatment routes and to localize and evaluate clinically interesting targets, their use in clinical interventions is still scarce. One of the reasons is the magnetic complexity of clinical settings, like an operating theater with all kinds of instrumentation. MRI or SQUID based techniques are difficult to implement in clinical interventions, because of their special requirements regarding magnetic field quality and adequate shielding. MRI and MPI are focusing on whole body imaging with relatively large magnetic fields. Smaller systems and handheld probes that enable local detection of magnetic nanoparticles during interventions with relatively low magnetic fields, are not well developed. In chapter 4 the detection and quantification of magnetic tracer in colorectal sentinel lymph nodes was performed using a vibrating sample magnetometer (VSM). The VSM is a typical laboratory instrument that is not suitable for clinical implementation. Measurements on individual lymph nodes took about 15 minutes and required high magnetic fields. These factors limit clinical use of the VSM technique. Therefore, development of a clinically suitable magnetometer was proposed, to realize specific and fast analysis of magnetic nanoparticles with

relatively low magnetic fields.

Inductive methods based on excitation with alternating magnetic fields are most suitable for detection of magnetic nanoparticles in larger tissue volumes, e.g. during interventions. The technique is fast and can operate with relatively low fields and without a magnetically shielded room. However, in simple alternating field magnetometry the linear magnetism of the body is also contributing to the signal, which prohibits selective detection of small amounts of magnetic tracer. To obtain a system with optimal sensitivity for magnetic particles in tissue, contributions from materials with a linear magnetic susceptibility have to be excluded from the detected signal. Existing techniques, like frequency mixing with alternating fields or MPI based methods, also exploit the nonlinear properties of magnetic nanoparticles with alternating field excitation [13, 14]. For larger samples and detection distances in clinical applications, these approaches are complicated, since they require high alternating field amplitudes for excitation and a large dynamic range for detection.

The purpose of this chapter is to investigate a new concept of magnetic nanoparticle detection for quick (quantitative) measurements which are not influenced by the presence of large tissue volumes. The aim of the concept is application in clinical interventions with a relatively inexpensive system using standard copper coils, low magnetic field amplitudes and low excitation frequencies.

Specific detection of nonlinear magnetism is achieved by probing the sample with a small alternating field and a sequence of static offset fields. The offset field saturates the magnetization of the nanoparticles and thus the response of the magnetic nanoparticles to the alternating field is modulated. This is expressed in a reduced voltage response in the induction coil. The amplitude of this signal modulation is linearly dependent on the amount of particles in the sample and can therefore be used for quantification. For characterization purposes, the magnetic response of particles to the alternating field can be measured at different offset field amplitudes. This provides information about nonlinear particle characteristics and optimal instrumentation settings for clinical applications.

5.2 Methods

5.2.1 Theory

Linear and nonlinear magnetization

The use of superparamagnetic nanoparticles for clinical purposes is driven by the beneficial nonlinear magnetization behavior that contrasts with the linear magnetic behavior of tissue. For materials with a linear magnetic susceptibility, the magnetization M_{lin} [Am^{-1}] is proportional to the applied magnetic field H [Am^{-1}] and can

be described by

$$M_{lin} = \chi H. \tag{5.1}$$

The (volume) susceptibility χ is positive for paramagnetic materials and negative for diamagnetic materials, the latter being more common in biomedical situations.

The susceptibility of superparamagnetic nanoparticles is nonlinear, which can be described by the Langevin function [15]. The average magnetization M_{MNP} of an ensemble of superparamagnetic nanoparticles as a function of the external field H is given by

$$M_{MNP}(xH) = M_s \left(\coth(xH) - \frac{1}{xH} \right), \tag{5.2}$$

with M_s is the saturation magnetization and

$$xH = \frac{m\mu_0 H}{k_B T}. \tag{5.3}$$

The constants μ_0, k_B and parameter T represent vacuum permeability, the Boltzmann constant and absolute temperature, respectively. The particle dependent parameter in the Langevin function is the magnetic moment m [Am^2]. The magnetic moment of a spherical superparamagnetic particle is related to its diameter D [m] by

$$m = \frac{\pi D^3 M_s}{6}. \tag{5.4}$$

using $\mu_0 M_s$= 0.55 T for Fe_3O_4/Fe_2O_3 [16, 17].

Equation 5.2 is defined for a single particle size. In practical situations, where samples contain an ensemble of particles with a lognormal size distribution, eq. 5.2 should be evaluated according to the actual particle size distribution [17].

Selective measurement of nonlinear magnetization

Alternating magnetic fields are commonly used to measure the magnetic susceptibility of samples. The material's response can simply be measured by a detection coil, according to Faraday's law of induction. Excitation with an alternating field is performed by a sinusoidally alternating excitation field

$$H(t) = H_0 \sin(\omega t), \tag{5.5}$$

with amplitude H_0 and angular frequency $\omega = 2\pi f$.

The sample's magnetization will change, according to its susceptibility, with the frequency of the alternating excitation field. The induction voltage in the coil is proportional to the time derivative of the magnetization

$$U(t) \propto \frac{dM}{dt}. \tag{5.6}$$

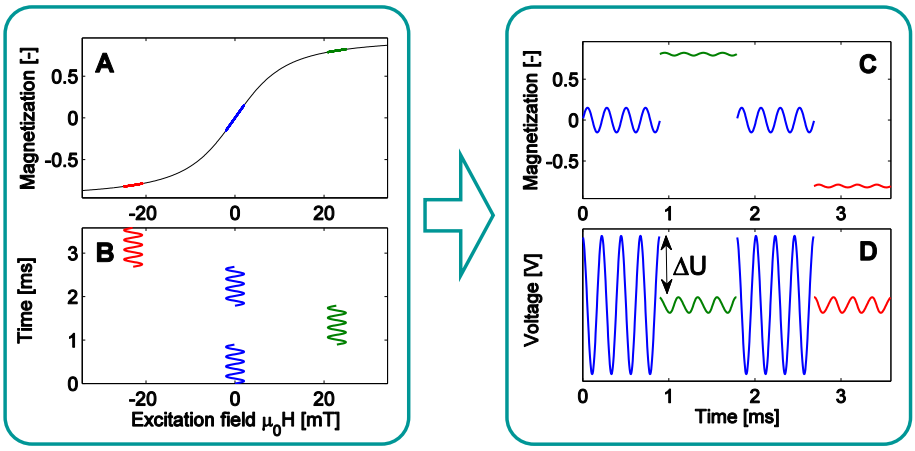

Figure 5.1: *The concept of differential magnetometry simulated for mono-disperse iron oxide particles with 16 nm diameter (A). The alternating excitation field is applied with intervals with a positive and negative offset field amplitude (B). The colors in each panel correspond with the offset field amplitude. Nonlinear magnetic susceptibility results in a reduced alternating magnetization response during periods with offset field (C), whichs is proportional to the ampltitude of inductively measured signal (D). The DiffMag voltage ΔU specifically represents the contribution from magnetic nanoparticles in a sample.*

In a tissue sample that contains superparamagnetic nanoparticles, both linear (M_{lin}) and nonlinear magnetization (M_{MNP}) contribute to the measured inductive voltage response.

$$M(t) = M_{lin}(t) + M_{MNP}(t). \tag{5.7}$$

The concept of differential magnetometry, presented in this chapter, uses first a standard alternating excitation field. If in a next interval an additional offset field $H_{offset} \neq 0$ is applied, the measured magnetization response of linear magnetic material does not change. However, for materials with a nonlinear susceptibility, the response to the alternating field will be reduced, since the magnetization moves towards saturation. The differential magnetometry concept is shown in figure 5.1. The contribution from superparamagnetic nanoparticles in the sample can be uniquely determined by calculation of the voltage drop ΔU, here defined as the differential magnetization or the *DiffMag* signal:

$$\Delta U \propto \Delta \frac{dM}{dt} = \left.\frac{dM_{MNP}}{dt}\right|_{H_{offset=0}} - \left.\frac{dM_{MNP}}{dt}\right|_{H_{offset\neq 0}}. \tag{5.8}$$

Subtraction of the measured induction voltages for both excitation conditions, provides a selective measure for the amount of magnetic nanoparticles present.

This algorithm can be rapidly executed (<100 ms) and is therefore suitable for implementation in clinical procedures that require real time feedback. Only a few periods of alternating field per offset field interval allow a reliable quantitative measure of the amount of particles. The response is independent of the magnetization of linear magnetic material (e.g. tissue). In this chapter, the procedure, which patent is pending, is referred to as *quantification protocol* or *DiffMag protocol* [18].

The alternating field excitation causes rotation of the magnetic moments of the nanoparticles. This process includes particle relaxation mechanisms known as Néel and Brownian relaxation. Néel relaxation is defined as rotation of the magnetic moment of the core without physical rotation of the entire particle. In Brownian relaxation the entire particle rotates, which thus includes rotation of the magnetic moment. Physical rotation of the particle is influenced by the volume of the particle and by the viscous drag acting on the particle. The Brownian relaxation time τ_B for particles with volume V is defined as

$$\tau_B = \frac{3V\eta}{k_B T}, \tag{5.9}$$

with η the viscosity of the medium surrounding the particle. Néel relaxation is independent of viscosity, but depends on temperature, size and anisotropy of the core [19].

Nonlinearity of the magnetization plays a key role in the DiffMag algorithm. There are two important parameters that determine the sensitivity of the procedure, as is shown in figure 5.2. The DiffMag response is calculated as a function of the offset field amplitude for different spherical iron oxide particle sizes using the Langevin model of superparamagnetism, all with identical saturation magnetization. For larger offset field amplitudes, the difference in local susceptibility (dM/dH) probed by the alternating field is stronger, resulting in a larger DiffMag response. Secondly, magnetic nanoparticles with a large diameter express a stronger magnetization for low fields and magnetization saturates at lower offset field amplitudes, which together results in a larger DiffMag response compared to smaller particles. In addition, the DiffMag response of Resovist and Endorem is calculated, based on particle size distributions obtained from VSM. The larger average particle diameter of Resovist compared to Endorem results in a stronger DiffMag response.

The two aspects of particle size and field amplitude have to be taken into account in the design of a system for a specific application. Depending on the size of the particles used for a typical application, the signal amplitude gained by increasing the offset field amplitude is limited. The differential magnetometry principle is most sensitive for particles with large core size, allowing a lower offset field amplitude. This is advantageous for clinical applications where magnetic field limits have to be considered [20].

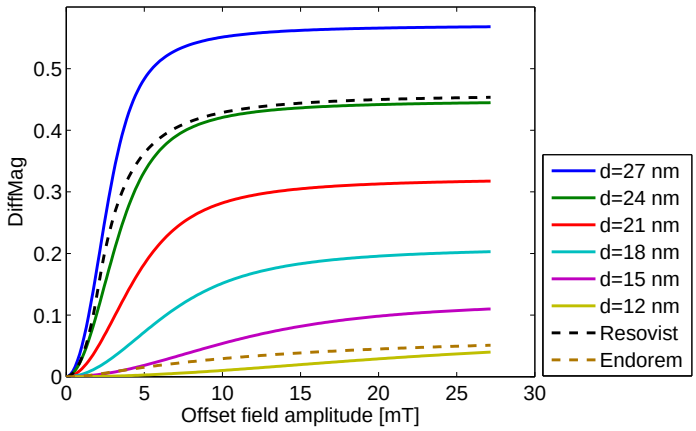

Figure 5.2: *Calculated response of differential magnetometry for mono-disperse particles with different size for various offset field amplitudes. The response of Resovist and Endorem was based on a bimodal lognormal particle size distribution, determined by VSM. Endorem shows a much smaller response compared to Resovist due to the differences in particle size distribution. For larger offset field amplitudes and larger particle sizes, the DiffMag response becomes stronger and saturates finally.*

Measurement of magnetization curve

In an alternative way, the method can be used for characterization purposes, by measuring the magnetization response to the small alternating field for a range of offset field amplitudes. The offset field is stepwise increased, while the alternating field is applied to probe the local susceptibility. The resulting response is the time derivative of the magnetic moment as a function of offset field amplitude. This can be used to reconstruct a (frequency dependent) dm/dH-curve that is equivalent with the point-spread-function (PSF) in x-space MPI [21]. Subsequently, the dm/dH-curve can be used to determine the magnetization vs. field curve of a sample material and the magnetic core size distribution of the particles in a sample that contribute to the signal.

5.2.2 Experimental setup

Magnetometer

The magnetometer is constructed of a set of coils that is placed in a homemade G10 fiberglass epoxy cryostat with vacuum insulation and MLI radiation shield. The cryostat filled with liquid nitrogen, provides optimal thermal and electrical stabilization of the excitation and detection coils. A schematic illustration of the coil geometry is shown in figure 5.3. To achieve optimal cooling, the coil set is constructed

Parameter	Excitation coil	Detection coils
Inner Diameter [mm]	25.9	16.6
Length [mm]	120	2×30
No. windings	646*	2×596
Wire diameter [mm]	1.07	0.10
Field homogeneity [%]	99**	92.5***
Sensitivity [mT A^{-1}]	2.9	19.9

**Including 184 counterwindings on a larger diameter of 45 mm to reduce stray field and to increase field homogeneity. **Over the entire volume of a detection coil. ***Over 20 mm axial coil length.*

Table 5.1: *Coil characteristics*

such, that the nitrogen also fills the space between the excitation and detection coils. However, the boiling nitrogen produces some bubbles near the detection coils, which causes mechanical vibrations and/or a varying capacitive coupling between the coils, thereby introducing noise in the signal.

The sample chamber is constructed as a small anti-cryostat, with a warm 11 mm bore to keep the sample at room temperature, which enables measurements on biological samples that have to remain intact for further processing (e.g. histopathology). A heater in the sample chamber is used to compensate remaining heat loss.

The coil set consists of an excitation coil and two co-axial pick-up coils. The parameters defining the coil characteristics can be found in table 5.1. Special effort is made to increase field homogeneity of the excitation and detection coils. This ensures accurate quantitative detection of magnetic nanoparticles independent of spatial distribution within a sample of about 2 mL. Vacuum insulation reduces the sample chamber diameter in the detection coil to 11 mm. The pick-up coils are wound 10 mm apart in series opposition, to cancel the contributions from the excitation field and environmental fields.

An alternating current and an offset current are applied to the excitation coil, to generate the alternating field with additional static offset field. Because of imperfections in fabrication and small alterations in coil geometry due to cooling, an imbalance in the response of both pick-up coils may occur. To compensate both the in-phase and out-of-phase imbalance component, a transformer circuit including a voltage divider is placed in series with the pick-up coils. The whole compensation circuit is placed in a separate (uncooled) box and is operated manually.

Electronic devices

The system comprises several electronic devices for signal generation and detection. A scheme of the electronic circuit is shown in figure 5.3. The excitation current

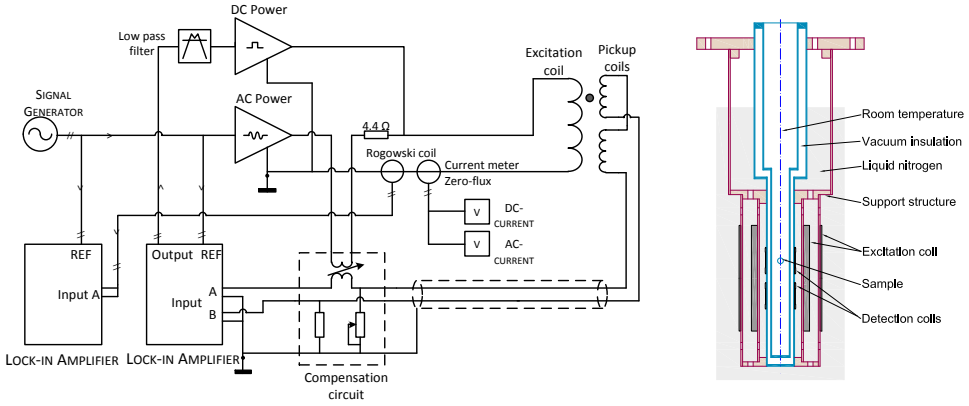

Figure 5.3: *Left: Electronic scheme of the setup including power amplifiers and measurement devices. Right: Schematic illustration of the geometrical arrangement of the coil set surrounding the room temperature sample space. The shaded area indicates the liquid nitrogen used to cool the setup. The outer part of the excitation coil is wound in opposite direction to optimize field homogeneity and to reduce stray field.*

to generate the magnetic field is supplied by two power amplifiers. The KEPCO amplifier (Kepco INC., Flushing, NY. U.S.A.) is used for the AC-current to produce an alternating magnetic field and is controlled by a waveform generator. The BOSS amplifier (TDK-Lambda Americas Inc., Neptune, NJ. U.S.A.) is controlled by the analog output channel of the lock-in amplifier and produces a DC-current to add an offset magnetic field. To smooth the effect of steps in the DC-current, a low-pass filter with a cut-off frequency of 1 Hz is placed between the lock-in amplifier and the BOSS amplifier.

A resistor in series with the AC-amplifier is used to avoid both amplifiers influencing each other and to reduce the load on the amplifier. To preserve thermal stability of the transformer in the compensation part, the compensation circuit is placed in series with the AC-amplifier, but not with the DC-amplifier. The AC and DC-excitation current is measured with high precision using a zero-flux meter (Hitec Macc+, Hitec Special Measuring Systems BV, Almelo, The Netherlands).

A lock-in amplifier (SR830, Research Systems, Inc., Sunnyvale, CA. U.S.A.) forms the main part in the detection circuit and is connected with the detection coils in differential mode. The phase of the AC-current was not stable with the different levels of the DC-current used to generate the offset field. To minimize phase errors, the alternating current and the sample response were measured with two separate lock-in amplifiers, with identical references from the waveform generator. A custom made

Rogowski coil was used to detect the alternating current. This enables reconstruction of the measured signal with minimal phase error relative to the generated alternating field.

Thermal control of the sample chamber is provided by a PT100 thermometer and a EUROTHERM 3208 PID temperature controller (Invensys Eurotherm, Alphen a/d Rijn, The Netherlands). The PID controls the power supply to the heater, which is placed just above the upper detection coil.

The setup was operated via a PC with MATLAB interface (The Mathworks Inc., Natick, MA, U.S.A.). All measurement devices and signal generators are connected to the PC via GPIB and were sampled with 2 Hz.

5.2.3 Samples and measurements

In the quantification protocol, samples are measured using a continuous alternating field with an amplitude of 2.0 mT and frequency of 4458 Hz. The offset field, with an amplitude of $\pm$23 mT, was applied in four separate periods of about seven seconds. The total measurement time of a sample, including five periods with zero offset field, was about 66 seconds.

The mean and standard deviation of the detected voltage were determined for each period in the offset field sequence. The mean difference between periods with offset field and without offset field were taken as the DiffMag response. The first two measuring points ($\sim$1 s) after each offset field switch were rejected, because of the inductive response caused by the offset field change.

To test the setup for background effects, measurements were performed with the empty sample coil and with only the sample holder. If there is response correlated with the offset field sequence, the background contribution is subtracted from measurements with nanoparticles.

The setup is calibrated for different types of magnetic nanoparticles. Samples of the commercially available magnetic tracers Resovist (Bayer Schering Pharma AG, Berlin, Germany), Endorem (Guerbet, Gorinchem, The Netherlands) and Sienna+ (Endomagnetics Ltd., Cambridge, U.K. / Sysmex Europe GmbH, Norderstedt, Germany) were prepared with concentrations between 0.5-28 μg μL^{-1} iron in suspension and iron mass in the range of 3-1568 μg. To minimize the errors of sample preparation affecting the calibration accuracy and to investigate reproducibility, 2-6 samples of all amounts of iron were prepared for each tracer type.

DiffMag quantification of tracer (Sienna+) in tissue was tested using nine porcine lymph nodes, which are retrieved from a sentinel lymph node procedure in the trial described in [22]. To check quantification accuracy, the lymph nodes were also measured with VSM (Physical Property Measurement System, Quantum Design Inc.,San Diego, CA, U.S.A.), calibrated for Sienna+, according to the protocol described in chapter 3.

To investigate the effect of immobilization of the particles on the *DiffMag* sensitivity, two samples of each iron mass of the Resovist and Sienna+ series were dried in vacuum. The particles stick to the wall of the container and free rotation (Brownian relaxation) of the particles is blocked.

Measurements of the dm/dH-curve were performed to characterize Resovist and Endorem in suspension and after drying. The measured response to the alternating field represents an average of the local susceptibility dM/dH of the sample. By decreasing the alternating field amplitude H_0, the resolution of the dM/dt response can be increased, which gives a more precise measurement of the local susceptibility. Therefore, the alternating field amplitude was decreased to 1.0 mT, compared to the *DiffMag* protocol. The offset field amplitude was cycled between ± 27.2 mT using log-spaced intervals, to increase the resolution for low offset field amplitudes. These measurements were analyzed using the Langevin model with a unimodal lognormal particle size distribution.

5.3 Results

5.3.1 Background measurements

The DiffMag response of the empty coil and the sample holder to the offset field sequence both show modulation as is shown in the upper panel of figure 5.4. Ideally empty coil measurements and materials with linear magnetic properties should not display a DiffMag response. However, after subtraction of the empty coil measurement from the sample holder measurement, the remaining DiffMag response is in the order of system noise ($\sim 10^{-7}$ V). This indicates that the modulation of empty coil measurement and sample holder is similar and therefore not related to any materials of the sample holder. The background response is attributed to nonlinearities in the amplifiers that generate the magnetic field causing current fluctuations and affecting the imbalance compensation, or to temperature dependent geometric changes of the excitation coil during subsequent periods in the offset field sequence. Therefore, before analysis of the DiffMag response of sample measurements, the empty sample holder measurement is subtracted.

5.3.2 Calibration

In figure 5.4, mid-panel, the DiffMag protocol is demonstrated in a measurement of a Resovist sample containing 100 μg of iron. During the four periods with an offset field of 22.9 mT, the response to the continuous alternating field is reduced by more than 90%. The average voltage difference between periods with and without offset field is 370 (± 1) μV.

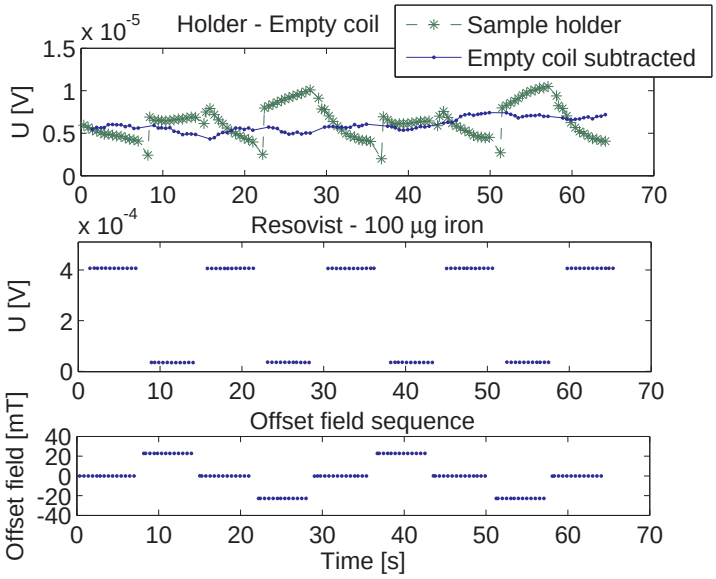

Figure 5.4: *DiffMag measurements of a sample holder and a Resovist sample containing 100 µg iron. The lower panel shows the offset field sequence. The upper panel shows the measured voltage response of a sample holder (glass vial with 50 µL of water) with the DiffMag quantification protocol. Although the sample holder consists of materials with linear magnetic susceptibilities, the response (green line) shows modulation that correlates with the offset field amplitude. This is attributed to nonlinearities in the current amplifier circuitry that generates the field or by a temperature dependent geometric change in the excitation coil. The empty coil measurements show the same type of modulation, and is therefore subtracted from the measurement. The remaining voltage response is more or less stable in the microvolts regime and reflects the diamagnetic response. The mean voltage difference between subsequent offset field periods is 0.45 ±0.39 µV. The mid panel shows the DiffMag measurement of a 100 µg iron containing suspension of Resovist.*

To determine the mass sensitivity S, the DiffMag voltage response of Endorem, Resovist and Sienna+ is plotted in figure 5.5 against the iron mass in a sample. For all different tracers, the DiffMag response scales linearly with iron mass. The response of Resovist and Sienna+ is similar, while the setup is relatively less sensitive for samples with Endorem that contain the same amount of iron. This could already be expected from the DiffMag performance analysis in figure 5.2, which shows the eminent difference between the DiffMag response of Resovist and Endorem, arising from the particle size distributions.

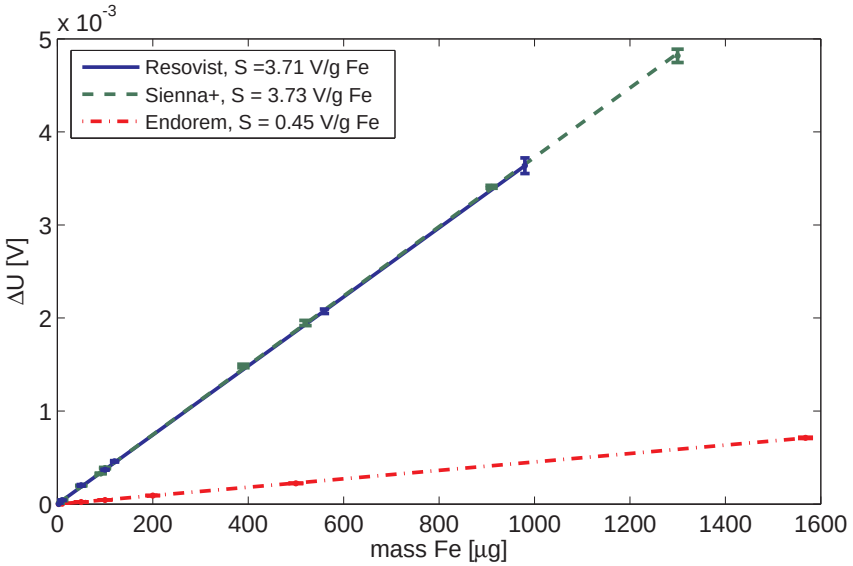

Figure 5.5: *Calibration curves of three different SPIO suspensions, with S the determined sensitivity in V g^{-1} iron. The DiffMag response (ΔU [V]) is plotted against the iron mass in the sample. Endorem gives a much smaller response for the same amount of iron compared to Resovist and Sienna+ that have a similar response.*

5.3.3 Quantification of tracer in a lymph node

The DiffMag concept is developed to selectively detect nonlinear magnetic nanoparticles in tissue which exhibits linear magnetic properties. Therefore, to test this concept, measurements are performed on porcine lymph nodes harvested in a sentinel lymph node procedure using Sienna+ as magnetic tracer. First, lymph node A was measured without tracer administration (figure 5.6). This sample only contains lymph node tissue, which is normally contributing in the background of DiffMag measurements and does not show modulation. The measured voltage drifts in the microvolts range, but does not show systematic modulation correlated with the offset field sequence. The average modulation of the subsequent periods with and without offset field was 0.44 $\pm$0.30 μV, which corresponds to 0.12 μg iron in Sienna+ tracer. This response is similar to the value found for a sample holder (see figure 5.4).

In addition, a series of 8 porcine lymph nodes from different sentinel lymph node procedures, is collected based on the presence of Sienna+ and measured with the DiffMag protocol and VSM. Two examples of the DiffMag measurement are shown in figure 5.6. In the first example, lymph node B, the response to the alternating field is reduced with 17.4 $\pm$0.5 μV during the periods with offset field. This corresponds to 4.6 μg iron according to the Sienna+ calibration in figure 5.5. In the second example,

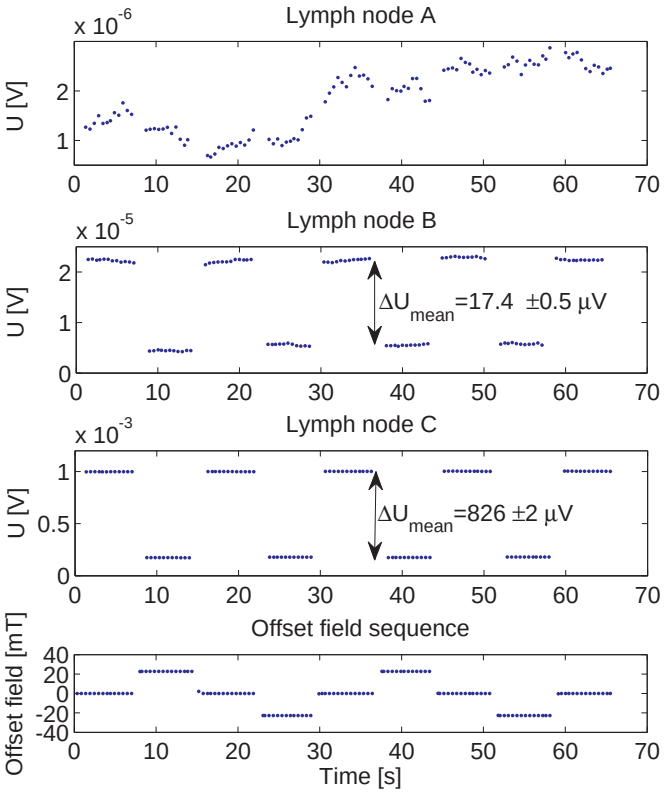

Figure 5.6: *DiffMag measurement of three different lymph nodes. Lymph node A: Control measurement of a lymph node not containing SPIO tracer. The voltage drifts in the microvolts range and does not show modulation on the offset field sequence (lower panel). The mean difference between subsequent offset field periods is 0.44 ±0.30 μV, which corresponds to 0.12 μg iron according to Sienna+ calibration (figure 5.5). Lymph node B: A porcine lymph node obtained in a sentinel lymph node procedure with Sienna+ tracer. The DiffMag response was about 17.4 ±0.5 μV corresponding to 6.95 μg iron. Lymph node C: A second porcine lymph node with Sienna+ tracer. The DiffMag response was about 826 ±2 μV corresponding to 223 μg iron.*

lymph node C, the DiffMag response is 826 ± 2 μV, corresponding with 223 μg iron. The amount of iron in both lymph nodes determined by VSM, was 6.95 and 328 μg respectively, using a calibration factor of $8.33 \cdot 10^{-8}$ Am^2 μg^{-1} iron for the magnetic moment saturation Sienna+ at 4.0 T. The quantified iron mass in these lymph node samples is 50% larger, compared to the DiffMag quantification.

To compare the DiffMag response of all lymph nodes with the response of the suspensions, the DiffMag response of lymph nodes is plotted against the iron mass as determined by VSM (figure 5.7). On average, the DiffMag sensitivity for Sienna+

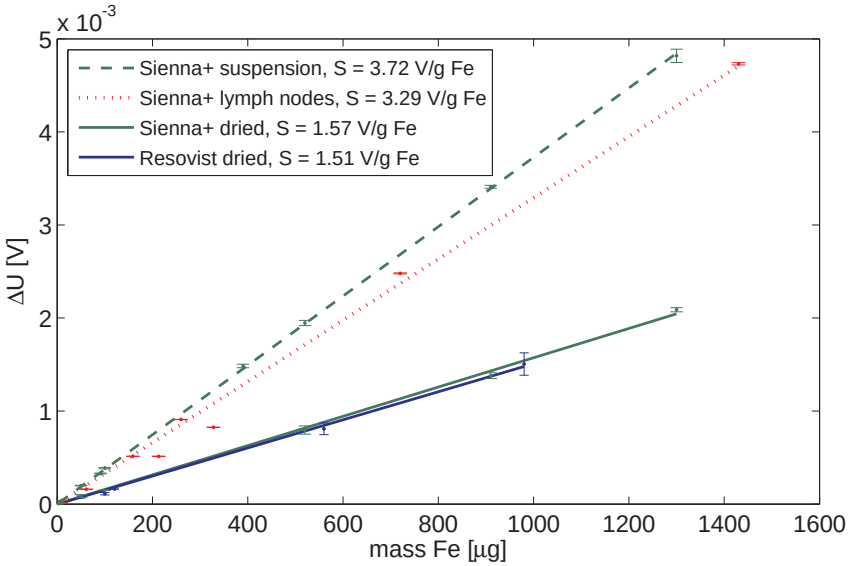

Figure 5.7: *DiffMag voltage response for Sienna+ in lymph nodes, where the iron content was determined by VSM, compared to the original calibration curve for Sienna+ suspensions (same as figure 5.5). The sensitivity for Sienna+ in lymph nodes was reduced by 12% compared to suspensions. The DiffMag response of dried samples with immobilized magnetic nanoparticles is shown against iron mass in Sienna+ and Resovist. The sensitivity determined by linear fit is similar for dried Resovist and Sienna+ and is reduced by a factor 2.3-2.4 compared to the sensitivity for the suspensions (see figure 5.5).*

content in lymph nodes, determined by VSM, was found to be 12% lower compared to the sensitivity for suspensions. The difference in sensitivity for Sienna+ in suspension and in lymph nodes can be explained by differences in particle dynamics. The mobility of the nanoparticles, important for the magnetic relaxation process, becomes altered in tissue, which apparently results in a signal reduction. This aspect is further investigated by measurements on immobilized magnetic nanoparticles in dried samples.

5.3.4 Quantification of immobilized particles

In figure 5.7, the DiffMag voltage response of the dried Resovist and Sienna+ samples is plotted against the iron content. Again, the sensitivity for both tracers is similar. With a sensitivity of 1.54 and 1.58 μV/μg iron for dried Resovist and Sienna+, the sensitivity is reduced by a factor 2.4 and 2.3 respectively compared to suspensions. It is concluded that, the contribution from Brownian relaxation is blocked and only Néel relaxation can still contribute to the DiffMag response. The sensitivity for immobilized Sienna+ particles is also lower compared to the sensitivity found for Sienna+ in

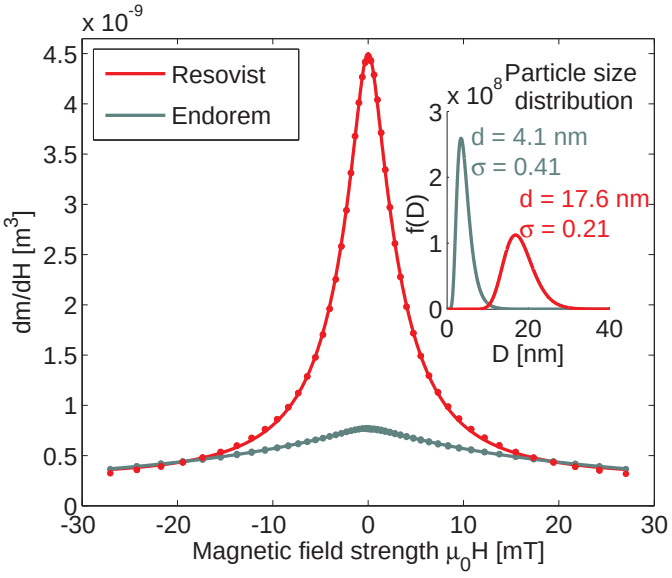

Figure 5.8: *The measured magnetic moment derivative of Resovist and Endorem (both 500 μg iron) fitted with a single lognormal particle size distribution (inset). The strong difference between the performance of both particles in differential magnetometry can be explained by a difference in effective particle size that contributes to the signal.*

lymph nodes, which indicates an intermediate field of Brownian relaxation in lymph nodes between dried samples and suspensions.

5.3.5 Characterization of magnetic nanoparticles: dm/dH-measurements

Endorem and Resovist samples with 500 μg iron were characterized by dm/dH-measurements, as shown in figure 5.8. The Resovist curve shows a much sharper peak compared to Endorem, which corresponds to the previous observation of the larger DiffMag sensitivity for Resovist compared to Endorem. The dm/dH-curves are fitted using the Langevin model for superparamagnetism and a lognormal particle size distribution. The particle size obtained for Resovist has a median of 17.6 nm with standard deviation of 0.21, which is much larger than the values found for Endorem, with median size 4.1 nm and standard deviation 0.41.

To characterize the difference between samples with particles in suspension and dried particles, the dm/dH-curve of two Resovist samples containing 560 μg iron, one suspension and one dried, was measured with the characterization protocol. As was observed before with the quantification protocol, the dm/dH-response for Resovist becomes significantly reduced after drying. The peak is broader and the particle

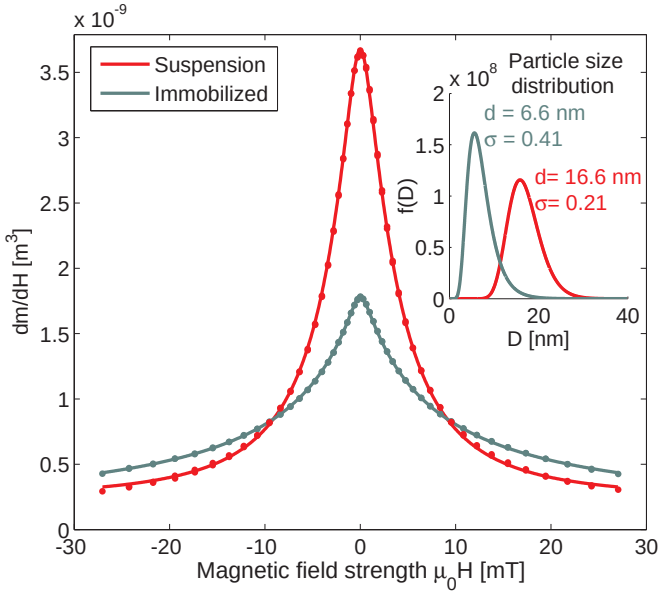

Figure 5.9: *The magnetic moment derivative of Resovist in suspension and after immobilization. Corresponding particle size distributions used to fit the measured data are displayed in the inset. There is an obvious signal reduction as well as a relative decrease in contribution from large particle sizes in dried samples.*

size obtained by the fit shows a shift to smaller sizes resulting in a median size of 6.6 ±0.41 nm. The median diameter of the particles in suspension, determined by a model assuming lognormal distributed particle size, was lower compared to the previous measurement in figure 5.8. However, the determined median core diameter of Resovist is in the range as was found in other studies [14, 23, 24].

5.4 Discussion

The differential magnetometry, presented in this chapter, shows similar mass sensitivity for the Resovist and Sienna+ tracers, whereas the sensitivity for Endorem is significantly lower. According to the DiffMag performance analysis (figure 5.2), this indicates the presence of larger core sizes contributing to the signal of Resovist and Sienna+. For Resovist and Sienna+, the reduction of the induction voltage due to the offset field is more than 93.5%. For these tracers the used offset field amplitude was near optimal, since for only a small signal increase, a significantly larger offset field amplitude is required. For Endorem the DiffMag response can still be significantly increased with offset field amplitude. However, in the present setup the current amplifiers that drive the excitation coil were used up to their functional limits.

The Sienna+ content in lymph node samples determined by DiffMag, was significantly lower compared to the quantity determined by VSM. This difference is attributed to the fundamental difference between both measuring techniques. The VSM measures magnetization of the particles in the sample in a (quasi) static field. The DiffMag concept uses at different static offset fields an alternating field to probe the magnetization and therefore Brownian and Néel relaxation can be involved. In this study, the frequency of the alternating field was 4458 Hz. Using equation 5.9 and the viscosity of water ($\eta = 10^{-3}$ N s m^{-2}), the maximum diameter of the particles with a relaxation time below the period of the field ($1/f$) is 83.9 nm. The mean hydrodynamic diameter of Resovist [23, 25–27] and Sienna+ [22] is below this limit. Therefore, most of the particles in Resovist and Sienna+ can contribute by Brownian relaxation if suspended in aqueous liquid.

After uptake of particles in lymph nodes, the viscosity of interstitial fluid, the uptake in macrophages, as well as binding of proteins in the lymph to the surface of the nanoparticles, may influence the hydrodynamic behavior of the Sienna+ particles. The Brownian relaxation that contributes in suspensions, becomes reduced or blocked in tissue. In other studies it is shown that the medium surrounding the particles affects the particle relaxation and interaction behavior, thereby reducing the response to alternating fields [14, 26, 28]. The detection of a change in Brownian relaxation is confirmed by the measurements of dried samples with immobilized particles. The DiffMag sensitivity for Resovist and Sienna+ tracer reduces by more than a factor of 2, which indicates the loss of Brownian relaxation. Only Néel relaxation of the individual cores could still contribute to the signal.

For the quantification of tracer in lymph nodes this means that the DiffMag response is still quantitative, but the setup should be calibrated with samples with matched Brownian response. Another route for reliable quantification in tissue is to increase the excitation frequency to the regime of Néel relaxation ($\geq$12.5 kHz for particles with hydrodynamic diameter of 60 nm), which will eliminate the effect of different Brownian contributions in suspensions and tissue. However, this solution is at the cost of the current system's sensitivity and detection limit and significantly increases the required power.

For Endorem the hydrodynamic size is reported most above the 83.9 nm limit [29, 30] and Brownian contributions are therefore not expected in the present study. This is confirmed by the fact that drying of Endorem samples has no effect on DiffMag sensitivity or dm/dH-response (data not shown). The Néel relaxation of Endorem particles is not affected in dry samples.

The dm/dH-measurements provide important information about magnetic nanoparticles and the nonlinear magnetization. The measurements illustrate the effects of particle size, offset field amplitude and particle relaxation effects on DiffMag sensitivity. This measurement is strongly related to the point-spread-function measure-

ments for x-space MPI [21]. The dm/dH-peak measurements can be fitted with the derivative of the Langevin function and a lognormal size distribution of spherical particles, to specifically reveal the size of particles contributing to the signal. The resulting size distribution is physically not representative for all particle sizes in the entire sample as with VSM measurements. It represents only the distribution of spherical particle sizes that similarly contribute to the signal. Therefore, the measurement of the dm/dH-curve can be used to characterize magnetic nanoparticles behavior in alternating fields and to determine optimal parameters for DiffMag measurements. The particle size distributions fitted for the suspensions with Resovist and Endorem were in agreement with other studies [14, 23–26, 31, 32].

The shift of the observed particle size distribution towards lower diameters in the dried Resovist sample, can be explained by blocking of Brownian relaxation of larger particles or clusters. The core size found by the fit of the dm/dH-curve of dried Resovist, corresponded with the size of individual cores determined by TEM in other studies [23, 25]. Using a similar excitation frequency but a larger alternating field amplitude, Goodwill *et al.* observed a reduction of particle size contributing to the signal from 15.9 in suspension to 11.0 nm in a frozen Resovist sample [14].

In the present study, samples are only investigated for one excitation frequency. The characterization of a frequency dependent field-derivative of the magnetization can be used as a tool to investigate the use of magnetic nanoparticles in other applications that use alternating excitation fields, like MPI.

For the experiments presented in this work it was necessary to subtract a background measurement from the sample measurements. This was due to some intrinsic system modulation, most probably caused by power instabilities or thermal effects during offset field excitation. The ideal setup is only sensitive for magnetic nanoparticles and does not require subtraction of a background response. In future work this issue can be solved by optimization of the excitation circuit and the measurement algorithm, or, in a less favorable solution, by a standard subtraction of the system modulation error.

In this study, the DiffMag concept was applied to a small series of selected magnetic sentinel nodes. For further validation and evaluation of both technical and clinical performance, a patient study for sentinel lymph node selection, in for example colorectal cancer, has to be executed. In addition, the possibility of detection of particle relaxation effects in 2 mL samples at room temperature is a promising tool for immunoassay or bio-molecular applications.

5.5 Conclusions

The DiffMag technique presented in this work, is developed as a detection method that is highly specific for nonlinear magnetic nanoparticles, without interference from

linear magnetic materials, like tissue. The DiffMag protocol provides exclusive quantitative detection of nanoparticles in the submicrogram range. For accurate quantification of nanoparticles in tissue samples, calibration samples with matching relaxation behavior should be used. The technique can be used with relatively low field strengths (1-10 mT) and simple detection electronics that do not require a high dynamic range. The method does not require a shielded room and can be performed by small sized, inexpensive systems, which facilitates application for both ex vivo and in vivo clinical procedures. For example, large numbers of lymph node samples from colorectal cancer, can be analyzed in only a few minutes or less, with higher specificity compared to the VSM used in a chapter 3 and 4. The method allows a quick measurement that can be brought to real-time detection, allowing implementation in surgical practice with a handheld probe for in vivo sentinel lymph node localization, as was already suggested by us [33].

In the present setup, the coil set was cooled with liquid nitrogen, which provided excellent thermal and electrical stability with minimal drift. The cooling with nitrogen and accompanying noise can be eliminated in future applications, since the field requirements for DiffMag are limited and the DiffMag protocol can be made robust for drift, by using a faster offset field sequence with lower duty cycle and lower energy consumption.

The DiffMag response strongly depends on both the core diameter of the magnetic nanoparticles and the offset field amplitude. Therefore, to optimize the DiffMag sensitivity for a specific type of magnetic nanoparticles, it is worth to consider the optimal offset field amplitude. This is also relevant for reduction of energy consumption and to remain below safety limits for in vivo applications. Regarding development of optimal tracers, it is clear that tracers with a larger core size, below the superparamagnetic limit, provide larger DiffMag signals.

References

[1] Q. A. Pankhurst, N. T. K. Thanh, S. K. Jones, and J. Dobson, “Progress in applications of magnetic nanoparticles in biomedicine”, Journal of Physics D: Applied Physics **42**, 224001 (2009).

[2] K. M. Krishnan, “Biomedical nanomagnetics: A spin through possibilities in imaging, diagnostics, and therapy”, IEEE Transactions on Magnetics **46**, 2523–2558 (2010).

[3] C. Rümenapp, B. Gleich, and A. Haase, “Magnetic nanoparticles in magnetic resonance imaging and diagnostics”, Pharmaceutical Research **29**, 1165–1179 (2012).

[4] D. Baumgarten and J. Haueisen, “A spatio-temporal approach for the solution of the inverse problem in the reconstruction of magnetic nanoparticle distributions”, IEEE Transactions on Magnetics **46**, 3496–3499 (2010).

[5] F. Wiekhorst, C. Seliger, R. Jurgons, U. Steinhoff, D. Eberbeck, L. Trahms, and C. Alexiou, “Quantification of magnetic nanoparticles by magnetorelaxometry and comparison to histology after magnetic drug targeting”, Journal of Nanoscience and Nanotechnology **6**, 3222–3225 (2006).

[6] H. Richter, M. Kettering, F. Wiekhorst, U. Steinhoff, I. Hilger, and L. Trahms, "Magnetorelaxometry for localization and quantification of magnetic nanoparticles for thermal ablation studies", Physics in Medicine and Biology **55**, 623 (2010).

[7] E. R. Flynn and H. C. Bryant, "A biomagnetic system for in vivo cancer imaging", Physics in Medicine and Biology **50**, 1273 (2005).

[8] S. Tanaka, H. Ota, Y. Kondo, Y. Tamaki, S. Kobayashi, and S. Noguchi, "Detection of magnetic nanoparticles in lymph nodes of rat by high t_c squid", IEEE Transactions on Applied Superconductivity **13**, 377–380 (2003).

[9] K. Enpuku, K. Soejima, T. Nishimoto, H. Tokumitsu, H. Kuma, N. Hamasaki, and K. Yoshinaga, "Liquid phase immunoassay utilizing magnetic marker and high T_C superconducting quantum interference device", Journal of Applied Physics **100**, 054701–5 (2006).

[10] B. Gleich and J. Weizenecker, "Tomographic imaging using the nonlinear response of magnetic particles", Nature **435**, 1214–1217 (2005).

[11] M. Shiozawa, A. Lefor, Y. Hozumi, K. Kurihara, N. Sata, Y. Yasuda, and M. Kusakabe, "Sentinel lymph node biopsy in patients with breast cancer using superparamagnetic iron oxide and a magnetometer", Breast Cancer 1–7 (2012).

[12] Y. Minamiya, M. Ito, Y. Katayose, H. Saito, K. Imai, Y. Sato, and J. I. Ogawa, "Intraoperative sentinel lymph node mapping using a new sterilizable magnetometer in patients with nonsmall cell lung cancer", Annals of Thoracic Surgery **81**, 327–330 (2006).

[13] H. J. Krause, N. Wolters, Y. Zhang, A. Offenhäusser, P. Miethe, M. H. F. Meyer, M. Hartmann, and M. Keusgen, "Magnetic particle detection by frequency mixing for immunoassay applications", Journal of Magnetism and Magnetic Materials **311**, 436–444 (2007).

[14] P. W. Goodwill, A. Tamrazian, L. R. Croft, C. D. Lu, E. M. Johnson, R. Pidaparthi, R. M. Ferguson, A. P. Khandhar, K. M. Krishnan, and S. M. Conolly, "Ferrohydrodynamic relaxometry for magnetic particle imaging", Applied Physics Letters **98**, 262502–3 (2011).

[15] C. P. Bean and I. S. Jacobs, "Magnetic granulometry and super-paramagnetism", Journal of Applied Physics **27**, 1448–1452 (1956).

[16] L. F. Gamarra, W. M. Pontuschka, J. B. Mamani, D. R. Cornejo, T. R. Oliveira, E. D. Vieira, A. J. Costa-Filho, and E. A. Jr, "Magnetic characterization by SQUID and FMR of a biocompatible ferrofluid based on Fe_3O_4", Journal of Physics: Condensed Matter **21**, 115104 (2009).

[17] D. X. Chen, A. Sanchez, E. Taboada, A. Roig, N. Sun, and H. C. Gu, "Size determination of superparamagnetic nanoparticles from magnetization curve", Journal of Applied Physics **105** (2009).

[18] S. Waanders, M. Visscher, T. Oderkerk, H. Krooshoop, and B. ten Haken, "Method and apparatus for measuring an amount of superparamagnetic material in an object", (European Patent application EP 12194029.0, 23 november 2012).

[19] B. H. Erné, K. Butter, B. W. M. Kuipers, and G. J. Vroege, "Rotational diffusion in iron ferrofluids", Langmuir **19**, 8218–8225 (2003).

[20] E. Saritas, P. Goodwill, G. Zhang, and S. Conolly, "Magnetostimulation limits in magnetic particle imaging", IEEE Transactions on Medical Imaging **32**, 1600–1610 (2013).

[21] P. W. Goodwill and S. M. Conolly, "The x-space formulation of the magnetic particle imaging process: 1-d signal, resolution, bandwidth, snr, sar, and magnetostimulation", IEEE Transactions on Medical Imaging **29**, 1851–1859 (2010).

[22] B. Anninga, M. Ahmed, M. Hemelrijck, J. Pouw, D. Westbroek, S. Pinder, B. Haken, Q. Pankhurst, and M. Douek, "Magnetic sentinel lymph node biopsy and localization properties of a magnetic tracer in an in vivo porcine model", Breast Cancer Research and Treatment **141**, 33–42 (2013).

[23] D. Eberbeck, F. Wiekhorst, S. Wagner, and L. Trahms, "How the size distribution of magnetic nanoparticles determines their magnetic particle imaging performance", Applied Physics Letters **98**, 182502–3 (2011).

[24] R. M. Ferguson, A. P. Khandhar, and K. M. Krishnan, "Tracer design for magnetic particle imaging (invited)", Journal of Applied Physics **111**, 07B318–5 (2012).

[25] D. X. Chen, N. Sun, and H. C. Gu, "Size analysis of carboxydextran coated superparamagnetic iron oxide particles used as contrast agents of magnetic resonance imaging", Journal of Applied Physics **106**, 063906–9 (2009).

[26] A. P. Khandhar, R. M. Ferguson, H. Arami, and K. M. Krishnan, "Monodisperse magnetite nanoparticle tracers for in vivo magnetic particle imaging", Biomaterials **34**, 3837–3845 (2013).

[27] R. Lawaczeck, H. Bauer, T. Frenzel, M. Hasegawa, Y. Ito, K. Kito, N. Miwa, H. Tsutsui, H. Vogler, and H.-J. Weinmann, "Magnetic iron oxide particles coated with carboxydextran for parenteral administration and liver contrasting", Acta Radiologica **38**, 584–597 (1997).

[28] H. Arami, R. M. Ferguson, A. P. Khandhar, and K. M. Krishnan, "Size-dependent ferrohydrodynamic relaxometry of magnetic particle imaging tracers in different environments", Medical Physics **40**, 071904–14 (2013).

[29] I. Raynal, P. Prigent, S. Peyramaure, A. Najid, C. Rebuzzi, and C. Corot, "Macrophage endocytosis of superparamagnetic iron oxide nanoparticles: Mechanisms and comparison of ferumoxides and ferumoxtran-10", Investigative Radiology **39**, 56–63 (2004).

[30] H. Y. Lee, S. H. Lee, C. Xu, J. Xie, J. H. Lee, B. Wu, A. Leen Koh, X. Wang, R. Sinclair, S. X. Wang, D. G. Nishimura, S. Biswal, S. Sun, S. H. Cho, and X. Chen, "Synthesis and characterization of PVP-coated large core iron oxide nanoparticles as an MRI contrast agent", Nanotechnology **19** (2008).

[31] C. W. Jung and P. Jacobs, "Physical and chemical properties of superparamagnetic iron oxide MR contrast agents: Ferumoxides, ferumoxtran, ferumoxsil", Magnetic Resonance Imaging **13**, 661–674 (1995).

[32] L. F. Gamarra, G. E. S. Brito, W. M. Pontuschka, J. B. Mamani, C. A. Moreira-Filho, and E. Amaro Jr, "Study of the ferrofluid drying process for morphological and nanostructural characterization", Brazilian Journal of Physics **37**, 1288–1291 (2007).

[33] S. Waanders, M. Visscher, T. Oderkerk, and B. ten Haken, "Finding the sentinel lymph node with a handheld differential magnetometer", in *Proc. of International Workshop on Magnetic Particle Imaging (IWMPI) 2013*, 1–1 (2013).

6

Environmental effects on magnetic nanoparticle relaxation investigated by single frequency alternating field magnetometry with varying offset field*

Abstract: In biomedical applications of magnetic nanoparticles (MNPs), detection methods based on particle relaxation enable to quantify the effect of the physiological environment on the MNP response. In this chapter, the effects of different physiological factors that influence hydrodynamic nanoparticle behavior are investigated in Resovist, Endorem and in house produced MNP samples. Changes in viscosity are investigated with MNP suspensions in agar and glycerol and immobilized MNP samples. To determine the effect of increased hydrodynamic volume by protein adhesion, MNP suspensions in serum are measured. The effect of cellular uptake of Resovist is investigated in a murine macrophage culture. Macroscopic (~ 0.5 mL) samples are measured in a magnetometer using a continuous alternating field with a single excitation frequency (2.2 or 4.4 kHz) and a sequence of offset fields. The response is analyzed using the derivative of the Langevin function and a lognormal distributed particle size. For Resovist, the increased viscosity influenced the signal amplitude and/or contributing particle size, indicating decreased Brownian relaxation and a shift towards Néel relaxation. The response in serum was significantly reduced, with a shift to contributions with a slightly smaller mean particle size. In Endorem only a minor effect of viscosity was observed. Uptake of Resovist in macrophages showed a relative loss of the contribution of large particles compared to the original suspension. The presented approach is a novel tool for quantitative evaluation of MNP performance in specific biomedical applications and for detection of biomolecular reactions that influence Brownian relaxation of MNPs.

*This chapter is submitted with contributing authors: M. Visscher, S. Waanders, K.M. Pondman, B. ten Haken

6.1 Introduction

Particle relaxation is an important process in many magnetic nanoparticle (MNP) applications, like AC-susceptometry, magnetorelaxometry, magnetic particle imaging (MPI) and magnetic hyperthermia. Magnetic nanoparticles (MNPs) are used for many different applications in medicine and biology. Their typical magnetic characteristics make them useful for detection and manipulation in different circumstances [1]. The performance of MNPs in a specific application is largely dependent on the core materials, core diameter, hydrodynamic diameter, coating and environment [2, 3].

For superparamagnetic nanoparticles, a changing magnetic excitation field causes a reorientation of the MNPs via rotation of the entire particle (Brownian relaxation) and/or rotation of only the magnetic moment in the core (Néel relaxation) (see figure 6.1). Néel relaxation is therefore only dependent on magnetic core properties and temperature. Brownian relaxation is influenced by environmental factors that affect the rotation of the particle in the medium. A different viscosity in bodily fluids or an increase in particle size by biomolecule adhesion can change the Brownian relaxation properties in (*in vivo*) biomedical MNP applications.

Brownian relaxation is therefore an important and interesting phenomenon in biomedical MNP applications. Effects of biological environment on MNP behavior are relevant in two ways for biomedial MNP detection. First, the change in MNP response can be used to detect a specific process of interest [4]. Secondly, the change in MNP response quantitatively affects the performance of a specific MNP detection application [5]. The observed discrepancy in MNP quantification in lymph nodes between the measurements with DiffMag and vibrating sample magnetometry (VSM) in chapter 5, is attributed to the change in particle relaxation after MNP uptake in lymph nodes. For MNP quantification in tissue, the calibration should be performed on samples with similar relaxation behavior. For development of MNPs and detection

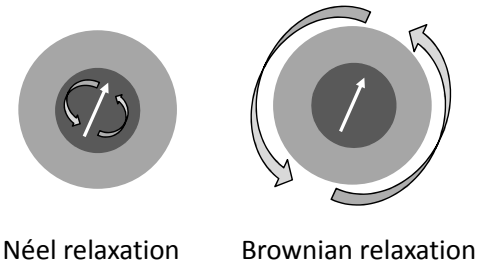

Figure 6.1: *Two types of MNP relaxation. In Néel relaxation only rotation of the magnetic moment orientation takes place. In Brownian relaxation the entire particle rotates in the surrounding medium.*

systems for quantitative MNP detection in biomedical applications, it is therefore important to investigate the factors that influence MNP performance under different circumstances.

Diagnostic and therapeutic MNP applications such as magnetic particle imaging (MPI), magnetic sentinel lymph node biopsy and magnetic hyperthermia, use alternating excitation fields and therefore require magnetic nanoparticles optimized for this technique. In addition, the techniques should be used with excitation field parameter settings that provide optimal performance for (clinically) available particles. The (field dependent) magnetic behavior and environmental effects of viscosity and adhesion of biomolecules in *in vivo* applications have to be taken into account for optimal performance.

We present an experimental method for particle specific characterization of magnetic and hydrodynamic properties. For these experiments we developed a protocol using single frequency alternating field magnetometry with a varying offset field. The measurements are performed in the same setup as used for the DiffMag measurements in chapter 5. Environmental effects on relaxation behavior of different MNP tracers are quantitatively investigated for different MNP tracers. The aim of this study is to develop a powerful tool for characterization of MNP performance in biomedical samples, with good prospects for specific biomolecular sensing.

6.2 Theory

The DiffMag concept, also described in chapter 5, is used for the dm/dH measurements. In figure 6.2 the concept of the measurement is shown. A single continuous alternating field $H(t) = H_0 \sin(\omega t)$ with a fixed frequency $\omega = 2\pi f$ and fixed amplitude H_0 is used to achieve an alternating magnetic moment m_a in the sample. In addition to the alternating field, a sequence of offset fields H_{offset} is applied to probe the alternating magnetic moment m_a at different amplitudes of magnetic moment m_{offset}. The sequence sweeps the offset field amplitude from zero over an identical positive and negative range. According to Langevin theory, the increasing offset field amplitude will bring superparamagnetic nanoparticles towards their saturation magnetization, thereby reducing the magnetic moment response to the alternating field (figure 6.2B). Using a first order gradiometer pick-up coil with sensitivity S, the sample induced voltage U provides us the alternating magnetic moment amplitude via [6],

$$U = -2\pi f m_a S. \tag{6.1}$$

The measured voltage is directly proportional to the time derivative of m_a. Using the time derivative of the alternating field, the dm/dH-response at each offset field can be determined. The resulting curve (figure 6.2C) is fitted with the derivative of the Langevin equation. As shown in the chapters 3 and 5, the $m(H)$ response of a sample

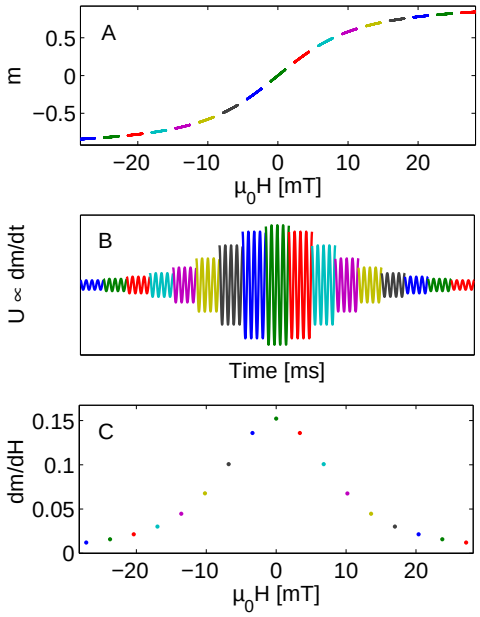

Figure 6.2: *The concept of the dm/dH measurements. A continuous alternating field H of a certain frequency is used with a sequence of offset fields to magnetize the sample. The nonlinear magnetization response of a 16 nm iron oxide particle is shown in panel A. Each color corresponds with the response to the alternating field at a certain offset field amplitude. The detected voltage is proportional to the time derivative of the magnetization response (panel B). Using the sensitivity of the detection coil and the time derivative of the alternating field, the dm/dH response for each offset field amplitude can be determined (panel C). For clarity, half of the time line of the response U is shown; the response in B starts at the negative maximum of the offset field. In the experiments the offset field made a full cycle, starting at $\mu_0 H$=0 mT.*

with MNPs is usually fitted with a lognormal distributed particle size. Therefore, in the present study, the dm/dH response is fitted using an unimodal lognormal distribution $f(D|d,\sigma)$ with d the mean diameter of the associated normal distribution with diameters D and σ the standard deviation.

Alternating magnetization of MNPs is associated with Néel and Brownian relaxation. Néel relaxation depends on the magnetic anisotropy K of the core, the volume V_c of the core and the temperature T of the system, and can be described by,

$$\tau_N = \tau_0 e^{KV_c/k_B T}, \tag{6.2}$$

where τ_0 is the characteristic relaxation time often chosen as 10^{-9} s [2], and k_B the Boltzmann constant. Since the Néel relaxation time is exponentially dependent on the

particle size, a small increase in particle diameter is already sufficient to influence the relaxation time by orders of magnitude.

In Brownian relaxation, where the entire particle rotates, the relaxation time is linearly dependent on the hydrodynamic particle volume V_h and the viscosity of the carrier liquid η:

$$\tau_B = \frac{3V_h\eta}{k_BT}. \tag{6.3}$$

The hydrodynamic volume is an effective volume, including the true particle volume and the volume of molecules and fluid that is moving when the particle rotates due to particle-fluid interactions [3, 7].

Both relaxation processes can take place in a particle, resulting in an effective relaxation time τ_{eff} [8],

$$\tau_{eff} = \frac{\tau_B\tau_N}{\tau_B + \tau_N}. \tag{6.4}$$

The relaxation process that dominates in a sample depends on which of the relaxation times is shorter. Using the alternating field H, MNPs with an effective relaxation time much shorter than $1/(2\pi f)$ are able to follow the field with relaxation. However, for particles with longer effective relaxation times, the relaxation process lags the alternating field and an out-of-phase component in m_a will occur. Finally, for MNPs with relaxation times much longer than $1/(2\pi f)$, the MNP is unable to follow the alternating field resulting in m_a to be zero.

The hydrodynamic volume and the viscosity are the variables that can change significantly in biomedical applications. The attachment of biomolecules in *in vivo* applications may change the hydrodynamic volume, increasing Brownian relaxation time. In typical biomedical fluids a different viscosity may also affect the Brownian relaxation time, compared to the original carrier liquid. For example, the viscosity of whole blood is about 3 times larger compared to the viscosity of water [9]. Therefore, MNPs showing Brownian relaxation are of particular interest to study these factors and its effect on performance for magnetic detection and manipulation. In this study the effect of particle volume is investigated by dm/dH-measurements of MNP suspensions added to serum. The dm/dH-response of MNPs suspended in agar and glycerol is measured to determine the effect of viscosity.

6.3 Methods

6.3.1 Experimental setup

For the characterization of magnetic nanoparticles in different situations, the same setup is used as described in chapter 5. The concept of the dm/dH-measurements, shown in figure 6.2, is based on a homogeneous alternating magnetic excitation field and an offset field using a single excitation coil. The sinusoidal alternating field

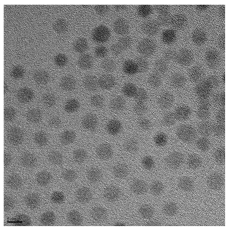

Figure 6.3: *Transmission electron microscopic image of the UTMNPs with a core size of 4 ± 1 nm. The scale bar is equivalent with 5 nm on the image.*

has an amplitude of 1 mT; to achieve sufficient resolution this is far below magnetic saturation of superparamagnetic nanoparticles. Excitation frequencies of 2229 Hz and 4458 Hz are used to investigate frequency dependency of the dm/dH response of MNPs in the samples. The offset field is swept with logarithmically spaced intervals between ±27 mT to increase resolution in the low field region, where the change in the dm/dH-curve is the largest.

Samples are placed in the upper coil of a first order gradiometer coil set, coaxially placed inside the excitation coil. The sample coil has a theoretical field profile of 92.5% homogeneity over 20 mm coil length, to obtain a sample volume independent sensitivity. The sample height of a 0.5 mL microcentrifuge tube is approximately equal to this 20 mm. The pick-up coils have an inner diameter of 16.6 mm, whereas the sample chamber has a diameter of 11.0 mm. The setup is cooled with liquid nitrogen in a cryostat. The sample chamber is constructed as an anti-cryostat to enable measurements at room temperature. After each offset field step the signal is measured over 5 seconds with a sampling frequency of 2 Hz. The data measured at each offset field step is averaged and analyzed using the Langevin model for superparamagnetism and an unimodal lognormal particle size distribution.

6.3.2 Samples

Samples with three different types of superparamagnetic iron oxide nanoparticles are prepared in 0.5 mL microcentrifuge tubes (Eppendorf Nederland B.V., Nijmegen, The Netherlands). The commercially produced MRI contrast agents Resovist (Bayer Schering Pharma AG, Berlin, Germany; 28 g Fe L^{-1}) and Endorem (Guerbet, Gorinchem, The Netherlands, 11.2 g Fe L^{-1}), as well as in house produced iron oxide nanoparticles with polyacrylic acid coating (UTMNPs, core size 4 ±1 nm, hydrodynamic size 10 nm, see figure 6.3) are measured to investigate the effect of different media on the MNP response. For each particle type a sample series containing 200 μg and 500 μg iron is prepared. The particles are measured as produced (Resovist) and diluted with water to 0.5 mL (all particle types), suspended in glycerol, 1 w%

and 2 w% agar and in human serum. Serum was chosen as medium since it is known that a protein corona will form around the nanoparticles. This increases the hydrodynamic particle volume V_h, which influences the Brownian dynamics of the sample [7, 10]. Glycerol and agar were chosen to investigate the effects of viscosity η on the dm/dH signal amplitude, separate from an increase in hydrodynamic volume. The extreme case of immobilized particles that lack Brownian relaxation is obtained by a vacuum dried Resovist sample with 560 μg iron, which is compared to an undiluted suspension also containing 560 μg iron. To investigate preparation accuracy, three undiluted Resovist samples of 17.9 μL containing 500 μg iron were prepared. After a first series of measurements, these samples were diluted to 500 μL to measure a possible effect of dilution and sample volume. The UTMNPs are dispersed in water and not investigated in other media.

To test the effect of particle uptake by the reticuloendothelial system on the dm/dH-response, Resovist (3 mL, 3 mg Fe) was added to a murine macrophage culture (RAW 264.7 cell line grown in DMEM with fetal calf serum and penicillin/streptomycin, 12 well plate, $5 \cdot 10^5$ cells/well) and incubated for 8 hours. One of the two samples prepared after incubation was extensively washed and resuspended in PBS (pH 7.4) to remove free Resovist from the sample, keeping only the macrophages with possible phagocytosed particles.

Background effects of the setup are eliminated by subtraction of the response of a sample not containing MNPs. For the blanco water, serum and macrophage samples, a linear response (dm/dH is constant) was measured over the whole offset field range after subtraction of an empty coil measurement. These samples are therefore suitable for background measurements, extract the MNP response and to eliminate the systems response. For the 4458 Hz alternating field, the noise level is in the order of $dm/dH = 2.2 \cdot 10^{-12} m^3$ for low offset field amplitudes and increases for larger offset fields, due to more evaporation of liquid nitrogen.

6.4 Results

6.4.1 Characterization of the technique

To investigate the effect of mass in different samples, dm/dH-measurements of 200 and 500 μg Fe samples are compared in figure 6.4a. The signal amplitude is proportional to the mass of iron in Resovist, with a deviation of about 12%. Normalization of the dm/dH-signal shows no significant deviation of peak shape, as is confirmed by the fit with very similar particle size distributions (not shown) with mean diameters of 17.6 (σ=0.21) and 17.8 (σ=0.20) nm, which indicates no clustering effects or sedimentation to occur in the larger concentration.

The effect of sample volume was assessed by comparing the dm/dH-results of a set of three high concentrated (28 gL^{-1} Fe, undiluted) small volume Resovist sam-

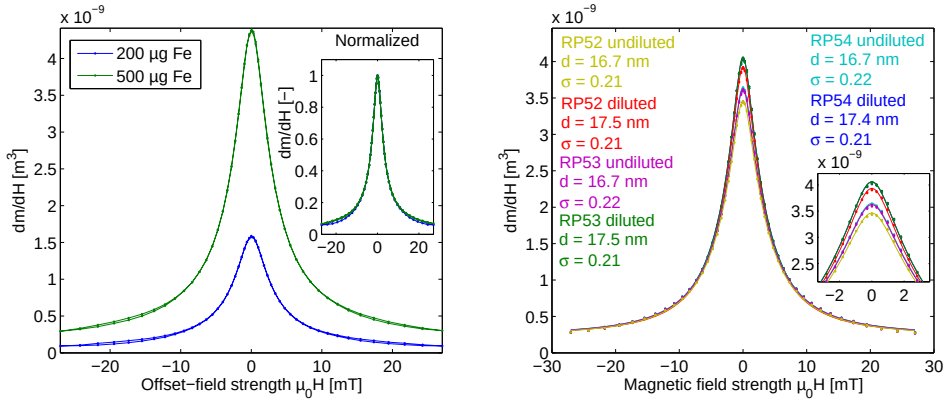

Figure 6.4: *a. Measured dm/dH-response vs. offset field of two samples of Resovist containing 200 µg and 500 µg iron, respectively. The amplitude of the response is proportional to the amount of iron in the sample. The inset shows overlapping normalized dm/dH curves for comparison of relative peak shape and indicates a similar response for different sample mass. b. Measured dm/dH-response vs. offset field for three 500 µg samples of Resovist before and after dilution. The inset focuses on the maximum peak amplitude.*

ples, with the results of the same samples after 28 times dilution (1 gL^{-1} Fe). In figure 6.4b the diluted samples systematically show a 10% increase of the peak maximum compared to the results of undiluted samples. However, this signal increase disappears for larger offset fields.

The results of the (diluted) 500 μg iron Resovist sample are reproduced with a period of two weeks (data not shown). Therefore, aging is not observed in the magnetic properties of aqueous suspensions.

6.4.2 Different particles compared

The dm/dH-measurements of the three different particle types Resovist, Endorem and an in house produced Fe_3O_4-particle (UTMNP) are shown in figure 6.5. Signal amplitude and relative peak shape is significantly different for the different particles. Samples displaying a wide peak and low signal amplitude are fitted with a small core size. For a narrow peak larger particles contribute to the signal in response to the alternating field. The values found for Resovist and Endorem are in accordance with values in literature [11–18]. The UTMNP core size of 4.0 nm (σ=0.35) obtained from the measurements is as expected from the TEM results in figure 6.3.

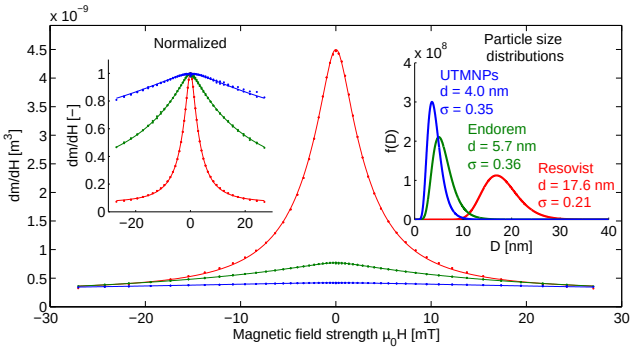

Figure 6.5: *Measured dm/dH-response vs. offset field of Resovist, Endorem and UTMNPs, all containing 500 µg iron. The left inset shows the normalized dm/dH curves for comparison of relative peak shape. The inset on the right shows the lognormal distributions fitted to the dm/dH curves.*

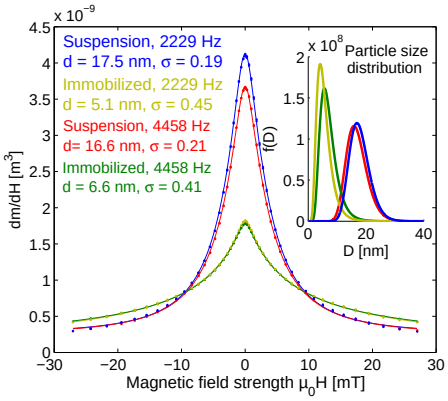

Figure 6.6: *The dm/dH response vs. offset field for a Resovist suspension and a immobilized Resovist sample, both containing 560 µg iron, measured at two excitation frequencies. Immobilization of the particles eliminates Brownian contributions and results in a significant signal loss and a shift in the contribution from large core size to small core size in the Langevin model with lognormal distributed particle size. The response of immobilized particles is not frequency dependent in the applied frequency range. Suspensions show a lower dm/dH response for a higher frequency, attributed to a loss of contributions from larger particles showing Brownian relaxation.*

6.4.3 Magnetic nanoparticles in different media

Resovist

The dm/dH-curves of Resovist particles in suspension and after immobilization are markedly different, as is shown in figure 6.6. Both samples have the same amount of iron oxide, but the maximum amplitude of the peak observed for the suspension, is more than halved after immobilization of the particles. The mean particle size of the distribution obtained for the immobilized particles is significantly smaller compared to the distribution fitted for the suspension. After immobilization the response from larger particles is lost. However, for offset fields larger than 10 mT, the signal from the immobilized particles is larger compared to the suspension. This corresponds to a quantitatively larger contribution of small particles in the immobilized sample.

The samples with Resovist in different media are measured at two excitation frequencies. In general, for larger excitation frequencies, only the fraction with smaller particle size and shorter relaxation times can contribute to the signal, as is also observed in other studies [4, 19–22]. For example, in figure 6.6 the dm/dH-response of the suspension is 15% reduced for the higher excitation frequency, with only a minor reduction of the estimated contributing particle size. This indicates the loss of the contribution of a specific part of the population of particles in the suspension.

For the immobilized particles there is no significant difference observed between both excitation frequencies. The larger particles, previously contributing in the suspension by Brownian relaxation, are blocked in this sample and the Néel relaxation of the fixated magnetic cores is not significantly diminished at the higher excitation frequency, which results in a fit with similar particle size distribution.

The biomedical relevance of these results is illustrated by the experiments with Resovist in different media. The result of Resovist in serum is remarkable (figure 6.7). Compared to the 500 μg suspensions in figure 6.4, the maximum signal is significantly reduced (35-50%) in serum. One of the two serum samples shows similar results for different excitation frequencies, as was the case with the immobilized sample. The mean diameter of the lognormal distribution obtained for the Resovist suspension reduced with only about 1-1.5 nm, whereas for both serum samples similar distributions were found with both excitation frequencies. The suspected volume increase, caused by the protein corona attached to the nanoparticles, is such that for both frequencies particle volume effects are similar.

The dm/dH-response of serum samples reduces after preparation over a period of 2 weeks, as is shown in figure 6.8. The growth and stabilization of the protein corona [23] and sedimentation both may contribute to a change in the signal response over time.

Figure 6.9 shows the effect of increased viscosity in agar on the dm/dH-response of Resovist in the alternating field. Compared to the maximum signal intensity of the

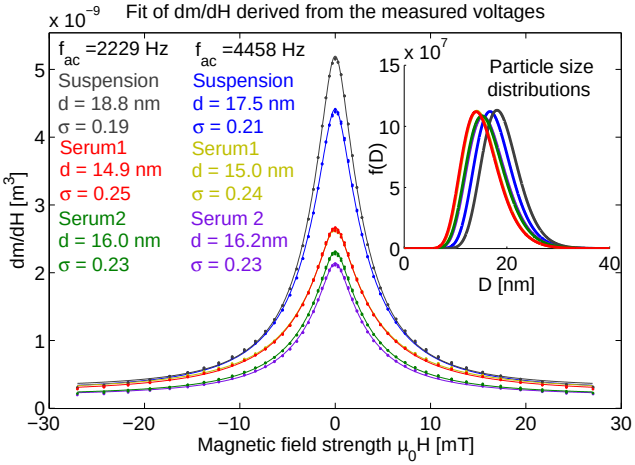

Figure 6.7: *The dm/dH response vs. offset field for two Resovist suspensions in serum measured at two different excitation frequencies. For both samples the response is very similar, as is confirmed by the particle size distributions. Differences between sample 1 and 2 can be explained by preparation errors. Two illustrate the signal reduction, the response of the original tracer is included.*

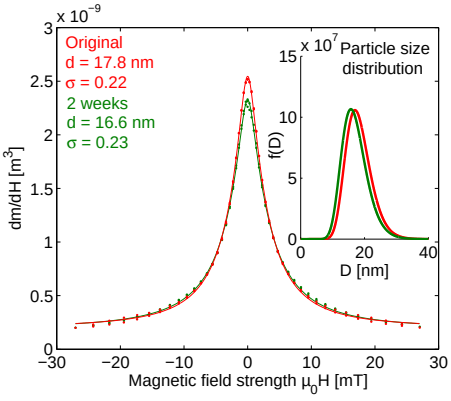

Figure 6.8: *The same sample with Resovist suspended in serum was measured after 2 weeks. Compared to the first measurement the peak reduces with 8% while there is a small reduction in contributing particle size.*

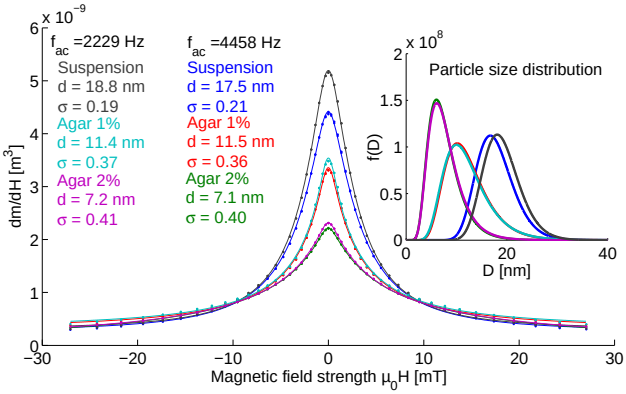

Figure 6.9: *The dm/dH response vs. offset field for Resovist suspensions in 1% and 2% agar measured at two different excitation frequencies. For both agar samples the response is very similar at different frequencies, with only a minor signal reduction at the higher frequency. The response of the 2%-agar sample results in a significantly lower mean particle size and lower signal strength, indicating the reduction of Brownian contributions by the increased viscosity. For the aqueous Resovist suspension with the same amount of iron (500 μg Fe), the mean diameter of the particle size distribution was smaller at higher frequencies.*

aqueous suspension, the signal reduces with 25-27% and 50-55% for 1%-agar and 2%-agar, respectively. The mean diameters of the particle size distributions are significantly smaller for the agar samples compared to the original suspension. The distribution for the 2%-agar sample approaches the distribution for immobilized particles, which indicates reduction of Brownian relaxation by the increased viscosity. The response of the agar samples is less affected by the higher excitation frequency, compared to the aqueous suspension.

For Resovist in glycerol the signal amplitude overall is reduced, while the estimated contributing particle size distribution is increased (see figure 6.10). In contrast to the results with agar, the suspected effect of decreased contributing particle size due to an increased viscosity is not observed.

The dm/dH-response of both samples with murine macrophages show a reduction of contributing particle size compared to the original suspension (figure 6.11). Uptake of Resovist in macrophages was confirmed by microscopy (not shown). Apart from the difference in amplitude, which is attributed to the loss of particles in the washing step, there is no significant difference observed in dm/dH-response after washing. This is confirmed by normalization and the very similar particle size distributions.

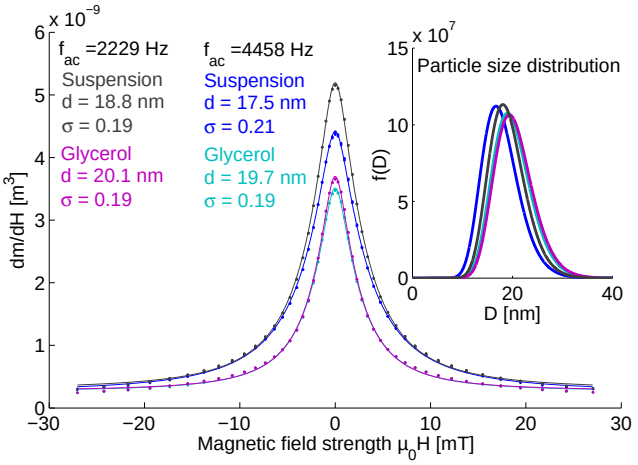

Figure 6.10: *The dm/dH response vs. offset field for Resovist suspensions in glycerol measured at two different excitation frequencies. For both glycerol samples the response is very similar at different frequencies, with only a minor signal reduction at the higher frequency. The response of the glycerol sample results remarkably in a larger mean particle size and lower signal strength, compared to the original aqueous suspension. The increased viscosity in glycerol seems to reduce mainly the contribution from smaller particle sizes.*

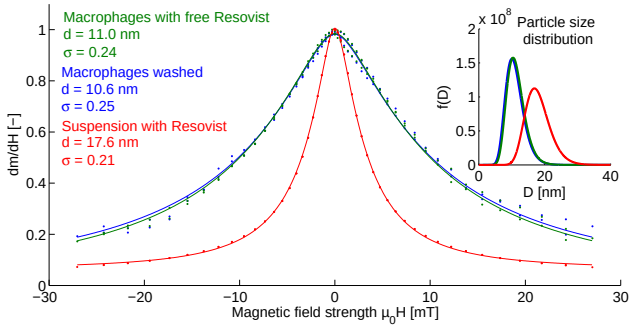

Figure 6.11: *The results of dm/dH-measurements with particles after uptake in macrophages and the Resovist in suspension. To compare the results of the washed and not washed sample the measurements are normalized with a factor $9.52 \cdot 10^{-11}$ and $1.56 \cdot 10^{-10}$ respectively. The difference in factors reflect the loss of Resovist particles in the washing step. The fitted particle size distributions are very similar for both macrophage samples, but show smaller particle size compared to Resovist in suspension.*

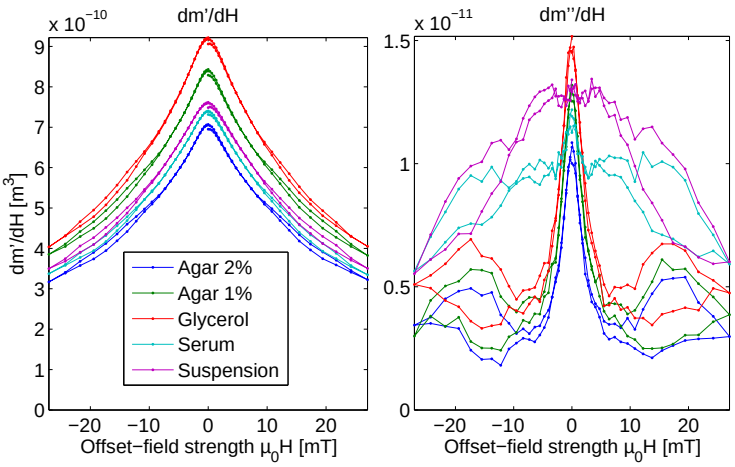

Figure 6.12: *The results of dm/dH-measurements of Endorem in different media. The most prominent differences are observed in the out-of-phase response (right panel). Samples with increased viscosity have a different peak shape compared to the original suspension and the serum sample. The amplitude differences for the in-phase component are attributed to sample preparation errors. It should be noted that the response of the out-of-phase component is much lower compared to the the in-phase component.*

Endorem

The dm/dH-measurements of Endorem in different media in figure 6.12 show different amplitudes and the estimated particle size distributions show a relatively small mean particle size (table 6.1). Deviations of the distributions can be largely explained by the relatively low signal amplitude and the small offset field range, resulting in a less accurate fit. The differences in signal amplitude between the samples is attributed to sample preparation inaccuracies. After normalization the dm/dH-curves are very similar (not shown), indicating the subtle difference in peak shape in this offset field region for small particles sizes. The most prominent differences are observed in the out-of-phase response of the glycerol and agar samples using an excitation frequency of 2229 Hz (see figure 6.12, right panel). Compared to the aqueous suspension and the serum sample, the peak shape of these samples is much sharper in the region below 10 mT. The increase in viscosity has a little effect on the magnetic particle response, but is not of large influence on the total (quadrature) signal amplitude and particle size contribution.

Sample	d [nm]	σ
Agar 2%	2.6	0.48
Agar 1%	2.6	0.48
Glycerol	4.1	0.41
Serum	4.7	0.39
Suspension	5.7	0.35

Table 6.1: *Particle size distribution parameters fitted to the quadrature dm/dH-curve of Endorem samples*

6.5 Discussion

The dm/dH-measurements presented here, indicate the potential of the DiffMag method to characterize the performance of magnetic nanoparticles in alternating fields under biomedical and physiological conditions, using only a single excitation frequency and a relatively low range of offset fields. The typical peak shape originates from the field dependent alignment of the MNPs. For $H_{offset} = 0$ all particles that can contribute at the excitation frequency f have a component in m_a. By increasing H_{offset}, more particles become aligned with the field, where larger particles are fully polarized for lower field amplitudes and the smaller particles saturate for larger fields with corresponding decreased contribution to m_a [8]. The contribution of particles in a sample is shown to be dependent on Néel and Brownian relaxation. For Brownian dependent contributions, factors reducing the possibility to align with both the offset field and the alternating field, influence the amplitude and shape of the dm/dH-response and consequently the estimated particle size distribution. The lognormal particle size distribution in the field-derivative of the Langevin equation is used for comparative purposes and represents the contribution of MNPs to the dm/dH-response for an equivalent population of spherical, non-interacting, superparamagnetic nanoparticles.

The analysis with a simple Langevin approach does not fully include the aspects of relaxation time as a function of alternating field amplitude H_0 [14, 22, 24, 25] and offset field amplitude H_{offset} [8, 21, 26, 27]. Furthermore, the particle size is modeled with an equivalent population of spherical shape and does not include factors of anisotropy, interaction and (complex) hydrodynamic shape (of clusters) [4, 8, 14, 25, 28, 29].

For dilution of Resovist samples, the increase of peak amplitude, combined with similar signal amplitudes for larger offset fields, indicates a change in the physical properties of the sample rather than optimized detection by changed coil filling. This is confirmed by the slight, but systematic, increase of particle size in the fitted lognormal distribution (d=16.7 nm, σ=0.22) to d=17.5 nm, σ=0.21). For stronger detection by larger coil filling, the signal increase would be over the whole offset field range.

Dilution of the suspension seems to enable detection of larger particles or clusters. Therefore, in the present DiffMag configuration, the dm/dH-response of Resovist is not fully concentration independent.

The dm/dH-response of Resovist indicates the contribution of particles with a relatively large magnetic core size, compared to the TEM results found for the individual cores in literature [13]. Therefore, we suggest the contribution of clustered particles, effectively resulting in a larger estimated particle size distribution. A diminished contribution at higher frequencies, was also observed by others [4, 30].

The different factors influencing particle mobility show a significant effect on the dm/dH signal amplitude of Resovist. These Brownian relaxation related effects are observed since we measure at relatively low excitation frequencies. Compared to the aqueous suspension, the estimated size distribution obtained for the dried sample and the agar sample is significantly reduced. Since we assume the drying process blocks free Brownian relaxation of particles, we conclude that the large sized particles in the suspension contribute to the signal via Brownian relaxation. Enpuku *et al.* already showed a significant partial Néel contribution for Resovist suspensions [4].

In our experiments, for offset fields larger than 10 mT, the signal from the immobilized particles in the agar and dried samples is larger compared to the suspension (see fig. 6.6 and 6.9). Combined with the estimated particle size distributions, this indicates that the contribution from large particles is not merely lost, but (partially) shifted to the lower particle size. This confirms the suggestion that the contribution of larger particles in suspension may originate from clusters composed of smaller magnetic cores that collectively contribute in suspension and individually contribute to the signal after immobilization [3, 4, 13].

The difference between the dm/dH-response of the Resovist suspension at both excitation frequencies and the existence of a contribution from Brownian relaxation, enables to estimate the hydrodynamic diameter of the particles. Other studies widely reported an hydrodynamic diameter of 60 nm by DLS analysis [12, 13, 16, 31, 32]. For 60 nm particles in water, the observed 15% signal decrease of the dm/dH peak is expected for frequencies larger than 7.5 kHz, whereas a 15% signal decrease at 4.4 kHz corresponds to particles with a hydrodynamic diameter of about 75 nm. The DLS analysis assumes spherical particle size and may therefore underestimate the size of non-spherical clusters. Therefore, we suggest the existence of particles in Resovist suspension with hydrodynamic behavior equivalent to spherical particles larger than 60 nm, also suggested by Enpuku [4].

The higher viscosity of agar samples, which mimics tissue properties, effectively decreased the Brownian contribution from large particles. Therefore, the present results give an indication for the particle response to alternating fields after in vivo administration of Resovist. The apparent shift from Brownian to Néel relaxation in agar and dried samples complicates the use of Resovist for quantitative information,

as was similarly observed in chapter 5. In addition to the inherent presence of Néel relaxation in Resovist, the shift makes the tracer unsuitable for immunoassay applications that desire pure Brownian relaxation [4, 30].

The regarding the Resovist response in glycerol, in other studies a more pronounced effect was observed by a more rapid decay of the harmonic magnitude for increasing harmonic number and increasing viscosity [24, 33]. In the present study, this would be equivalent to a reduced contributing particle size. Apparently, the structure and molecular size of glycerol, which is different from the elongated polysaccharides in agar, seems to affect mainly the smaller particles. The particles with a larger magnetic moment are probably relatively less influenced by the glycerol molecules.

For serum samples only a minor reduction of mean diameter of the contributing size distribution was obtained, but the signal amplitude is significantly reduced compared to the aqueous suspension which is attributed to an increased hydrodynamic diameter by protein adhesion. This should be studied more precisely, to discriminate effects of sedimentation and stabilization of the corona. The fast and sample sparing DiffMag concept, can be valuable to study the effect of particle coating, protein concentration, protein type and time on corona formation [3, 7, 23, 34].

The smaller particle size fitted to the signal after uptake by macrophages, indicates a change in Brownian relaxation, compared to the aqueous suspension. This can be explained by internalization of particles in the macrophages, which might be size dependent [35]. Factors of protein adhesion, change in viscosity and particle degradation may play a role in macrophages. These phenomena of particle uptake and protein corona formation are expected to occur after (intravenous) injection of magnetic tracer and should therefore be taken into account in the performance of an MNP tracer in biomedical applications. Similar changes in particle dynamics by particle uptake and protein adhesion were observed in other studies [3, 7, 10, 36, 37].

The results with Endorem in different media show only minor differences, mostly caused by increased viscosity. Since differences between samples with different Brownian conditions are minor, the response of Endorem is mostly attributed to Néel relaxation. The fraction of the particles with a small hydrodynamic particle size in the range of 80-150 nm can still follow the alternating field by Brownian relaxation. However, for a more accurate fit of small particle size contributions, a larger offset field range and a lower system noise would help to discriminate small differences between samples and Brownian relaxation conditions. A bimodal distribution as was used in chapter 3, is oversized for the small field range and low number of data points of the dm/dH-curves, while the assumption of a lognormal size distribution is still questionable, especially for samples with very broad distributions [14].

The currently presented approach is sensitive for changes in Brownian relaxation and can therefore be applied for immunoassays [4, 30] or measurements on target size and bio-molecular processes [37]. Because the magnetic approach for immunoassays

can discriminate free and bound markers in (complex) liquids, substrate binding and time consuming washing steps, used in spectrophotometry based methods, are not required.

6.6 Conclusions

The currently presented method, using a small alternating field with a single frequency and a relatively low range of offset fields, provides specific characterization of biomedical MNP samples, to assess the performance of MNPs in alternating fields and to detect physiological interactions. For different types of MNPs, the dm/dH response is shown to be influenced by viscosity, hydrodynamic volume (protein corona formation), agglomeration and excitation frequency. The results emphasize the importance to consider changing viscosity and particle volume increase to achieve optimal performance of MNPs in *in vivo* biomedical applications.

References

[1] Q. A. Pankhurst, N. T. K. Thanh, S. K. Jones, and J. Dobson, "Progress in applications of magnetic nanoparticles in biomedicine", Journal of Physics D: Applied Physics **42**, 224001 (2009).

[2] F. Ludwig, E. Heim, and M. Schilling, "Characterization of magnetic core-shell nanoparticles by fluxgate magnetorelaxometry, ac susceptibility, transmission electron microscopy and photon correlation spectroscopy-a comparative study", Journal of Magnetism and Magnetic Materials **321**, 1644–1647 (2009).

[3] D. Eberbeck, M. Kettering, C. Bergemann, P. Zirpel, I. Hilger, and L. Trahms, "Quantification of the aggregation of magnetic nanoparticles with different polymeric coatings in cell culture medium", Journal of Physics D: Applied Physics **43**, 405002 (2010).

[4] K. Enpuku, H. Watanabe, Y. Higuchi, T. Yoshida, H. Kuma, N. Hamasaki, M. Mitsunaga, H. Kanzaki, and A. Kandori, "Characterization of magnetic markers for liquid-phase immunoassays using brownian relaxation", Japanese Journal of Applied Physics **51** (2012).

[5] L. R. Croft, P. W. Goodwill, and S. M. Conolly, "Relaxation in x-space magnetic particle imaging", IEEE Transactions on Medical Imaging **31**, 2335–2342 (2012).

[6] D. I. Hoult, "The principle of reciprocity in signal strength calculationsa mathematical guide", Concepts in Magnetic Resonance **12**, 173–187 (2000).

[7] A. Prieto Astalan, F. Ahrentorp, C. Johansson, K. Larsson, and A. Krozer, "Biomolecular reactions studied using changes in brownian rotation dynamics of magnetic particles", Biosensors and Bioelectronics **19**, 945–951 (2004).

[8] P. C. Fannin and A. T. Giannitsis, "Investigation of the field dependence of magnetic fluids exhibiting aggregation", Journal of Molecular Liquids **114**, 89–96 (2004).

[9] W. Boron and E. Boulpaep, *Medical Physiology - Ch. 17: Organization of the cardiovascular system* (Elsevier Health Sciences) (2008).

[10] D. Eberbeck, F. Wiekhorst, U. Steinhoff, and L. Trahms, "Aggregation behaviour of magnetic nanoparticle suspensions investigated by magnetorelaxometry", Journal of Physics Condensed Matter **18** (2006).

[11] P. W. Goodwill, A. Tamrazian, L. R. Croft, C. D. Lu, E. M. Johnson, R. Pidaparthi, R. M. Ferguson, A. P. Khandhar, K. M. Krishnan, and S. M. Conolly, "Ferrohydrodynamic relaxometry for magnetic particle imaging", Applied Physics Letters **98**, 262502–3 (2011).

[12] D. X. Chen, N. Sun, and H. C. Gu, "Size analysis of carboxydextran coated superparamagnetic iron oxide particles used as contrast agents of magnetic resonance imaging", Journal of Applied Physics **106**, 063906–9 (2009).

[13] D. Eberbeck, F. Wiekhorst, S. Wagner, and L. Trahms, "How the size distribution of magnetic nanoparticles determines their magnetic particle imaging performance", Applied Physics Letters **98**, 182502–3 (2011).

[14] R. M. Ferguson, K. R. Minard, A. P. Khandhar, and K. M. Krishnan, "Optimizing magnetite nanoparticles for mass sensitivity in magnetic particle imaging", Medical Physics **38**, 1619–1626 (2011).

[15] R. M. Ferguson, A. P. Khandhar, and K. M. Krishnan, "Tracer design for magnetic particle imaging (invited)", Journal of Applied Physics **111**, 07B318–5 (2012).

[16] A. P. Khandhar, R. M. Ferguson, H. Arami, and K. M. Krishnan, "Monodisperse magnetite nanoparticle tracers for in vivo magnetic particle imaging", Biomaterials **34**, 3837–3845 (2013).

[17] C. W. Jung and P. Jacobs, "Physical and chemical properties of superparamagnetic iron oxide MR contrast agents: Ferumoxides, ferumoxtran, ferumoxsil", Magnetic Resonance Imaging **13**, 661–674 (1995).

[18] L. F. Gamarra, G. E. S. Brito, W. M. Pontuschka, J. B. Mamani, C. A. Moreira-Filho, and E. Amaro Jr, "Study of the ferrofluid drying process for morphological and nanostructural characterization", Brazilian Journal of Physics **37**, 1288–1291 (2007).

[19] B. H. Erné, K. Butter, B. W. M. Kuipers, and G. J. Vroege, "Rotational diffusion in iron ferrofluids", Langmuir **19**, 8218–8225 (2003).

[20] B. W. M. Kuipers, I. A. Bakelaar, M. Klokkenburg, and B. H. Erné, "Complex magnetic susceptibility setup for spectroscopy in the extremely low-frequency range", Review of Scientific Instruments **79**, – (2008).

[21] P. Fannin, C. Marin, and C. Couper, "Investigation of magnetic fluids exhibiting field-induced increasing loss peaks", Journal of Magnetism and Magnetic Materials **322**, 1677 – 1681 (2010), proceedings of the Joint European Magnetic Symposia.

[22] T. Yoshida, K. Ogawa, K. Enpuku, N. Usuki, and H. Kanzaki, "AC susceptibility of magnetic fluid in nonlinear brownian relaxation region: Experiment and comparison with numerical simulation", Japanese Journal of Applied Physics **49**, 053001 (2010).

[23] E. Casals, T. Pfaller, A. Duschl, G. Oostingh, and V. Puntes, "Time evolution of the nanoparticle protein corona", ACS Nano **4**, 3623–3632 (2010).

[24] A. M. Rauwerdink and J. B. Weaver, "Harmonic phase angle as a concentration-independent measure of nanoparticle dynamics", Medical Physics **37**, 2587–2592 (2010).

[25] P. Déjardin and Y. Kalmykov, "Relaxation of the magnetization in uniaxial single-domain ferromagnetic particles driven by a strong ac magnetic field", Journal of Applied Physics **106**, – (2009).

[26] F. Ludwig, A. Guillaume, M. Schilling, N. Frickel, and A. M. Schmidt, "Determination of core and hydrodynamic size distributions of cofe[sub 2]o[sub 4] nanoparticle suspensions using ac susceptibility measurements", Journal of Applied Physics **108**, 033918–5 (2010).

[27] J. B. Weaver, A. M. Rauwerdink, C. R. Sullivan, and I. Baker, "Frequency distribution of the nanoparticle magnetization in the presence of a static as well as a harmonic magnetic field", Medical Physics **35**, 1988–1994 (2008).

[28] J. Weizenecker, B. Gleich, J. Rahmer, and J. Borgert, "Micro-magnetic simulation study on the magnetic particle imaging performance of anisotropic mono-domain particles", Physics in Medicine and Biology **57**, 7317 (2012).

[29] S. Sarangi, I. C. Tan, and A. Brazdeikis, "Brownian relaxation of interacting magnetic nanoparticles in a colloid subjected to a pulsatile magnetic field", Journal of Nanoscience and Nanotechnology **11**, 4136–4141 (2011).

[30] A. K. Bhuiya, M. Asai, H. Watanabe, T. Hirata, Y. Higuchi, T. Yoshida, and K. Enpuku, "Characterization of magnetic markers and sensors for liquid-phase immunoassays using brownian relaxation", IEEE Transactions on Magnetics **48**, 2838–2841 (2012).

[31] R. Lawaczeck, H. Bauer, T. Frenzel, M. Hasegawa, Y. Ito, K. Kito, N. Miwa, H. Tsutsui, H. Vogler, and H.-J. Weinmann, "Magnetic iron oxide particles coated with carboxydextran for parenteral administration and liver contrasting", Acta Radiologica **38**, 584–597 (1997).

[32] Y. Ishihara, T. Honma, S. Nohara, and Y. Ito, "Evaluation of magnetic nanoparticle samples made from biocompatible ferucarbotran by time-correlation magnetic particle imaging reconstruction method", BMC Medical Imaging **13**, 15 (2013).

[33] J. Weaver and E. Kuehlert, "Measurement of magnetic nanoparticle relaxation time", Medical Physics **39**, 2765–2770 (2012).

[34] J. Dieckhoff, A. Lak, M. Schilling, and F. Ludwig, "Protein detection with magnetic nanoparticles in a rotating magnetic field", Journal of Applied Physics **115**, – (2014).

[35] C. D. Walkey, J. B. Olsen, H. Guo, A. Emili, and W. C. W. Chan, "Nanoparticle size and surface chemistry determine serum protein adsorption and macrophage uptake", Journal of the American Chemical Society **134**, 2139–2147 (2012).

[36] F. Wiekhorst, C. Seliger, R. Jurgons, U. Steinhoff, D. Eberbeck, L. Trahms, and C. Alexiou, "Quantification of magnetic nanoparticles by magnetorelaxometry and comparison to histology after magnetic drug targeting", Journal of Nanoscience and Nanotechnology **6**, 3222–3225 (2006).

[37] S.-H. Chung, A. Hoffmann, K. Guslienko, S. D. Bader, C. Liu, B. Kay, L. Makowski, and L. Chen, "Biological sensing with magnetic nanoparticles using brownian relaxation (invited)", Journal of Applied Physics **97**, 10R101 (2005).

7

General Discussion and Outlook

In this final chapter a general discussion, which summarizes the main conclusions and gives a short outlook, recapitulates the research described in this thesis. In the first sections the use of magnetic nanoparticle detection in medicine is discussed, with a focus on sentinel lymph node detection. The subsequent sections discuss the technical aspects of DiffMag and its possibilities for biomedical applications.

7.1 Magnetic detection of sentinel lymph nodes

The increasing interest for magnetic detection of sentinel lymph nodes stimulated to investigate the technical aspects related to clinical implementation. The existing tracers, blue dye and technetium colloid, have significant drawbacks in clinical practice. The magnetic route for sentinel lymph node mapping (SLNM) is a promising alternative. The study to ex vivo colorectal SLNM in the present thesis shows the feasibility of this approach. The performance of the procedure was only tested on 10 patients, which should be at least 5 to 10 times larger to draw firm conclusions with clinical value. However, the results obtained so far encourage further investigations.

7.2 VSM detection of MNPs in biological samples

The clinical use of MNPs in MRI is still very limited and direct magnetic detection of MNPs in clinically relevant samples outside MRI is in an early stage of development. This work opens the perspective of clinical MNP use in the operating room. A rapidly emerging application is magnetic detection of sentinel lymph nodes with an MNP tracer. Since this application requires new detection technology to assist surgeons or pathologists to search for sentinel nodes filled with MNP tracer, an important objective of the present research was to reveal the requirements, optimal characteristics and detection limits of such a device. At present sentinel lymph node mapping for colorectal cancer is increasingly investigated and can be performed in an *ex vivo* fashion [1, 2]. In this perspective the VSM measurements as a gold standard in the chapters 3 and 4 have provided quantitative insight in magnetic measurements on clinical samples, while the magnetic *ex vivo* procedure for colorectal cancer is tested on its feasibility.

The iron content in lymph nodes could be well estimated by VSM with microgram precision. Initially, the varying and strong linear response of the individual lymph node samples hindered the analysis of the measurements with all parameters in the Langevin model. For very small amounts of Endorem, the nonlinear contribution could not be accurately determined. In addition, the combination of soft tissue and sample vibrations makes the small signal vulnerable for noise contributions from parasitic movements. The magnetization measurements of lymph nodes were therefore analyzed using a model with predetermined, fixated parameters for the nonlinear

contribution, based on the calibration measurements with a pronounced nonlinear response. For these samples the parameters defining the linear response and the amplitude of the MNP response (the saturation magnetic moment) were estimated. Even the lowest amounts of Endorem in the lymph nodes, equivalent to about 1 μg of iron, were all confirmed by microscopic iron staining, whereas no lymph nodes free of MNPs by VSM analysis were indicated to contain MNPs by microscopy. Therefore, the procedure developed for lymph node analysis showed to work well as there were no indications of failure in magnetic SLN selection.

Still the VSM was the best choice to perform a first magnetic analysis of magnetic SLNM. The availability of an existing technique with a proven capability for quantitative measurements on MNPs facilitated the fast onset of the first experiments. A detection coil set with a larger bore size that could fit the tissue samples was available, as well as a fixation system enabling an effective fixation of samples with different size. The VSM procedure was optimized for accurate magnetic measurements on fresh or formalin fixated tissue. Aside from the clinical relevance of patients, the *ex vivo* character of the SLNM procedure for colorectal cancer enabled implementation without significant patient risks or alterations of clinical procedures. The relevance of *ex vivo* measurements for MNP tracer detection in selected lymph nodes, supported the use of VSM at a distant laboratory location.

The VSM measurements have provided insight in several aspects of magnetic measurements in lymph nodes. The amount of Endorem tracer accumulated in the lymph nodes indicates the required detection limit for a clinical probe for both *in vivo* and *ex vivo* use. The linear magnetic contribution from tissue can significantly interfere with a small contribution of a few micrograms iron in MNPs. This observation is in accordance with the theoretical analysis in 2 and confirms the necessity of an MNP specific detection method for high sensitive *in vivo* measurements. MNPs with a stronger nonlinear response enable a lower mass detection limit, since for a lower amount of iron the signal surpasses the signal from tissue.

Since the measurements with VSM were time consuming and not specificly designed for unique detection of MNPs, magnetic methods that are developed with the purpose of MNP detection in tissue with linear magnetic properties, will increase the possibilities of a fast protocol for clinical MNP application. The differential magnetometry concept, as developed in chapter 5, exploits the nonlinear magnetic properties of MNPs with a fast measurement that is not sensitive for tissue and can be performed with small and efficient systems suitable for a clinical environment like the operating theatre. This concept is discussed in the following sections.

In conclusion, the VSM measurements of lymph nodes retrieved from SLNM colorectal cancer with Endorem and blue dye, could quantitatively reveal the feasibility of *ex vivo* magnetic SLNM. The magnetic moment response of the Endorem tracer was best fitted with a bimodal lognormal distribution for the quantification of

unknown amounts of tracer in lymph nodes. VSM is useful for quantification of magnetic content in tissue samples for research to new magnetic clinical procedures and for complementary analysis in clinical studies with MNPs in MRI or other clinical detection technologies.

7.3 Differential magnetometry for MNP detection

The differential magnetometry procedure in chapter 5 is developed for high sensitive and selective MNP detection with the purpose of clinical application in interventions. The intrinsic sensitivity of VSM and standard AC-magnetometry for diamagnetic tissue, demonstrated in the chapters 2 and 3, was reason to develop a method only sensitive for nonlinear superparamagnetic magnetic materials. The DiffMag protocol achieved a detection limit in the submicrogram iron range with superparamagnetic iron oxide nanoparticles (SPIOs). Compared to VSM, the much faster measurement procedure (15 minutes vs. a few seconds) can be performed with a simple copper coil based setup suitable for implementation in clinical practice. The following sections discuss the technical aspects, preclinical experiments and clinical applications of the DiffMag research as described in chapter 5 and 6.

7.3.1 Technical performance

As is shown in chapter 5, the mass sensitivity of a DiffMag probe depends on the MNP relaxation properties, which are strongly related to core size and hydrodynamic particle size. In general, particles with a large core size show a larger initial susceptibility with saturation for lower field amplitudes and thus give a larger response for a small excitation field.

For probes with only alternating field excitation MNPs with a larger initial susceptibility provide increased sensitivity and a better contrast with the linear magnetic response of tissue (see chapter 2, section 2.4). Therefore, to improve clinical performance it is more sensible to invest in a suitable MNP tracer than simply increasing the alternating field frequency or field amplitude of the probe.

For the DiffMag concept the situation is different, since the signal is not only based on the initial susceptibility. The DiffMag sensitivity for MNPs is based on the combination of alternating field frequency, field amplitudes and MNP properties as is shown in chapter 5 and 6. Therefore, to optimize DiffMag performance for a specific application both the MNP tracer and the different parameters of excitation have to be balanced. Since the tissue contribution is eliminated, the detection limit depends only the sensitivity and the noise level of the sensor.

With the excitation and detection parameters chosen for the sensor as presented in this thesis, the noise level was in the order of 0.5 μV, which corresponds to a

detection limit of about 0.14 μg iron for Resovist or Sienna+. As will be discussed further in 7.3.3, it is expected that the detection limit of the present sensor can be further improved to the nanogram level by optimization of thermal and mechanical stabilization.

7.3.2 Protocol optimization

To show the suitability of the DiffMag protocol for specific MNP detection, measurements with different MNPs and tissue samples were presented. The results demonstrated the concept of a simple MNP specific detection method which can be applied for clinical purposes. The combination of the applied field amplitudes and alternating field frequencies were optimal for the presented setup. For clinical implementation, optimization of the measurement protocol is desired which is very well feasible with some minor adaptations.

To facilitate progress of clinical analysis of larger sample sets in for example *ex vivo* SLN selection for colorectal cancer, detection speed can be further optimized. In the present setup detection speed was rather low, partly due to the relatively high noise contribution from liquid nitrogen. Longer averaging times with a low sampling frequency were used to obtain a stable response. Measurement times up to 1 minute for quantification or identification and 15-20 minutes for MNP characterization can be largely reduced to hundreds of milliseconds to a few minutes respectively. The detection speed can be increased by shortening of the periods in the offset field sequence. A limiting factor for minimization of the periods in the offset field sequence, is the inductive response of the field switch in the pick-up coils. A fast MNP detection algorithm requires less than 5 seconds per sample, which enables the entire SLN selection procedure for a patient (10-20 lymph nodes) to be completed in less than a few minutes.

For medical *in vivo* applications, magnetic field amplitude and the rate of field change are limited by the biomedical effects of magnetostimulation and tissue heating. For MRI, MPI and magnetic hyperthermia these limits are already investigated or defined [3, 4]. Therefore, the increase of the detected MNP response that can be achieved by larger alternating field frequencies and offset field amplitudes is always limited by the undesired biomedical response in the body.

The magnetic excitation field limits have also consequences for the suitability of different MNPs. Generally speaking, the magnetization response of MNPs with a large magnetic core is stronger compared to MNPs with a small magnetic core, as was shown in figure 5.2. Depending on the clinical application of DiffMag, probably in combination with other techniques like MRI, MPI, frequency mixing, hyperthermia or other (experimental) MNP applications, the excitation field characteristics of the DiffMag algorithm have to be optimized for the applied tracer. As long as particles show a strong nonlinear response, a relatively low offset field amplitude is sufficient

for optimal detection. However, in some applications, like for example magnetic hyperthermia, only MNPs with a small hydrodynamic size show optimal biodistribution, which limits the allowable size of the magnetic core [5, 6]. In those cases, optimal DiffMag detection can only be achieved for large offset field amplitudes, even beyond the maximum allowable amplitude. So, ideally optimization of biomedical DiffMag detection technique should go hand in hand with MNP development, similar to what is going on in the field of MPI [7–13].

7.3.3 Sensor optimization

The first DiffMag prototype worked well to investigate the technical possibilities of MNP detection in small biological samples. Sample chamber and coil dimensions were suitable to contain small lymph nodes, whereas the homogeneity of the excitation field and sensitivity of the detection coils provided optimal detection of inhomogeneously distributed MNPs. However, the bore size of 11 mm was sometimes to small to fit the larger lymph nodes. Therefore, for lymph node analysis, a bore size in the order of 25 mm is recommended [14, 15].

Depending on the actual application of DiffMag the configuration and geometry of the coil set can be changed. For specific, quantitative analysis of small sample volumes ($\sim$1-10 mL) the configuration with a sample enclosing coil is desired. For a handheld sensor for clinical interventions there are more approaches thinkable to design a suitable coil configuration in terms of excitation field production, depth sensitivity and geometry. In this case there can be thought of splitting the detection part and the excitation part. With large excitation coils positioned below the patient and a small handheld detector operated by the surgeon, the handheld part can be kept small while depth sensitivity of the sensor improves compared to detectors with integrated excitation coils [16].

The electrical, thermal and mechanical stability of the setup was achieved by cooling with liquid nitrogen. The balanced geometry of the coil set is susceptible to minor changes due to thermal expansion related to the excitation current. The low temperature of liquid nitrogen allowed larger excitation currents while the coil set remains stable. The initial idea to decrease the sensor's noise level by cooling the detection coil with liquid nitrogen was not successful. Instead, cooling with liquid nitrogen resulted in a larger noise contribution, which is attributed to bubble formation causing capacitive fluctuations and mechanical vibrations in the setup [17, 18]. Therefore, the thermal noise level of the detection coil was not reached.

The DiffMag measurements work with significant offset field amplitudes and thus require relatively large currents, compared to the current that produces the alternating field. For copper coils this implies a considerable heat production which demands adequate cooling. The heat production can be minimized by reducing the relative period of offset field excitation in a low duty cycle. To maintain the advantageous stability

while avoiding the noise contribution of liquid nitrogen cooling, another coolant, like water or oil, or another cooling mechanism will improve the minimum noise level. For the research presented here, liquid nitrogen was only essential to provide stability and to lower the load on the current sources by reducing the excitation coil resistance, which allowed larger excitation field amplitudes. Low temperature cooling does not improve detection as long as the system's noise does not approach thermal noise level of the detection coil.

To obtain probes with a high sensitivity and specificity for MNPs, specialized excitation and detection algorithms, functional hardware and accurate signal analysis are required to exploit the nonlinear properties of MNPs. The complexity of clinical practice, demands a multidisciplinary approach to achieve magnetic systems that can be successfully applied. In addition to the physical and electromagnetic aspects, the clinical environment, procedures and requirements have to be taken into account. Sensors for intra-operative use should not hamper the workflow, spending costly operating time. Furthermore, the sensor design should enable smooth implementation in the surgical practice, with proper size, optimal handling, minimal sight impediment and robustness against interference with other instruments. In the design of new detection technology, it is important to consider these aspects as early as possible.

7.3.4 dm/dH measurements

The sequence that was developed to measure the field derivative of the magnetization response is useful to investigate the relaxation properties of MNPs in different media. The MNP characteristic peak curves are analyzed using the field derivative of the Langevin and a lognormal distributed particle size. Since the particle response is based on alternating field excitation, only particles that can contribute by particle relaxation are detected. Particles with characteristic relaxation times much longer than the period of the excitation field do not contribute to the signal and remain undetected. The estimated particle size distribution obtained from the measured data is therefore regarded as the distribution of the population fraction that is contributing to the signal.

Compared to the MPI-relaxometers and spectrometers, the approach of dm/dH-measurements has a relatively low alternating field amplitude, while the offset field range determines the degree of magnetic saturation. Therefore the MNP response is mainly dominated by the excitation frequency and the offset field amplitude, while field velocity has not a large impact on the MNP response.

Since the MNP relaxation can take place via Neél and Brownian relaxation, the dm/dH measurements are suitable to investigate the conditions for these phenomena. This aspect is further discussed in the context of biomedical applications in section 7.4.5.

7.4 Clinical applicability of DiffMag

The DiffMag concept presented in this thesis, is developed with a focus on clinical magnetic detection during interventions. To obtain a technique that can specificly detect a small amount of MNPs in a large tissue volume using a small and efficient system, the DiffMag concept was developed. Since the diamagnetic contribution of tissue is eliminated, tiny amounts of MNP deep located in tissue are detectable. Although magnetic SLNM was used as a leading case in the present thesis, there are also possibilities to use DiffMag for other, probably more demanding, clinical diagnostic and therapeutic methods that require sensitive and specific detection of a tracer (deep) in the body. A short discussion and outlook about the clinical applicability of DiffMag can be found in the next sections.

7.4.1 Sentinel lymph node detection in colorectal cancer

As discussed in 4 the traditional visual and radioactive SLNM tracers, currently applied in colorectal cancer, have significant drawbacks in terms of handling, timing, detection rates and safety. For this procedure in colorectal cancer there are several reasons to use an MNP tracer in combination with a high sensitive, MNP specific detector. Magnetic measurements on lymph nodes retrieved from colorectal cancer patients showed the feasibility of the magnetic detection route for SLNM. The results so far are promising and encourage further investigations of magnetic SLNM in colorectal cancer, with for each patient a thorough analysis of MNP accumulation in all lymph nodes retrieved from a specimen. The time consuming VSM protocol allowed the analysis of only selected blue nodes, but the much faster DiffMag protocol is suitable to perform the desired analysis of all lymph nodes. Then, the magnetic route of SLNM makes significant optimization of SLNM for colorectal cancer possible.

Compared to the use of magnetic tracer, (postsurgical) SLN dissection using blue dye or ratio-isotopes is much more time critical. The lasting magnetic properties and the colloidal nature of an MNP tracer that retains in the sentinel lymph node after resection, enable SLN detection for longer time after surgery. Furthermore, the other drawbacks of the traditional SLNM tracers, concerning safety or visibility in deeper locations, are solved by safe chemical and magnetic properties and increased detection depth (in the order of centimeters) of magnetic systems compared to optical systems. In addition, it has been reported the magnetic tracer is suitable to be used as a visual tracer for SLNM [19].

It remains to be seen whether intraoperative SLNM is the preferred technique for magnetic detection in colorectal cancer. For intraoperative detection the probe design should be suitable for surgical handling and the surgical practice. The increasing portion of laparoscopic interventions for colorectal cancer requires a different approach of probe design compared to the probes used for open surgery in breast cancer or

lung cancer [19–24]. The inner diameter of a trocar as well as the properties of typical surgical instruments used in laparoscopy are of importance to consider in design of a magnetic probe. Small detector size is possible with DiffMag by splitting the coil geometry in a handheld detector and static excitation coils, as was suggested before.

In the present thesis, postsurgical *ex vivo* SLNM was performed, which saved the administration of a tracer in patients and prevented the use of intraoperative instruments. In the standard surgical treatment of colorectal cancer with complete resection of the nodal basin, the surgeon does not necessarily need to know the actual position or status of the sentinel node to determine the surgical strategy. Only in cases of aberrant drainage ($\leq$4%), the surgical approach may be altered [1, 2]. This justifies for most cases postsurgical SLNM analysis of the resected specimen and enables separate measurements on individual sentinel and non-sentinel nodes found by the pathologist.

For postsurgical analysis, both the use of a handheld probe handled by a surgeon or a pathologist is sensible to localize the SLN in the specimen. For specimens with a thick mesenterium and limited possibilities for optical SLNM, a handheld DiffMag probe specificly sensitive to MNPs can assist the surgeon or pathologist to identify the SLNs. A standalone, sample enclosing magnetic probe is suitable for magnetic selection of the SLN out of all retrieved lymph nodes. Especially for the small lymph nodes usually found in the mesenterium, a high sensitive MNP sensor that encloses the sample will improve unambiguous MNP detection. The DiffMag concept with its high MNP-specificity and potentially fast measurement, is very suitable to perform this analysis, in particular for larger series of lymph nodes.

7.4.2 Sentinel lymph node detection in breast cancer

In chapter 2 the current status of magnetic SLNM for breast cancer has been shortly reviewed. For these studies different magnetic probes have been used for intraoperative detection of the sentinel node. The SentiMag probe that is used in the European study, is based on a single alternating excitation field and a gradiometer detector [19]. However, a sensor using simple alternating field detection is not specificly sensitive for MNPs as long as nonlinear properties (e.g. higher harmonics) are not collected or analyzed. Depending on the excitation field produced by the probe, the nonlinear magnetic response of a little amount of MNPs in the tissue can be fully hidden by the variations of the diamagnetic tissue response, as was shown by the calculations in section 2.4.

Especially for the so called 'hotspot' detection, the selective MNP detection of DiffMag will be valuable. The surgeon uses the probe to detect the location of the sentinel node noninvasively, to determine the optimal location of the incision. For this part of the SLN procedure in breast cancer a good depth sensitivity in the order of 3-5 centimeters and effective elimination of tissue detection are crucial. For a sensor

with only (homogeneous) alternating field excitation, the lymph node should contain at least about 100 micrograms of iron (see section 2.4). In practice, for a sensor like the SentiMag, the excitation field decays with the distance from the probe and thus the resulting magnetization and the relative voltage response for deeper located sentinel nodes is even lower. Depth sensitivity of a DiffMag handheld sensor can be improved by increasing the amplitudes of the excitation field, while the increased diamagnetic response is effectively eliminated and the MNP response increases.

The complex and variable environment of surgical interventions requires a detection technique that is specificly sensitive for MNPs. When contributions from tissue and environment can be effectively eliminated, variations in these contributions can no longer bias MNP detection. Therefore the DiffMag approach is a very promising approach. In addition to its MNP specificity, the DiffMag approach has increased depth sensitivity in a single sided handheld probe, since for larger excitation fields the increasing linear contribution from tissue is effectively removed. Therefore the DiffMag sensor can principally detect deeper located lymph nodes compared to a single alternating field sensor, like the SentiMag.

In contrast to the case of colorectal cancer, SLNM in breast cancer is a typical diagnostic, surgical method, used to determine the therapeutic path for a patient. The earlier the status of (sentinel) nodes are known, the better the optimal treatment can be determined. The use of a magnetic tracer for SLNM provides new possibilities for preoperative and intraoperative diagnostics. Therefore, magnetic SLNM in breast cancer has to be developed keeping in mind the most optimal diagnostic route for the sentinel node. In this perspective, DiffMag can play a valuable role in magnetic SLNM for breast cancer.

7.4.3 Other clinical interventions

In addition to magnetic sentinel lymph node detection, the DiffMag concept can intensify development of MNP application in other clinical interventions. Several preclinical studies already reported on the possibility of magnetic detection of tumors. The localization of tumor tissue is especially important for nonpalpable or small tumors [25, 26]. For this purpose a handheld DiffMag sensor can be used intraoperatively to localize MNP labeled tumor sites. The success of this intraoperative localization depends on the probe sensitivity and the amount of particles that can specificly localized at the tumor site. For tumors located deep in the body, the promising perspective of DiffMag regarding depth sensitivity will be crucial for successful implementation. For magnetic labeling of tumors different approaches can be used, including intratumoral injection and intravenous administration of tumor targeted MNPs labeled with an antigen. The intratumoral injection suggested by Ahmed *et al.* provides a better dose control at the lesion, whereas targeted MNPs via intravenous administration probably give a better distribution through the entire

tumor volume [25].

After resection of the tumor, the resection surface can be scanned with a probe to check whether tumor resection was complete. If there is some marginal tumor tissue left, the resection can be completed until the DiffMag signal is zero. The very tiny amounts of iron to be detected in a large body, in the order of tens of picograms per cell [27], require the high specificity for MNPs as is achieved by the DiffMag protocol.

7.4.4 Combinations with other diagnostic and therapeutic techniques

In sentinel lymph node detection, the MNP based intra-operative technique with DiffMag can be combined with a preoperative MRI as is shown by Shiozawa [28]. The present use of lymphoscintigraphy lacks detailed anatomical information, leading to the introduction of SPECT/CT-imaging with undesired, additional radiation exposure [29]. With the magnetic alternative the anatomical information can be obtained by MRI, as the MNPs can be used as a MRI contrast agent. The loss of resolution power at the cost of the elimination of radiation exposure is acceptable [28].

The MNP tracer distribution in lymph nodes, visualized by MRI, can reveal the metastatic state of lymph nodes [30]. Preoperative staging of lymph nodes is of importance, to reduce the number of operative procedures, needed to accurately treat a patient. For a patient with a positive preoperative diagnosis of lymph nodes, the SLNB procedure as well as a second surgery to remove the whole nodal basin can be omitted. After the preoperative scan, the MNP tracer in the lymph nodes can still be used for intra-operative detection with a handheld sensor. In case of inconclusive MRI results or metastatic areas smaller than the resolution of MRI, microscopic analysis after the magnetic SLNB can give a decisive answer about metastatic stage. SLNB may be avoided when the sentinel node is diagnosed as disease-free by the preoperative MRI.

Similar to what is done in MR-lymphography [31, 32], photoacoustics can be used to image the MNP distribution in the sentinel lymph node to determine the presence of metastases after resection [33]. The combined modality of magnetic and photoacoustic detection using the same tracer can bring a complete SLN-analysis platform in the operating theater with a relatively simple detection and imaging system. Similar to MPI, photoacoustic imaging mainly images the tracer and lacks therefore an anatomical reference. Therefore, it remains to be seen whether diagnostic accuracy of photoacoustic imaging (or MPI) lymph node staging will be high enough. Especially the physiological filling of the lymph nodes can be different from what is expected from intravenous administration as is used in MR-lymphography [31], because of the time course and the interstitial injection of MNP tracer in SLNM. However, the transition to magnetic SLNM using a DiffMag sensor can be combined with the application of additional diagnostic techniques that potentially improve the

clinical path in cancer diagnosis.

A combination of DiffMag with intra-operative diagnostics that gives a decisive answer about the status of the sentinel node may introduce a larger uncertainty in surgical planning. The conclusion of metastatic sentinel nodes is usually followed by gross nodal resection, which takes significantly more operating time. The uncertainty about the diagnostic outcome of SLNM during surgery, complicates scheduling with estimated operation times, with consequent effects on clinical flow and costs. On the other hand, for patients with positive SLNs, the intraoperative analysis saves another surgery for axillary lymph node dissection and thus reduces personal, clinical and financial burden [34].

7.4.5 Detection of cellular and biochemical phenomena and MNP characterization

In the development of MNPs for *in vivo* applications, surface chemistry is an important issue to achieve optimal performance. As follows from the results in chapter 6, the DiffMag dm/dH measurements can play a valuable role to investigate the interaction between MNP and environment.

Aside from the effect of the coating on magnetic properties [35], the surface of the MNPs is particularly important for blood circulation time and biomolecular interactions. The large surface to volume ratio causes the MNPs to agglomerate and absorb plasma proteins. Hydrophobic surface properties accompany increased uptake by the reticuloendothelial system. Therefore, coverage of MNPs with surfactant that minimizes protein adsorption is important to increase blood circulation time [35]. To investigate the effect of surface modification, MNPs with different surface chemistry can be tested with DiffMag characterization in larger *in vitro* samples and probably even *in vivo*, in small animals.

The sensitivity of DiffMag for changes in MNP relaxation can be used to observe specific processes of MNP binding to cells or biomolecules, which includes a wide range of possibilities for therapeutics and diagnostics [36]. After *in vitro* or *in vivo* MNP internalization in cells or attachment to molecules or cell membranes using functional groups, like antibodies or fragments directed to a receptor, magnetic systems can be used for monitoring and manipulation [35, 37, 38]. *In vitro* applications have already been developed to enter the market for biomedical applications [39]. *In vivo* applications are still in the phase of animal experiments [37, 40]. The advantage of DiffMag in this context will be the exclusive magnetic method using a single excitation frequency, which can be realized in a rather simple setup.

7.5 Closing remarks

The increasing interest for MNP detection during clinical interventions, driven by the desire of radiation free procedures and by development of new clinical procedures, requires development of high-sensitive, MNP specific detection technology that is suitable for clinical use. The promising possibilities of MNPs for sentinel lymph node detection have been quantitatively demonstrated in a feasibility study for colorectal cancer. The development of DiffMag as an MNP specific detection method that eliminates the diamagnetic contribution of tissue, provides a route for implementation of safe and user-friendly magnetic probes with increased depth sensitivity in different clinical interventions. Finally, the DiffMag dm/dH measurements have shown to be a valuable tool to characterize MNP samples in different environmental conditions, which can be used to detect specific MNP related biomolecular and cellular processes.

References

[1] E. S. Van der Zaag, W. H. Bouma, P. J. Tanis, D. T. Ubbink, W. A. Bemelman, and C. J. Buskens, "Systematic review of sentinel lymph node mapping procedure in colorectal cancer", Annals of Surgical Oncology **19**, 3449–3459 (2012).

[2] M. H. G. M. Van der Pas, S. Meijer, O. S. Hoekstra, I. I. Riphagen, H. C. W. de Vet, D. L. Knol, N. C. T. van Grieken, and W. J. H. J. Meijerink, "Sentinel-lymph-node procedure in colon and rectal cancer: a systematic review and meta-analysis", The Lancet Oncology **12**, 540–550 (2011).

[3] E. U. Saritas, P. W. Goodwill, G. Z. Zhang, and S. M. Conolly, "Magnetostimulation limits in magnetic particle imaging", Medical Imaging, IEEE Transactions on **32**, 1600–1610 (2013).

[4] S. Dutz and R. Hergt, "Magnetic nanoparticle heating and heat transfer on a microscale: Basic principles, realities and physical limitations of hyperthermia for tumour therapy", International Journal of Hyperthermia **29**, 790–800 (2013), pMID: 23968194.

[5] I. Hilger, "In vivo applications of magnetic nanoparticle hyperthermia", International Journal of Hyperthermia **29**, 828–834 (2013), pMID: 24219800.

[6] M. Bañobre-López, A. Teijeiro, and J. Rivas, "Magnetic nanoparticle-based hyperthermia for cancer treatment", Reports of Practical Oncology & Radiotherapy **18**, 397 – 400 (2013), selected Papers Presented at the {XVII} {SEOR} Congress, Vigo, 1821 June 2013.

[7] D. Eberbeck, F. Wiekhorst, S. Wagner, and L. Trahms, "How the size distribution of magnetic nanoparticles determines their magnetic particle imaging performance", Applied Physics Letters **98**, 182502–3 (2011).

[8] R. M. Ferguson, K. R. Minard, and K. M. Krishnan, "Optimization of nanoparticle core size for magnetic particle imaging", Journal of Magnetism and Magnetic Materials **321**, 1548–1551 (2009).

[9] R. M. Ferguson, K. R. Minard, A. P. Khandhar, and K. M. Krishnan, "Optimizing magnetite nanoparticles for mass sensitivity in magnetic particle imaging", Medical Physics **38**, 1619–1626 (2011).

[10] R. M. Ferguson, A. P. Khandhar, and K. M. Krishnan, "Tracer design for magnetic particle imaging (invited)", Journal of Applied Physics **111**, 07B318–5 (2012).

[11] F. Ludwig, T. Wawrzik, T. Yoshida, N. Gehrke, A. Briel, D. Eberbeck, and M. Schilling, "Optimization of magnetic nanoparticles for magnetic particle imaging", IEEE Transactions on Magnetics **48**, 3780–3783 (2012).

[12] J. Weizenecker, J. Borgert, and B. Gleich, "A simulation study on the resolution and sensitivity of magnetic particle imaging", Physics in Medicine and Biology **52**, 6363 (2007).

[13] J. Weizenecker, B. Gleich, J. Rahmer, and J. Borgert, "Micro-magnetic simulation study on the magnetic particle imaging performance of anisotropic mono-domain particles", Physics in Medicine and Biology **57**, 7317 (2012).

[14] S. Thakur, U. Somashekar, S. K. Chandrakar, and D. Sharma, "Anatomic study of distribution, numbers, and size of lymph nodes in mesorectum in indians: A cadaveric study", International Journal of Surgical Pathology (2011).

[15] M. Memarsadeghi, C. C. Riedl, A. Kaneider, A. Galid, M. Rudas, W. Matzek, and T. H. Helbich, "Axillary lymph node metastases in patients with breast carcinomas: Assessment with nonenhanced versus USPIO-enhanced MR imaging", Radiology **241**, 367–377 (2006), pMID: 17057065.

[16] S. Waanders, M. Visscher, T. Oderkerk, and B. ten Haken, "Finding the sentinel lymph node with a handheld differential magnetometer", in *Magnetic Particle Imaging (IWMPI), 2013 International Workshop on*, 1–1 (2013).

[17] J. Allen, "The University of Illinois spiral-ridge cyclotron", Proceedings of Sector-Focused Cyclotrons 89–96 (1959).

[18] Y. Khatami, M. Alavi, F. Sarreshtedari, M. Vesaghi, M. Banzet, J. Schubert, and M. Fardmanesh, "Low noise SQUID based NDE with non-magnetic scanning system in unshielded environment", Journal of Physics: Conference Series **97**, 012064 (2008).

[19] M. Douek, J. Klaase, I. Monypenny, A. Kothari, K. Zechmeister, D. Brown, L. Wyld, P. Drew, H. Garmo, O. Agbaje, Q. Pankhurst, B. Anninga, M. Grootendorst, B. Haken, M. Hall-Craggs, A. Purushotham, and S. Pinder, "Sentinel node biopsy using a magnetic tracer versus standard technique: The sentimag multicentre trial", Annals of Surgical Oncology 1–9 (2013).

[20] T. Nakagawa, Y. Minamiya, Y. Katayose, H. Saito, K. Taguchi, H. Imano, H. Watanabe, K. Enomoto, M. Sageshima, T. Ueda, and J. I. Ogawa, "A novel method for sentinel lymph node mapping using magnetite in patients with non-small cell lung cancer", Journal of Thoracic and Cardiovascular Surgery **126**, 563–567 (2003).

[21] Y. Minamiya, M. Ito, Y. Katayose, H. Saito, K. Imai, Y. Sato, and J. I. Ogawa, "Intraoperative sentinel lymph node mapping using a new sterilizable magnetometer in patients with nonsmall cell lung cancer", Annals of Thoracic Surgery **81**, 327–330 (2006).

[22] Y. Minamiya, M. Ito, Y. Hosono, H. Kawai, H. Saito, Y. Katayose, S. Motoyama, and J.-i. Ogawa, "Subpleural injection of tracer improves detection of mediastinal sentinel lymph nodes in non-small cell lung cancer", European Journal of Cardio-Thoracic Surgery **32**, 770–775 (2007).

[23] T. Ono, Y. Minamiya, M. Ito, H. Saito, S. Motoyama, H. Nanjo, and J. Ogawa, "Sentinel node mapping and micrometastasis in patients with clinical stage ia non-small cell lung cancer", Interactive CardioVascular and Thoracic Surgery **9**, 659–661 (2009).

[24] M. Shiozawa, A. Lefor, Y. Hozumi, K. Kurihara, N. Sata, Y. Yasuda, and M. Kusakabe, "Sentinel lymph node biopsy in patients with breast cancer using superparamagnetic iron oxide and a magnetometer", Breast Cancer **20**, 223–229 (2013).

[25] M. Ahmed, R. T. M. de Rosales, and M. Douek, "Preclinical studies of the role of iron oxide magnetic nanoparticles for nonpalpable lesion localization in breast cancer", Journal of Surgical Research **185**, 27 – 35 (2013).

[26] H. Hathaway, K. Butler, N. Adolphi, D. Lovato, R. Belfon, D. Fegan, T. Monson, J. Trujillo, T. Tessier, H. Bryant, D. Huber, R. Larson, and E. Flynn, "Detection of breast cancer cells using targeted magnetic nanoparticles and ultra-sensitive magnetic field sensors", Breast Cancer Research **13**, R108 (2011).

[27] C. Sun, O. Veiseh, J. Gunn, C. Fang, S. Hansen, D. Lee, R. Sze, R. G. Ellenbogen, J. Olson, and M. Zhang, "In vivo MRI detection of gliomas by chlorotoxin-conjugated superparamagnetic nanoprobes", Small **4**, 372–379 (2008).

[28] M. Shiozawa, S. Kobayashi, Y. Sato, H. Maeshima, Y. Hozumi, A. Lefor, K. Kurihara, N. Sata, and Y. Yasuda, "Magnetic resonance lymphography of sentinel lymph nodes in patients with breast cancer using superparamagnetic iron oxide: a feasibility study", Breast Cancer 1–8 (2012).

[29] I. M. C. Van Der Ploeg, R. A. Valdés Olmos, O. E. Nieweg, E. J. T. Rutgers, B. B. R. Kroon, and C. A. Hoefnagel, "The additional value of spect/ct in lymphatic mapping in breast cancer and melanoma", Journal of Nuclear Medicine **48**, 1756–1760 (2007).

[30] K. Motomura, M. Ishitobi, Y. Komoike, H. Koyama, A. Noguchi, H. Sumino, Y. Kumatani, H. Inaji, T. Horinouchi, and K. Nakanishi, "SPIO-enhanced magnetic resonance imaging for the detection of metastases in sentinel nodes localized by computed tomography lymphography in patients with breast cancer", Annals of Surgical Oncology **18**, 3422–3429 (2011).

[31] M. G. Harisinghani, M. A. Saksena, P. F. Hahn, B. King, J. Kim, and R. Torabi, Maha T. Weissleder, "Ferumoxtran-10-enhanced mr lymphangiography: Does contrast-enhanced imaging alone suffice for accurate lymph node characterization?", American Journal of Roentgenology **186**, 144–148 (2006).

[32] J. O. Barentsz, J. J. Fütterer, and S. Takahashi, "Use of ultrasmall superparamagnetic iron oxide in lymph node mr imaging in prostate cancer patients", European Journal of Radiology **63**, 369–372 (2007).

[33] D. J. Grootendorst, R. M. Fratila, M. Visscher, B. T. Haken, R. J. A. van Wezel, S. Rottenberg, W. Steenbergen, S. Manohar, and T. J. M. Ruers, "Intra-operative ex vivo photoacoustic nodal staging in a rat model using a clinical superparamagnetic iron oxide nanoparticle dispersion", Journal of Biophotonics **6**, 493–504 (2013).

[34] S. Lanitis, C. Poulou, V. Armoutidis, V. Samaras, G. Sgourakis, C. Karaliotas, M. Korontzi, C. Tsikos, K. Barbatis, and C. Karaliotas, "Intraoperative assessment via imprint cytology and frozen section or postoperative assessment of the sentinel lymph node in breast cancer?", Hellenic Journal of Surgery **84**, 214–219 (2012).

[35] A. K. Gupta and M. Gupta, "Synthesis and surface engineering of iron oxide nanoparticles for biomedical applications", Biomaterials **26**, 3995–4021 (2005).

[36] J. Connolly and T. G. S. Pierre, "Proposed biosensors based on time-dependent properties of magnetic fluids", Journal of Magnetism and Magnetic Materials **225**, 156 – 160 (2001), proceedings of the Third International Conference on Scientific and Clinical Applications of Magnetic Carriers.

[37] S. Laurent, D. Forge, M. Port, A. Roch, C. Robic, L. Vander Elst, and R. N. Muller, "Magnetic iron oxide nanoparticles: Synthesis, stabilization, vectorization, physicochemical characterizations, and biological applications", Chemical Reviews **108**, 2064–2110 (2008).

[38] J. W. M. Bulte and D. L. Kraitchman, "Iron oxide mr contrast agents for molecular and cellular imaging", NMR in Biomedicine **17**, 484–499 (2004).

[39] D. Issadore, C. Min, M. Liong, J. Chung, R. Weissleder, and H. Lee, "Miniature magnetic resonance system for point-of-care diagnostics", Lab Chip **11**, 2282–2287 (2011).

[40] R. Di Corato, F. Gazeau, C. Le Visage, D. Fayol, P. Levitz, F. Lux, D. Letourneur, N. Luciani, O. Tillement, and C. Wilhelm, "High-resolution cellular MRI: Gadolinium and iron oxide nanoparticles for in-depth dual-cell imaging of engineered tissue constructs", ACS Nano **7**, 7500–7512 (2013).

Summary

The research described in this thesis focuses on the development of a high sensitive, specific detection technology for clinical magnetic nanoparticle (MNP) applications during interventions like surgery. Up to now, the clinical use of MNPs is mainly as a contrast agent in MRI. An upcoming surgical application is the use of MNPs in the sentinel lymph node procedure.

Of all lymph nodes, the sentinel lymph node (SLN) has the highest chance to receive metastases due to its direct drainage of the tumor area. Therefore, the SLN is essential to determine the stage of metastatic spread. The SLN is usually identified by an injection of a tracer which flows from the tumor area and finally accumulates in the SLN. MNP tracers are a good alternative for the presently applied radionuclides and blue dyes. Since SLNs can be located centimeters deep in tissue, successful application of optical methods is limited. The application of radionuclides is limited and complicated by logistics and safety regulations. With their unique magnetic properties, MNPs are detectable at a distance. In addition, MNPs are stable and safe for storage and clinical application. The research in this thesis focuses on different aspects of MNP detection for clinical procedures.

In chapter 2 the current status of clinical MNP application is shortly described. The limitations of standard AC-magnetometry are quantitatively analyzed for clinical detection during interventions. In clinical application of MNPs, depth sensitivity of the sensor is crucial, while the magnetic contribution of tissue has to be taken into account. The (variable) magnetic contribution of tissue masks the MNP signal, which increases the detection limit of MNPs. The model-based analysis has shown that only with coils smaller than 2 cm diameter an amount of 1 μg iron can be detected within 1 cm deep in tissue. For larger detection coils the tissue contribution dominates the MNP signal which increases the detection limit. At a depth of 5 cm in tissue the MNPs can only be detected if the spot contains more than about 120 μg iron.

In chapter 3 a method is developed to reliably quantify the amount of iron oxide nanoparticles (Endorem) in lymph node tissue with vibrating sample magnetometry (VSM). Using a especially designed sample fixation system, the abusive effects of additional vibrations due to the soft tissue properties could be minimized. The measured magnetic moment response as a function of the applied field is analyzed with the Langevin function to determine the superparamagnetic contribution of the MNPs,

while a linear component was estimated to determine the contribution of the linear magnetic tissue and sample holder. For a good approximation of the nonlinear contribution a particle size distribution was required to include in the Langevin function. For Endorem calibration samples a bimodal particle size distribution was determined. MNP quantification in tissue is accurately performed with a detection limit of 1 μg iron. This is achieved by fixing the parameters of the bimodal lognormal particle size distribution while for each sample the amplitude of the nonlinear component and the linear contribution are independently determined. Especially for very low MNP quantities this approach is essential, because the estimation of the particle size distribution is difficult in those cases.

Chapter 4 describes a feasibility study to demonstrate MND application in *ex vivo* sentinel lymph node mapping in a small group of 10 colorectal cancer patients (11 tumors), using the VSM method developed in chapter 3. There is increasing evidence that the identification of micrometastases, revealed by the sentinel lymph node procedure, justifies additional treatment in stage I and II patients. After standard resection of the tumor in 10 patients, the colonic or rectal segment was opened and Endorem and Patent Blue V was injected submucosally around the tumor, followed by a gentle massage. At histopathological dissection, the three blue nodes closest to the tumor were selected as the sentinel nodes. The SLNs were subjected to VSM and histological staining to determine Endorem content. To determine nodal status, multi-level sectioning and immunohistochemistry was applied.

VSM detected nonlinear magnetism from Endorem in 9 patients in the range of 1.1-51.4 μg iron, which was confirmed by histology with iron staining. In only one patient no Endorem was detected in the SLNs, neither with VSM nor with iron staining. In one patient metastases were detected by standard histology. In four conventionally node negative patients (44%) micrometastases and isolated tumor cells were detected only by additional histology, which can be fully attributed to the SLN procedure and focused histology. Although SLN selection was based on selection with blue dye, the Endorem containing nodes accurately predicted status of the nodal basin in all patients. The results show the feasibility of Endorem for SLNM in colorectal cancer as a probably more specific and stable tracer compared to Patent Blue V. The *ex vivo* circumstances of the procedure did not hamper the distribution of nanoparticles through the lymphatic system. Development of a clinical magnetometer that exploits the nonlinear properties of SPIO will facilitate the introduction of magnetic *ex vivo* SLN mapping in colorectal cancer as a fast and cost-effective method to improve staging.

Chapter 5 describes a new, patented concept of magnetic detection, named differential magnetometry or shortly DiffMag, that can be used for fast and selective measurements on magnetic nanoparticles and which eliminates the contribution of materials with a linear magnetic susceptibility, like tissue. In the clinical practice of

SLN detection, it is important to detect the MNPs at a substantial depth of several centimeters within maximally a few seconds. The DiffMag concept is a solution for this problem and can be realized in a simple setup using copper coils. Using an alternating excitation field ($f \sim 5$kHz, $\mu_0 H \sim 2$ mT) with a sequence of static offset fields ($\mu_0 H \sim$20 mT), the magnetometer is selectively sensitive for the nonlinear properties of magnetic nanoparticles in samples. The offset amplitude brings the magnetization of the MNPs to saturation, which reduces the MNP response on the alternating field. Because this reduction does not occur for linear magnetic materials like tissue, the signal reduction is specific for the MNPs and is therefore useful for selective MNP detection. By subtraction of the subsequent periods in the sequence (with and without offset), the constant response of tissue is eliminated, while the remaining difference is a quantitative measure for the MNPs. As was shown in chapter 2, elimination of the tissue contribution is essential for detection of a small amount of MNPs. A detection limit for superparamagnetic iron oxide nanoparticles is demonstrated in the sub-submicrogram (iron) range.

For different types of MNP suspensions the sensitivity of DiffMag was determined. In general, the mass sensitivity of the procedure increases with offset field amplitude and particle core size. Compared to the sensitivity for particles in suspension, the sensitivity reduces for particles accumulated in lymph node tissue or immobilized by drying, which is attributed to a change in Brownian relaxation. This hypothesis was confirmed by measurements with dried samples. The differential magnetometry concept is used as a tool to perform non-destructive analysis of magnetic nanoparticles in clinically relevant tissue samples at room temperature. In addition, the differential magnetometer can be used for fundamental quantitative research of the performance of magnetic nanoparticles in alternating fields. The method is a promising approach for in vivo measurements during clinical interventions, since it suppresses the linear contribution of the surrounding body volume and effectively picks out the nonlinear contribution of magnetic tracer.

Since in biomedical applications the biological environment can largely influence the original magnetic relaxation properties of the applied MNPs, this aspect has been further investigated in chapter 6. An extended DiffMag measurement, using a sequence with a range of offset field amplitudes, provides the dm/dH response of a sample. This curve is analyzed by the first derivative of the Langevin function, including a core size distribution. Macroscopic (~ 0.5 mL) samples are measured in a magnetometer consisting of a first order gradiometer pick-up coil, using a continuous alternating field with a single excitation frequency ($f \sim 2.2$ or 4.4 kHz, $\mu_0 H$=1 mT) and a sequence of offset fields ($\mu_0 H = \pm 27$ mT).The effects of different environments that influence hydrodynamic nanoparticle behavior are investigated in samples with Resovist, Endorem and an in house produced MNP. Changes in viscosity are investigated with MNP suspensions in agar and glycerol and with immobilized,

dried samples. MNP suspensions in serum are measured to investigate the effect of increased hydrodynamic volume by protein adhesion. Resovist uptake in murine macrophages is succesfully detected by a change in response relative to the original suspension.

For Resovist, the increased viscosity of the medium reduced the signal amplitude and/or contributing particle size, indicating decreased Brownian relaxation and a shift towards Néel relaxation. The mean size of the contributing particle size distribution shifts from 18 nm in suspension, to 12 nm in 1% Agar and 7 nm in 2% Agar. Except from a lower amplitude in the response of the glycerol sample, no clear effect of viscosity was observed in the contributing particle size distribution. The signal response in serum was significantly reduced and shows a shift to contributions with a slightly smaller mean particle size. Uptake of Resovist in macrophages showed a relative loss of the contribution of large particles to the magnetic signal, compared to the original suspension. In contrast to Resovist, for Endorem only a minor effect of viscosity was observed.

With the dm/dH measurements the environmental effects of viscosity and hydrodynamic volume on particle relaxation in alternating fields, could be observed in milliliter sized samples. This can be used as a tool to characterize performance of MNPs in biomedical alternating field applications. The presented approach provides a novel method for specific, non-invasive detection of biomolecular reactions that influence Brownian relaxation of MNPs in cells, animals and patients.

In conclusion, this thesis has shown (1) the feasibility of MNPs for clinical use in detection of sentinel lymph nodes in colorectal cancer, (2) the importance of high sensitive and selective MNP detection by elimination of magnetic contributions of tissue, (3) a successful realization of selective MNP detection with DiffMag in a simple setup with copper coils and (4) the environmental, physiological factors responsible for signal reduction in differential magnetometry.

Samenvatting

Dit proefschrift beschrijft een onderzoek naar het detecteren van magnetische nanodeeltjes (MND's) voor medische toepassingen. Het doel is daarbij om deze deeltjes met een hoge gevoeligheid en selectiviteit te kunnen detecteren tijdens operaties of andere klinische interventies. Tot nu toe is het klinisch gebruik van magnetische nanodeeltjes hoofdzakelijk beperkt tot contrastvloeistof in MRI. Een opkomende chirurgische toepassing van deze deeltjes is de poortwachterlymfklier (PLK) procedure.

Vanwege directe drainage van het tumorgebied heeft een PLK van alle lymfklieren de grootste kans op uitzaaiingen. De PLK is daarmee essentieel om uitzaaiing van de tumor te bepalen. De PLK wordt opgespoord door via een injectie een markeringsvloeistof vanuit het tumorgebied te laten vloeien, welke zich vervolgens ophoopt in de PLK. Voor de huidige technieken, gebruikmakend van radio-isotopen of blauwe kleurstof, zijn magnetische nanodeeltjes een goed alternatief. De lymfklieren bevinden zich centimeters diep in weefsel waardoor detectie op afstand noodzakelijk is en optische technieken ontoereikend zijn. Het gebruik van radio-isotopen is gecompliceerd en beperkt toepasbaar door logistiek en veiligheidsmaatregelen. MND's zijn detecteerbaar op afstand met unieke magnetische eigenschappen. Daarnaast zijn ze stabiel en veilig in opslag en klinisch gebruik. In het licht van deze toepassing heeft het onderzoek in dit proefschrift zich gericht op diverse aspecten van de detectie van MND's voor klinsche procedures.

In hoofdstuk 2 is de huidige stand van zaken in het klinisch gebruik van MND's belicht, waarbij een kwantitatieve analyse is gemaakt van de beperkingen van standaard AC-magnetometrie. Essentieel in klinische detectie van MND's is de detectiediepte, waarbij rekening moet worden gehouden met de magnetische bijdrage van weefsel. Bij systemen gebaseerd op een enkel wisselend magneetveld maskeert de (variabele) magnetische bijdrage van het weefsel het MND-signaal, wat zorgt voor verhoging van de detectielimiet van MND's. Alleen met kleine spoelen met een diameter tot 2 cm kunnen hoeveelheden van 1 μg ijzeroxide gedetecteerd worden tot ongeveer 1 cm diepte. Voor grotere spoelen overheerst de weefselbijdrage en wordt de detectielimiet hoger. Op 5 cm diepte kunnen MND's pas gedetecteerd worden als het meer is dan 120 μg ijzer.

In hoofdstuk 3 is een methode ontwikkeld om op een betrouwbare manier de

hoeveelheid ijzeroxidedeeltjes (Endorem) in lymfklierweefsel te bepalen met een zogenaamde 'vibrating sample magnetometer' (VSM). Door een speciaal ontworpen samplefixatiesysteem konden eventuele bij-effecten in de trillingen ten gevolge van de zachte eigenschappen van weefsel geminimaliseerd worden. Het gemeten magnetisch moment is als functie van het aangelegde veld geanalyseerd. De niet-lineaire, superparamagnetische component afkomstig van de MND's wordt benaderd met de Langevin functie. Een lineaire functie benadert de diamagnetische of paramagnetische component van het weefsel en het fixatiesysteem. Om een goede bepaling te doen van de niet lineaire magnetisatie van de MND's was het nodig om een deeltjesgrootteverdeling in de Langevin vergelijking op te nemen. Voor de magnetische deeltjesgrootte van Endorem is een bimodale lognormaalverdeling bepaald op basis van kalibratie samples. De kwantificatie van de MND's in weefsel kon nauwkeurig gedaan worden tot op 1 μg ijzer door de deeltjesgrootteverdeling te fixeren en alleen de amplitude en de lineaire bijdrage te bepalen. Met name voor kleine hoeveelheden MND's is deze aanpak essentieel, omdat de deeltjesgrootteverdeling bij een zeer kleine niet-lineaire bijdrage moeilijk te bepalen is.

Met behulp van de VSM-methode uit hoofdstuk 3 is in hoofdstuk 4 een studie gedaan naar de bruikbaarheid van MND's in een *ex vivo* poortwachterlymfklierprocedure in een kleine groep van 10 patiënten (11 tumoren) met colorectaal carcinoom. Er is toenemend bewijs dat de micrometastasen die met deze procedure aan het licht gebracht worden, extra behandeling van deze patiënten rechtvaardigt. Na het uitsnijden van de tumor is de colon geopend en is 1.5-2 mL Endorem en 1-1.5 mL Patente Bleu V rondom de tumor submucosaal geïnjecteerd gevolgd door lichte massage. Direct daarna is het preparaat onderzocht op aanwezigheid van blauwe klieren in het mesocolon of mesorectum. Na fixatie in formaline is het preparaat gelamineerd door de patholoog, waarbij de drie blauwe klieren het dichtst bij de tumor als poortwachterlymfklier zijn geselecteerd. Van deze lymfklieren is vervolgens met VSM de hoeveelheid Endorem in de klieren bepaald. Tenslotte is van de poortwachterlymfklieren een microscopische analyse gedaan, met ijzerkleuring (Perls pruisisch blauw) om de aanwezigheid van Endorem aan te tonen en met Cam 5.2 om micrometastasen aan te tonen.

In negen patiënten bevatte minstens één van de drie blauwe klieren ijzer op basis van de VSM. In totaal is in 19 van de 33 gevonden klieren (58%) de aanwezigheid van Endorem vastgesteld, in een range van 1.1-51.4 μg ijzer. De VSM bepalingen van alle klieren werden alle bevestigd door de ijzerkleuring. In slechts 1 patient werd zowel met VSM als met microscopie geen Endorem in de poortwachterlymfklieren gevonden. In 1 patiënt werden metastasen geconstateerd op basis van standaard histologisch onderzoek. In 4 patiënten is de aanwezigheid van micrometastasen en geïsoleerde tumorcellen vastgesteld op basis van de aanvullende histologische analyse van de poortwachterlymfklieren. Deze bevinding van occulte tumorcellen in

44% van de patienten die met de conventionele benadering als metastase-vrij wordt beschouwd, kan volledig worden toegeschreven worden aan het gebruik van de PLK-procedure en het meer gefocuste histologisch onderzoek. Hoewel de PLK's geselecteerd werden op basis van blauwe kleur, zou voor deze patiënten de diagnose niet anders worden als alleen op basis van Endorem geselecteerd zou worden. De studie toont dus aan dat Endorem geschikt is voor de *ex vivo* PLK-procedure bij colorectaal kanker, waarbij er waarschijnlijk een hogere selectiviteit voor de PLK bestaat vergeleken met Patente Bleu V. De *ex vivo* omstandigheden hebben de distributie van deeltjes door het weefsel niet volledig verhinderd. De ontwikkeling van een klinisch bruikbare magnetometer die de niet-lineaire eigenschappen van de MND's benut, zal de introductie van een snelle en kosten-effectieve magnetische ex vivo PLK-procedure voor colorectaal kanker ter verbetering van de stadiëring bevorderen.

In hoofdstuk 5 is een nieuw, gepatenteerd, technisch concept, differentiële magnetometrie of kortweg DiffMag, ontwikkeld voor het snel en selectief meten van MND's in biologisch weefsel. De lineaire magnetische bijdrage, die een rol speelt in de meettechnieken in voorgaande hoofdstukken, is daarbij geëlimineerd. In de klinische praktijk van bijvoorbeeld de PLK-procedure, is het van belang dat de detectie van de MND's met een redelijke diepte van meerdere centimeters en in maximaal een paar seconden kan plaatsvinden. Het ontwikkelde DiffMag concept, gerealiseerd in een eenvoudige opstelling met koperen spoelen, biedt daarvoor een oplossing. De niet-lineaire magnetische eigenschappen van MND's worden benut door met een sinusoïdaal magneetveld met een constante frequentie ($f \sim 5$ kHz, $\mu_0 H \sim 2$ mT) te exciteren en daarbij steeds een vaste offset ($\mu_0 H \sim$20 mT) aan en uit te schakelen. De amplitude van de offset zorgt voor magnetische saturatie van de MND's, waardoor de MND-respons op het wisselend veld reduceert. Omdat deze reductie niet optreedt bij lineair magnetisch materiaal, zoals weefsel, is deze reductie specifiek voor de MND's en is dus bruikbaar voor selectieve detectie. Door de respons van opeenvolgende periodes (met en zonder offset) van elkaar af te trekken, wordt de constante bijdrage van weefsel geëlimineerd, terwijl het verschil van het signaal een kwantitatieve maat is voor de MND's. Zoals hoofdstuk 2 heeft aangetoond, is het wegwerken van de weefselbijdrage essentieel om de kleinere hoeveelheden MND's te kunnen detecteren. In het huidige onderzoek is daarmee een detectielimiet behaald in het sub-microgram gebied voor ijzeroxidedeeltjes. Door het ruisniveau van de opstelling te verlagen, is de verwachting dat detectie in de orde van nanogrammen haalbaar is.

Met het ontwikkelde DiffMag-concept is voor diverse soorten MND-suspensies de gevoeligheid bepaald. Deeltjes met een grotere magnetische kern satureren bij een lagere veldsterkte en geven dus een hoger DiffMag-signaal. Verder zijn PLK's uit een varkensstudie zowel met VSM als met DiffMag gemeten, waarbij de VSM resultaten structureel hoger uitkomen dan de DiffMag-bepalingen. Dit verschil wordt verklaard

door het verschil in de omstandigheden van de deeltjes in suspensie en in weefsel en het gebruik van een hoogfrequent wisselend veld in DiffMag. Bij brownse relaxatie van MND's, waarbij het gehele deeltje roteert, spelen viscositeit en deeltjesvolume een rol. Vergeleken met de oorspronkelijke suspensie veranderen deze omstandigheden na opname van MND's in weefsel, zodat de brownse relaxatie beperkt wordt. Omdat voor de kalibratie de originele suspensies gebruikt zijn, is de hoeveelheid MND's met DiffMag onderschat. Bij de bepaling met quasi-statische VSM speelt de brownse relaxatie geen rol en is kwantificatie niet beïnvloed door omstandigheden. De invloed van de omstandigheden in weefsel op de DiffMag-bepaling is bevestigd door metingen waarin suspensies en gedroogde samples vergeleken zijn. DiffMag blijkt uitermate geschikt om met een hoge selectiviteit de hoeveelheid MND's te bepalen in intact klinisch relevant weefsel. Voor correcte kwantificatie moeten daarvoor wel kalibratiesamples worden gebruikt waarin de deeltjes zich vergelijkbaar gedragen als in weefsel.

Omdat de biologische omgevingsfactoren, zoals viscositeit en binding van biomoleculen, een groot effect op de kwantitatieve magnetische respons van MND's kunnen hebben, is in hoofdstuk 6 verder onderzoek hiernaar gedaan. Een uitbreiding op de DiffMag-metingen geeft de zogenaamde dm/dH-curve. Daarbij wordt de offset van het excitatieveld over een reeks van waarden gevarieerd. Deze curve kan met de afgeleide van de Langevin functie en een deeltjesgrootteverdeling benaderd worden. Samples met een volume van 0.5 mL zijn gemeten met een alternerend excitatieveld van 1 mT en frequenties van 2.2 en 4.4 kHz en een sequentie van offsetvelden tot $\pm$27 mT. Resovist, Endorem en een in huis geproduceerd MND zijn gebruikt om hydrodynamische effecten op het signaal te meten. Het effect van viscositeit is onderzocht met suspensies in agar en glycerol en met gedroogde samples. Het effect van hydrodynamisch volume is onderzocht met suspensies in serum, waarbij de MND's in volume kunnen toenemen door eiwitten die hechten aan de MND's. Tenslotte is voor Resovist onderzocht wat het effect is op het gemeten signaal als de deeltjes worden opgenomen in macrofagen van muizen.

De meest duidelijke resultaten zijn verkregen voor Resovist. Een toename in viscositeit leidt tot een verbreding en verlaging van de dm/dH-piek. De gemiddelde deeltjesgrootteverdeling die bijdraagt aan het signaal verschuift van 18 nm in suspensie, naar 12 nm in 1% Agar en 7 nm in 2% Agar. De verschuiving duidt op een verlaging van de brownse relaxatie en een toename van een Néel-bijdrage. Bij Resovist in glycerol is geen duidelijk effect van viscositeit waargenomen. Het signaal voor Resovist in serum is sterk verlaagd, waarbij de gemiddelde diameter van de bepaalde deeltjesgrootteverdeling iets lager uitkomt. De opname van Resovist in macrofagen laat een relatieve verlaging zien in de deeltjesgrootte die bijdraagt aan het signaal. In tegenstelling tot Resovist, is voor Endorem slechts een licht effect van viscositeit waargenomen. Dat wijst erop dat relaxatie bij Endorem hoofdzakelijk via

het Néel-proces verloopt.

In het gebruikte DiffMag-concept zijn de effecten van viscositeit en hydrodynamische deeltjesgrootte op brownse relaxatie duidelijk waarneembaar in milliliter volumes. Deze nieuwe techniek kan daarom ook gebruikt worden om relaxatie eigenschappen van MND samples in wisselende magneetvelden te karakteriseren. Daarmee liggen ook toepassingen op het gebied van biomoleculaire interacties in cellen, proefdieren en patiënten binnen handbereik.

Dit proefschrift heeft laten zien: (1) MND's zijn geschikt voor klinisch gebruik bij de detectie van de poortwachterlymfklier bij colorectaal carcinoom, (2) het belang van selectieve MND detectie met een hoge gevoeligheid en verwijdering van de magnetische bijdrage van weefsel, (3) een succesvolle realisatie van selectieve MND detectie met DiffMag gebruikmakend van een eenvoudige opstelling met koperspoelen die te vertalen is naar een intra-operatieve situatie en (4) de invloed van fysiologische omgevingsfactoren die zorgen voor reductie van het gemeten DiffMag signaal.

Dankwoord

Na de vele jaren werk die in dit proefschrift gestoken zijn, is het onmiskenbaar dat dit slechts tot stand heeft kunnen komen, dankzij velen die op enige manier een bijdrage hebben geleverd. Daarom wil ik graag mijn dank aan hen uitspreken.

Allereerst gaat mijn dank uit naar mijn promotor, prof. Wiendelt Steenbergen en co-promotor dr. Bennie ten Haken. Vanwege een wisseling van de wacht was jij, Wiendelt, pas op het laatst betrokken bij dit proefschrift. Temeer mijn dank voor de bereidheid om als promotor op te treden en voor de wijze waarop je hierin ruimte gaf om het geheel af te ronden.

In het bijzonder dank ik Bennie ten Haken, die als co-promotor het gehele traject van dit proefschrift heeft begeleid. Ik dank je voor het vertrouwen dat je in mij gesteld hebt. Je enthousiasme, optimisme, geduld en onverminderde vertrouwen in de waarde van dit onderzoek hebben het gebracht waar het nu is. En we zien dat de betekenis van detectie methoden voor magnetische nanodeeltjes in medische toepassingen alleen maar toeneemt. Veel discussies hebben we gevoerd en daarbij heb ik altijd veel vrijheid ervaren in het kiezen van de richting die me interesseerde. Daarnaast dank ik je voor de verschillende mogelijkheden die je me bood om buiten het onderzoeksgebied andere dingen te doen.

Ik ben de leden van de commissie erkentelijk voor het beoordelen van het werk en de bereidheid om deel te nemen aan de openbare verdediging. Especially, I would like to acknowledge prof. Pankhurst from Univesity College London for his inspiring contributions in earlier discussions and meetings. Moreover, I appreciate his readiness to evaluate the thesis and to come over for the public defence. In het bijzonder wil ik ook noemen dr. Klaase die samen met zijn collega-chirurgen in het MST en dr. Van Baarlen als patholoog een belangrijke bijdrage geleverd hebben voor de eerste twee hoofdstukken van het proefschrift. Door een eerste demonstratie van magnetische detectie poortwachterlymfklier in darmkankerpatiënten, is een goed beeld verkregen van de mogelijkheden voor en de waarde van detectie van magnetische nanodeeltjes in de (oncologische) chirurgie. Regelmatig herinner ik me de zeer motiverende besprekingen met dr. Klaase, waarbij het diepdoordrongen belang van de patiënt het belangrijkste motief was voor het inzetten van een nieuw onderzoek. De medewerking vanuit het MST en het Laboratorium Pathologie Oost-Nederland is door mij als zeer waardevol ervaren.

Anderen die heel belangrijk voor mij zijn geweest in de afgelopen jaren, zijn mijn directe collega's. Ik denk als eerste aan Erik Krooshoop die vanaf het begin als technicus bij het werk betrokken is geweest. Dankzij jou inzet, ervaring en hulp is dit werk gelukt. Je stond altijd klaar om te helpen, even mee te kijken of een probleem op te lossen. Hierbij wil ik ook Tasio Oderkerk noemen. Hoewel meer op afstand van mijn project, was je altijd geïnteresseerd en hebben we veel met elkaar besproken. Daarin heb ik je als een waardevolle collega leren kennen. Ook dank ik de andere promovendi, Martin, Bas-Jan, Kirsten, Joost en Sebastiaan voor hun interesse, samen optrekken, hulp en gezelligheid. Joost en Sebastiaan, dank dat jullie mij ook op de dag van de promotie als paranimfen willen bijstaan. In de afgelopen jaren hebben we op veel momenten samen opgetrokken, gediscussieerd, geluncht en gewoon gesproken over de dingen van het leven. Ik heb dat als zeer waardevol ervaren. Door jullie inbreng vanuit de medische praktijk of fysica ervoer ik het onderzoek als een gezamelijke prestatie waarin we elkaar konden versterken. De uren samen in ons kantoor, het lab of de operatie kamer zijn onvergetelijk.

Tijdens het onderzoek hebben diverse studenten op verschillende manieren bijgedragen. Françoise, Hans, Ben, Ellis, Joost, Matthias en Bart: veel dank voor jullie inzet.

De ondersteuning van het secretariaat in allerhande zaken is altijd als heel goed ervaren. In het begin bij de vakgroep Lage Temperaturen waren daar Ans en Inke die, zeer behulpzaam, meewerkten en meeleefden. Ik dank jullie voor het vele goede werk en persoonlijke interesse. Ook dank ik Esmeralda en Jolanda van het secretariaat van Neuro-Imaging. Jolanda, ook heel veel dank voor al het werk in het voorbereiden van de dag van de promotie.

Daarnaast zijn er velen op de UT geweest die de afgelopen jaren tot fijne jaren hebben gemaakt, door hun interesse, gezelligheid of medewerking. Alle collega's van ICE, EMS, ECTM, CNPH, RAM en TG: veel dank. Ook noem ik de oud-kamergenoten van EMS en RAM, waarmee ik veel heb kunnen delen tijdens het werk of in de pauzes. Hierbij wil ik ook Heidi Witteveen noemen. Als oud-studiegenoot en collega hebben we elkaar veel gesproken, ook tijdens het reizen of lunchen. Ik hoop dat we elkaar de komende jaren niet uit het oog verliezen.

Het werken aan een proefschrift zou niet vol te houden zijn als er niet momenten van rust en ontspanning zouden zijn. Familie, vrienden, en bekenden zijn daarbij heel belangrijk geweest. Ik wil daarom alle vrienden, bekenden en buren bedanken voor de momenten van ontspanning en hun interesse in de voortgang van het werk. Ook mijn broers, (schoon)zussen, zwagers, dank ik voor hun meeleven en momenten van relativering. Het werken aan een promotie onderzoek is in zekere zin niet meer dan de uitoefening van enig ander beroep. Ik heb het altijd wat lastig gevonden om de nuance en relativering over te brengen, waarbij ik meer en meer respect ervaar voor hen die met reeële risico's hun werk doen. Ik hoop ook dat er in de komende tijd wat

meer ruimte ontstaat om de contacten met familie en vrienden te onderhouden.

De schitterende omslag van het proefschrift heb ik te danken aan de zeer toegewijde, enthousiaste en deskundige inzet van mijn zwager Martijn Duifhuizen. Ik ben zelf heel blij dat er bij een proefschrift de ruimte voor zo'n bijdrage is en dat je bereid was om hier aan mee te werken. Met het vertrouwen in een goed resultaat, heeft het mij veel moeite en tijd bespaard.

In het bijzonder wil ik mijn schoonouders danken. Pa en ma van Woerden, veel dank dat jullie op zoveel momenten en met zoveel dingen klaarstonden. Heel fijn was het dat er op dinsdag op Hadassah en Gerline gepast kon worden. Ook de maaltijden uit de keuken in Oene op dinsdagavond waren altijd royaal en heerlijk. En dan blijft er nog zoveel op te noemen waarin jullie met raad en daad terzijde stonden. Heel veel dank!

Heel dankbaar ben ik voor alles wat ik van en door mijn ouders ontvangen heb. Lieve papa en mama, vele herinneringen zijn er aan de voorbije jaren. Veel hebben jullie voor mij betekend, tot aan dit moment dat ik mijn promotie mag afronden. Ik dank jullie voor de vrijheid die jullie mij gaven om te studeren, waardoor ik ook deze promotie kon beginnen. Ook jullie interesse tijdens het werk heb ik gewaardeerd. Daarnaast hebben jullie vaak voor mij en mijn gezin op allerlei manieren klaargestaan. Ik ben daar heel dankbaar voor.

Anne-Esther, mijn lieve vrouw, ik dank je voor wie je voor mij bent. Jij bent er altijd voor mij geweest. Je hebt me in alles gesteund, geduld met me gehad en zo vaak de ruimte gegeven om verder te werken. Daarbij heb je ook zo vaak iets op je genomen waar ik niet de gelegenheid voor had om het zelf te doen. Tijdens mijn promotie zijn we getrouwd en hebben we samen twee prachtige dochters gekregen en mogen we een derde kindje verwachten. Heel veel dank wat je ook in hen aan mij gegeven hebt. Ik hoop dat we samen nog vele mooie, goede en gezonde jaren tegemoet gaan. Lieve Hadassah en Gerline, ik hou van jullie. Elke dag weer kan ik genieten van jullie onbevangenheid en leergierigheid. Ik hoop dat er weer tijden komen waarin ik me thuis ook meer op jullie kan richten.

In de wetenschap dat het vele goede van de afgelopen jaren ontvangen is uit de hand van de Gever van het leven, dank ik allermeest God de Heere.

Soli Deo gloria.

Martijn

About the author

Martijn Visscher was born in Apeldoorn (1983) and obtained his BSc degree in Biomedical Engineering from the University of Twente in 2005. At the same university, he received his MSc degree in 2008 with a study on the cortical processing of electrocutaneous stimuli, using EEG and source localization algorithms. In the same year, he started with a PhD programme at the MIRA Institute for Biomedical Engineering and Technical Medicine, focussing on clinical detection of magnetic nanoparticles in tissue samples. This research is performed in close collaboration with Medisch Spectrum Twente and the Technical Medicine Department as well as various research chairs in the MIRA and MESA+ institutes at the University of Twente. In the meantime, he contributed to several granted research proposals and practical courses for the educational programmes of Biomedical Engineering and Technical Medicine.

List of Abbreviations

CRC	colorectal cancer
DiffMag	differential magnetometry
DLS	dynamic light scattering
H&E	hematoxylin and eosin
ITC	isolated tumor cells
MM	micro-metastases
MNPs	magnetic nanoparticles
MPI	magnetic particle imaging
MRI	magnetic resonance imaging
NMR	nuclear magnetic resonance
PPMS	physical property measurement system
RES	reticuloendothelial system
RT-PCR	reverse transcription polymerase chain reaction
SLN	sentinel lymph node
SLNB	sentinel lymph node biopsy
SLNM	sentinel lymph node mapping
SPIOs	superparamagnetic iron oxides
SQUID	superconducting quantum interference device
TEM	transmission electron microscopy
USPIO	ultra-small superparamagnetic iron oxide nanoparticles
VSM	vibrating sample magnetometry

List of Publications

Journal papers

- Selective detection of magnetic nanoparticles in biomedical applications using differential magnetometry **M. Visscher**, S. Waanders, H.J.G. Krooshoop, B. ten Haken, Journal of Magnetism and Magnetic Materials, Vol.365, pp. 31-39, 2014,

- Quantitative analysis of superparamagnetic contrast agent in sentinel lymph nodes using ex vivo vibrating sample magnetometry **M. Visscher**, J. J. Pouw, J. van Baarlen, J. M. Klaase, B. ten Haken, IEEE Transactions on Biomedical Engineering, vol. 60, pp. 2594-2602, 2013.

- Intra-operative ex vivo photoacoustic nodal staging in a rat model using a clinical superparamagnetic iron oxide nanoparticle dispersion Diederik J. Grootendorst, Raluca M. Fratila, **Martijn Visscher**, Bennie Ten Haken, Richard J. A. Wezel, Sven Rottenberg, Wiendelt Steenbergen, Srirang Manohar and Theo J. M. Ruers Journal of Biophotonics, Vol. 6, Issue 6-7, pp. 493504, June 2013

- Evaluation of superparamagnetic iron oxide nanoparticles (Endorem) as a photoacoustic contrast agent for intra-operative nodal staging Diederik J. Grootendorst, Jithin Jose, Raluca M. Fratila, **Martijn Visscher**, Aldrik H. Velders, Bennie Ten Haken, Ton G. Van Leeuwen, Wiendelt Steenbergen, Srirang Manohar and Theo J. M. Ruers Contrast Media & Molecular Imaging Vol. 8 (1), pp. 83, January/February 2013

- Magnetic properties and paleointensities as function of depth in a Hawaiian lava flow Lennart de Groot, Mark Dekkers, **Martijn Visscher**, Geertje ter Maat G3 Geochemistry Geophysics Geosystems vol. 15(4), pp. 10961112, 2014, doi:10.1002/2013GC005094

Patent

- Method and apparatus for measuring an amount of superparamagnetic material in an object S. Waanders, **M. Visscher**, T.O.B. Oderkerk, H.J.G. Krooshoop, B. ten Haken EU-patent 12194029.0 2216, November 23 2012

Conference contributions

- Depth limitations for In-vivo Magnetic Nano-Particle detection with a Handheld Device **M. Visscher**, S. Waanders J.J. Pouw, B. ten Haken (oral), *(Proceedings paper submitted)* 10th International Conference on the Scientific and Clinical Applications of Magnetic Carriers, Dresden, Germany, June 10-14 2014

- Analyzing Magnetic Nanoparticle Content In Biological Samples: AC Susceptometry Using Offset Fields **M. Visscher**, S. Waanders, B. ten Haken (oral) 3rd International Workshop on Magnetic Particle Imaging, Berkeley, California USA, March 23-24 2013

- Finding the sentinel lymph node with a handheld differential magnetometer S. Waanders, **M. Visscher,** T.O.B Oderkerk, B. ten Haken (oral) 3rd International Workshop on Magnetic Particle Imaging, Berkeley, California USA, March 23-24 2013

- Photoacoustic intra-operative nodal staging using clinically approved superparamagnetic iron oxide nanoparticles D.J. Grootendorst, R.M.Fratila, **M. Visscher**, B. Ten Haken, R. Van Wezel, W. Steenbergen, S. Manohar, T.J.M. Ruers Progress in Biomedical Optics and Imaging - Proceedings of SPIE , 8581 , art. no. 858102, 2013

- Ex vivo quantification of magnetic nanoparticles in clinical samples at room temperature with high specificity and improved stability **M. Visscher**, S. Waanders, J.J. Pouw, H.J.G. Krooshoop, B. ten Haken (poster) 9th International Conference on the Scientific and Clinical Applications of Magnetic Carriers Minneapolis, MN, USA, May 22-26, 2012

- A magnetometer cooled with liquid nitrogen for the characterization and quantification of magnetic nanoparticles in biological samples at room temperature **Martijn Visscher**, Matthias Holling, Joost Pouw, Bennie ten Haken (poster) 2nd International Workshop on Magnetic Particle Imaging, Lbeck, Germany, March 15-16 2012

- A Magnetometer for Biological Samples Using Frequency Mixing Detection **Martijn Visscher**, Matthias Holling, Joost Pouw, Bennie ten Haken, Horst Rogalla (poster) 20th Soft Magnetic Materials Conference 2011, Kos Island, Greece, 18-22 September 2011

- Superparamagnetic Iron Oxides as Contrast Agent for Magnetic Detection of Sentinel Lymph Nodes in Colorectal Cancer **M. Visscher**, J.J. Pouw, B. ten

Haken, J.M. Klaase, J. van Baarlen, H. Rogalla (poster) 3rd Dutch Biomedical Engineering Conference 2011, Egmond aan Zee, The Netherlands, 20-21 January 2011

- Magnetic Sensing Methods and Materials for Medical Applications Bennie ten Haken, **Martijn Visscher**, Martin Sobik, Aldrik H. Velders (oral) International Workshop on Magnetic Particle Imaging, Lbeck, Germany, March 18-19 2010

- Magnetic Particles and Sensing Methods for Medical Applications **M. Visscher**, M. Sobik, B. ten Haken, J.J. Pouw, J.M. Klaase, J.J. Galindo Millan, A.H. Velders, H. Rogalla (poster) 11th European Symposium on Controlled Drug Delivery, Egmond aan Zee, The Netherlands, 7-9 April 2010

- Magnetic Detection of the Sentinel Lymph Node in Ex Vivo Tissue with Colorectal Cancer B. ten Haken, **M. Visscher**, J.J. Pouw, J.M. Klaase, Q.A. Pankhurst, A.H. Velders, H. Rogalla (poster) 17th International Conference on Biomagnetism BIOMAG 2010, Dbrovnik, Croatia, 28 March-1 April 2010

- Magnetic Detection of the Sentinel Lymph Node **M. Visscher**, B. ten Haken, A.H. Velders, J.J. Pouw, J.M. Klaase, H. Rogalla (poster) IEEE-EMBS Benelux Chapter Symposium, Enschede, The Netherlands, November 9-10, 2009

Poster

- Sentinel Lymph Node Detection Using Superparamagnetic Iron Oxides **M. Visscher**, B. ten Haken, J.J. Pouw, J.M. Klaase, Q.A. Pankhurst, A.H. Velders, H. Rogalla 1st Event MIRA Institute for Biomedical Engineering and Technical Medicine, Hengelo, The Netherlands, 1-2 April 2010

Stellingen

behorend bij het proefschrift

Detection of Magnetic Nanoparticles for Clinical Interventions

1. Succesvolle introductie van poortwachterlymfklierprocedures op basis van detectie van magnetische nanodeeltjes is zowel klinisch-technisch als maatschappelijk een mijlpaal.
2. Het DiffMag concept verschaft de mogelijkheid voor het ontwikkelen van *handheld* sensoren met een superieure dieptegevoeligheid voor magnetische nanodeeltjes, waarbij de eenvoud van het concept een minimale aanpassing van de chirurgische omgeving en handelwijze acceptabel maakt.
3. Voor het optimaliseren van detectietechnieken van magnetische nanodeeltjes in klinische toepassingen, is het noodzakelijk rekening te houden met het gedrag van de deeltjes in de fysiologische context.
4. Een deeltjesgrootteverdeling verkregen bij data, gemeten met een wisselend magneetveld, kan niet zomaar beschouwd worden als representatief voor de gehele deeltjespopulatie.
5. Omdat veel nieuwe medisch-technische ontwikkelingen uiteindelijk sneuvelen door een hoge mate van complexiteit die moeilijk verenigbaar is met de klinische praktijk, is het van het grootste belang om in een vroeg stadium gebruikers en ontwikkelaars bij elkaar te brengen.
6. Het doen van ontdekkingen is vergelijkbaar met magnetisatie: hoe meer wetenschapsdomeinen geordend zijn, hoe meer de kennis verzadigd wordt; verzadiging is veelal nog lang niet bereikt.
7. De vermeerdering van kennis verhoogt de nieuwsgierigheid en toont de, voor onze waarneming, oneindige diepte van het universum.
8. De beperktheid van 's mensen kennis veroorlooft, voedt en continueert het bestaan van wetenschappelijke instituten, als universiteiten.
9. Wetenschap spreekt zich uit over de dingen die waargenomen zijn; over zaken die niet zijn waargenomen zijn, dient het zich niet uit te spreken, maar kan het slechts speculeren.
10. Zelfkennis is de beste kennis.

Martijn Visscher

Propositions

accompanying the thesis

Detection of Magnetic Nanoparticles for Clinical Interventions

1. A successful introduction of sentinel lymph node procedures based on detection of magnetic nanoparticles is in clinical as well as social perspective a milestone.
2. The DiffMag concept delivers the possibility to develop handheld detectors with superior depth sensitivity for magnetic nanoparticles, while the simplicity of the concept makes a minimal adaptation of surgical environment and practice acceptable.
3. To optimize detection techniques for magnetic nanoparticles in clinical applications, it is necessary to take into account the particle behavior in physiological context.
4. A particle size distribution obtained from data measured using an alternating field, cannot unquestioningly be regarded as representative for the whole particle population.
5. Since a lot of new medical technological developments finally get stranded by a high complexity which is hardly compatible with clinical practice, it is of great importance to bring users and developers together in an early phase of development.
6. Making discoveries is comparable with magnetization: the more scientific domains are ordered, the more our knowledge becomes saturated; generally, saturation is by far not reached.
7. The increase of knowledge arouses one's curiosity and shows the, for our perception, infinite depth of the universe.
8. The limitations of human knowledge permit, feed and continue the existence of scientific institutions, like universities.
9. Science speaks about things that are observed; it should not speak about things that are not observed, but can only speculate about it.
10. Self-knowledge is the best knowledge.

Martijn Visscher